Development and characterization of novel microelectrode arrays for neurophysiology

Ph.D. dissertation

Gergely Márton

Semmelweis University
János Szentágothai School of Neurosciences

Supervisor: Dr. István Ulbert, D.Sc.

Opponents: Dr. András Czurkó, Ph.D.
Dr. László Négyessy, Ph.D.

Qualifying exam commitee, chair: Dr. Béla Halász, member of the HAS
Qualifying exam commitee: Dr. László Acsády, Ph.D.
Dr. Zoltán Somogyvári, Ph.D.

Budapest
2015

Contents

List of abbrevations

AP	Anteroposterior
BBB	Blood-brain barrier
BMI	Brain-machine interface
CED	Convection enhanced delivery
CMOS	Complementary metal–oxide–semiconductor
CPE	Constant phase element
CSD	Current source density
CV	Cyclic voltammetry
DG	Dentate gyrus
DL	Double layer
DRIE	Deep reactive ion etching
ECoG	Electrocorticography
EDC	Electronic depth control
EEG	Electroencephalography
EMG	Electromyography
FDA	U.S. Food and Drug Administration
FIB	Focused ion beam
LFP	Local field potential
LTP	Long term potentiation
MEA	Microelectrode array
MEMS	Microelectromechanical systems
MFA	Institute for Technical Physics and Materials Science of the RCNS-HAS (Műszaki Fizikai és Anyagtudományi Kutatóintézet, MTA-TTK)
ML	Mediolateral
MUA	Multiunit activity
nRT	Thalamic reticular nucleus
PDMS	Polydimethylsiloxane
Pt/Pt	Platinized platinum

RCNS-HAS	Research Centre for Natural Sciences of the Hungarian Academy of Sciences (MTA-TTK)
RIE	Reactive ion etching
RF	Roughness factor
RMS	Root mean square
SEM	Scanning electron microscope
SNR	Signal-to-noise ratio
SOI	Silicon-on-insulator
SUA	Single unit activity
TC	Thalamocortical
UIEA	Utah intracortical electrode array
VPL	Ventral posterolateral nucleus (of the thalamus)
VPM	Ventral posteromedial nucleus (of the thalamus)

1. INTRODUCTION

1.1. Electrophysiology

1.1.1. Overview

Electrodes make the detection of potential changes within, or in the vicinity of a domain containing living cells possible by converting ionic currents, propagating in aqueous solutions into currents of electrons, propagating in metals or semiconductors. They are utilized by the majority of clinical and experimental neuroscience techniques, such as in vitro and in vivo electrophysiology, electrocorticography (ECoG), electromyography (EMG), electroencephalography (EEG), etc.

During in vitro experiments cultured neurons or brain slices are typically observed. In the majority of these studies, micropipettes are used in order to detect potential changes within the extracellular space, monitor membrane potentials of specific cells, or determine conductivity values of membrane regions, which are regulated by ion channels. Insulated metal wires can also be utilized for extracellular recordings, or for regulating the membrane potentials. In vivo extracellular electrophysiology allows neuroscientists to observe behavior of cells, cell populations or more extent neural structures in their natural physiological environment, without violating their - usually extremely complex - connections with other parts of the brain. This is achieved by implanting probes into the tissue. ECoG and EEG are practices of recording electric activity from the surface of the cerebral cortex and the scalp, respectively. Spontaneous activity and evoked potentials can be examined with both methods. A great advantage of EEG is its noninvasivity, however, its spatial and temporal resolution is low due to the filtering effect of the skull.

EEG and in vitro measurements are not directly related to this thesis, whereas in vivo extracellular measurements and ECoG are. Therefore the latter two methods are detailed in the following sections.

1.1.2. In vivo extracellular measurements

Local field potential

Cell membranes can be described as high impedance elements, with mostly capacitive characteristics, yet as a result of the conductive extracellular space, the neural tissue can be approximated as an ohmic conductor medium, with inhomogenity and anisotropy (Goto et al., 2010; Hoeltzell and Dykes, 1979). Due to the finite conductivity of the tissue, transmembrane currents give rise to a potential field. The fluctuations of the voltage at a certain point of the brain, which can be measured with respect to the voltage in a reference point, are usually divided into two signal types: unit activities, i.e. the spikes generated by action potentials of neurons in the vicinity of the observed location, and variations of the local field potential (LFP), i.e. potential changes of other sources. The fact that LFP is not simply the result of superposing action potentials has been revealed early by Eccles (Eccles, 1951), who proposed that LFP is rather generated by postsynaptic currents. Since then, the contribution of other factors to the LFP has been described, e.g. afterhyperpolarization following action potentials, calcium spikes, transmembrane currents of glial cells, etc. (Buzsáki et al., 2012).

LFP signals are frequently utilized for current source density (CSD) analysis, during which current sinks and sources observed from the viewpoint of the extracellular space are evaluated. Assuming the potential field (φ) and the conductivity tensor (σ) are known in a domain, and the magnetic effects can be neglected, the source distribution (I) can be calculated:

$$I = - \qquad (1.1.)$$

where $\nabla^2\varphi$ is the second spatial derivative of the potential field. CSD allows the analysis of neural events with superior resolution compared to field potentials (Freeman and Nicholson, 1975; Nicholson and Freeman, 1975).

Unit activities

With an electrode implanted into the extracellular space, the detection of action potentials is possible as well (Woldring and Dirken, 1950). These single and multiple unit activities (SUAs, MUAs) can vastly increase the information content of extracellular recordings. The firing patterns of cells that contain their soma or axon in the vicinity of the probe yield information about the functions of the monitored tissue region. This allows functional mapping of most parts of the brain, e.g. the thalamus and neocortical regions (Komura et al., 2005; Metin and Frost, 1989). Hippocampal place cells of a rat are active when the animal is in a certain place of its environment (O'Keefe and Conway, 1978; O'Keefe and Dostrovsky, 1971), while grid cells in the entorhinal cortex fire when the rat positions itself into a node of a triangular spatial array (Hafting et al., 2005; Moser et al., 2008). SUA recordings in the human hippocampus revealed neurons that correspond to other, non-spatial related memory elements as well (Gelbard-Sagiv et al., 2008). Activity patterns of some neurons in the human amygdala showed that cells in the nuclei encode or compute stimulus values during decision making (Jenison et al., 2011).

Usually, SUAs of many neurons can be detected during a recording session. Unit activity clustering, or spike sorting is a technique used for reproducing spike trains of individual neurons (Takekawa et al., 2010). Simulations showed that action potential waveforms of maximum 8-10 cells can be classified (Lewicki, 1998; Pedreira et al., 2012). Mathematical algorithms have been developed in order to automate the sorting process (Quiroga et al., 2004; Rutishauser et al., 2006; Vargas-Irwin and Donoghue, 2007).

Determining the location of a neuron that generates unit activities, with respect to the electrode is a much more complicated matter than spike sorting. A special CSD method (spike CSD) was developed in order to reconstruct current source distributions of a single neuron during action potential generation and to determine cell-electrode distance (Somogyvari et al., 2012).

The information extracted from unit activity analysis can be exploited for developing high quality brain-machine interface (BMI) systems with cortically implanted extracellular microelectrodes. Such systems can be used to offer a speech-

deprived person a new channel of communication, which circumvents the individual's sub-cortical nervous system in case of its impairment (Bartels et al., 2008; Brumberg et al., 2010; Guenther et al., 2009; Hochberg et al., 2006). Signals gained by extracellular electrodes implanted into the motor cortex can be utilized to control prosthetic limbs purely with thoughts (Hochberg et al., 2006; Homer et al., 2013; Truccolo et al., 2008; Velliste et al., 2008).

1.1.3. Electrocorticography

ECoG, which is sometimes referred to as intracranial EEG, is a method comprising electrodes placed onto the brain surface (Matsuo et al., 2013). It can be used for functional mapping of various cortical regions, e.g. in the vibrissa/barrel field of rat neocortex (Jones and Barth, 1999).

In the clinics, ECoG is widely used during treatment of patients suffering from epilepsy, whose condition necessitates surgical resection (Asano et al., 2005; Kuruvilla and Flink, 2003; Ojemann, 1997; Sugano et al., 2007). Such surgeries require precise localization of the epileptogenic zones. Due to its high spatial resolution and signal-to-noise ratio (SNR) compared to EEG, ECoG is more suitable for this purpose (Hashiguchi et al., 2007). The technique is employed not only to assess the location of the irritative zones from ictal spike and interictal epileptiform activity, but also for functional mapping to avoid causing damage to critical regions. Furthermore, ECoG is employed to ascertain that the entire epileptogenic zone was resectioned.

Similarly to extracellular electrophysiology, ECoG is also a promising method in the aspect of creating BMIs for either brain-actuated prosthetic limbs (Graimann et al., 2004; Scherer et al., 2009) or speech restoration (Kanas et al., 2014; Spencer et al., 2010).

1.1.4. Acute in vivo measurements on laboratory animals

The in vivo characterization of neural probe prototypes and other novelties presented in this thesis will confine itself to acute measurements on laboratory rats. Chronic implantation of the probes for neuroscientific experiments, as well as their

utilization in the clinics open further possibilities, yet they are more complex, and exceed the subject of this thesis.

Acute in vivo experiments revealing the principals of long term potentiation (LTP) were carried out on anesthetized rabbits (Bliss and Lomo, 1973). Pairs of stimulating (tungsten wire) and recording (NaCl filled glass pipette) electrodes were implanted into the perforant path and the dentate gyrus (DG) of the hippocampus, respectively, into both hemispheres of the animals, with micromanipulators. The experiments showed that the strength of the synapses between the entorhinal cortex neurons and the granule cells of the DG can be increased by tetanic stimulation of the perforant path. Further findings based on these experiments gave insight to the cellular mechanisms of synaptic plasticity, which plays a fundament role in learning and memory functions of the brain (Bliss and Collingridge, 1993; Cooke and Bliss, 2006).

Acute in vivo experiments are performed for the analysis of neural activity during sleep, too. In the majority of these studies, the animals are anesthetized with urethane (Metherate and Ashe, 1993; Toth et al., 2008) and/or a mixture of ketamine-xylazine (Sachdev et al., 2004). During deep anesthesia and natural sleep, spontaneous activity in the neocortex shows low frequency oscillations. Each period of the oscillation can be divided to two alternating states. Active (upstate) periods, when cortical cells generate action potentials frequently are followed by inactive (downstate) periods, when spikes occur sparsely (Chauvette et al., 2011; Chauvette et al., 2010). The firing rate strongly correlates with membrane potential fluctuations (Metherate and Ashe, 1993). The effects of peripheral stimulations can be measured on the cortex during sleep as well, including evoked field potentials and elevated unit activity (Toth et al., 2008). This allows e.g. the investigation of mechanisms in the barrel field that are triggered by whisker stimuli (Sachdev et al., 2004), or the mapping of auditory functional topography (Hackett et al., 2011).

1.2. Electrode properties

Before demonstrating various types of neural electrodes and electrode arrays, I touch upon some properties that need to be kept in sight during development and utilization of such devices.

1.2.1. Surface conditions

The surface conditions of a microelectrode are of high importance, since this is the area through which the ionic currents of the neural tissue communicate with the electron-currents of the sensor or stimulator devices. Non-toxic noble metals such as gold (Au), platinum (Pt) and iridium (Ir) are commonly used as microelectrode materials, because of their corrosion resistance (Heim et al., 2012b). According to the Gouy-Chapman model, when such metals are immersed into electrolytes, an electrical double layer (DL) will develop in the vicinity of their surface. The DL contains the Helmholtz planes, formed by dehydrated ions adsorbed to the surface and hydrated ions closely attracted to it by the Coulomb force. The thickness of the Helmholtz layer is of the order of an ionic radius, i.e., 2 to 4 Å. The diffuse, or Gouy-Chapman layer is much less compact. It contains mobile ions, which are distributed according to the mechanics of electrostatic interaction and thermal diffusion (Yang et al., 2004). The electric field (i.e. the negative of the potential gradient) generated by the charges which are accumulated on the surface of the metal is shielded by the ion concentration gradient in the DL, making the complete structure electroneutral in a relaxed state.

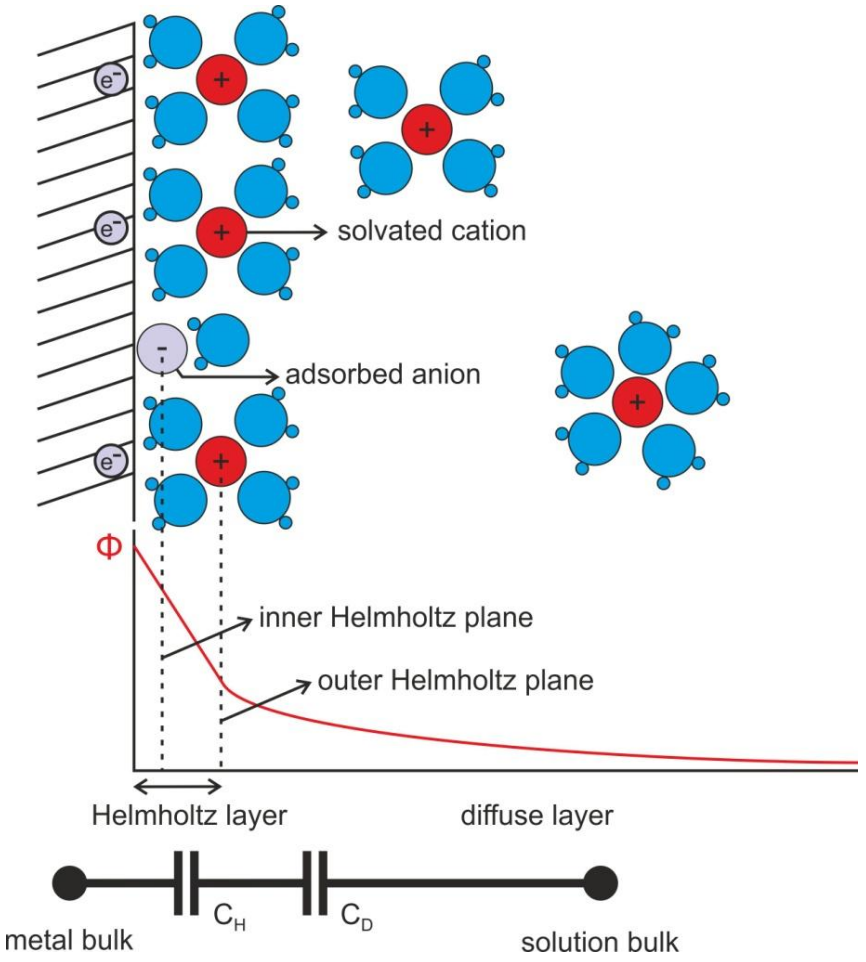

Fig. 1.1. Schematics illustrating the electrical double layer on the surface of a polarizable electrode. The Helmholtz layer contains ions adsorbed or electrostatically attracted to the surface. The diffuse layer contains mobile, solvated ions. Illustration based on Fig. 9. of (Wise et al., 1970).

1.2.2. Impedance

Considering the system illustrated in Fig. 1.1. as an electrical circuit, the Helmholtz and diffuse layers can be roughly approximated as capacitances (C_H and C_D, respectively), which will dominate the response of a polarizable electrode to an alternating current or voltage. The impedance of the electrical DL can be unified into a total capacitance, yet due to a phenomenon called frequency dispersion, a more precise approximation can be obtained by using a constant phase element (CPE) (Pajkossy et al., 1996; Zoltowski, 1998), which has an impedance of

$$Z_{CPE}(\omega) = \qquad (1.2)$$

where i is the imaginary unit, ω is the angular frequency, Q and α are frequency-independent parameters of the CPE. For α = 1, the CPE is a capacitance, for α = 0.5, it is a Wartburg element, and for α = 0, a resistance. The CPE can only model ideally polarizable electrodes. In order to achieve a more realistic illustration, a parallel resistive element (R_{CT}) is often included, corresponding to faradic charge transfer between the metal and the electrolyte. Furthermore, a spreading resistance (R_S) is applied serially, which represents the resistance of the solution around the electrode. In case of microelectrodes with small geometric area, this is an important element.

The thus assembled model was detailed previously (Franks et al., 2005; Zoltowski, 1998) and is shown in Fig. 1.2. In reality, the situation can be even more complex, if we take into consideration e.g. the resistance of the wiring, or the finite impedance between two different channels in a multielectrode system. In case of neural electrodes, the relatively low (< 20 kHz) biologically relevant frequencies ensure the usefulness of this simple model.

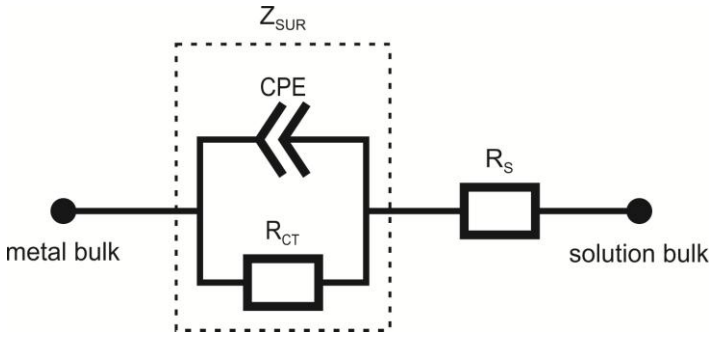

Fig. 1.2. Advanced equivalent circuit model of a non-ideally polarizable electrode. The constant phase element (CPE) corresponds to the double layer, the charge transfer resistance (R_{CT}) models the behavior of faradic processes. These two elements are characteristics to the electrode surface conditions, while the solution resistivity (R_S) depends on the chemical and

geometric properties of the aqueous media surrounding the electrode. The model was adapted from (Zoltowski, 1998) and (Franks et al., 2005).

Electrodes must be as noiseless as possible, when functioning as recording devices and they must be capable of injecting sufficient amount of charge into the tissue, when employed as stimulators. Although the influence of electrode impedance to the performance is subtle and not thoroughly understood, most theories and experiments indicate that decreased impedance results in improved recording and stimulation capabilities (Du et al., 2011; Ferguson et al., 2009; Heim et al., 2012a; Keefer et al., 2008; Liu et al., 2008; Scott et al., 2012). The root mean square (RMS) of thermal noise is proportional to the square root of the real part of the impedance (Ferguson et al., 2009; Liu et al., 2008), and reducing it has proven to be an effective way to increase SNR of recording electrodes (Du et al., 2011; Scott et al., 2012). Lowering the impedance of stimulating devices allows higher amount of charge to be injected into the extracellular space of the targeted tissue before causing electrolysis (Mailley et al., 2004; Merrill et al., 2005).

1.2.3. Roughness factor

As shown in Fig. 1.3., the effective surface area of an electrode determines the extent of the surface where the electrolyte comes into contact with the electron-conductive material. This area contains the microscopic irregularities of the surface and differs from the geometric area of the electrode, i.e. its "footprint" size from a macroscopic point of view. The roughness factor is the ratio of the effective surface and the geometric areas.

Increased electrode surface area causes higher double layer capacitance and lower charge transfer resistance, which both mean lower impedance, therefore higher SNR. Increasing the geometric area of the electrodes in order to reduce their impedance is not only limited by probe shaft dimensions, but could worsen recording properties of action potentials from individual neurons (Moffitt and McIntyre, 2005). A theoretical study on factors determining the SNR suggests that increasing geometric area of the microelectrode sites does not improve recording quality (Lempka et al., 2011). It is

rather beneficial if only the effective surface area can be increased (i.e. the area calculated with taking into account the microscopic irregularities of the surface).

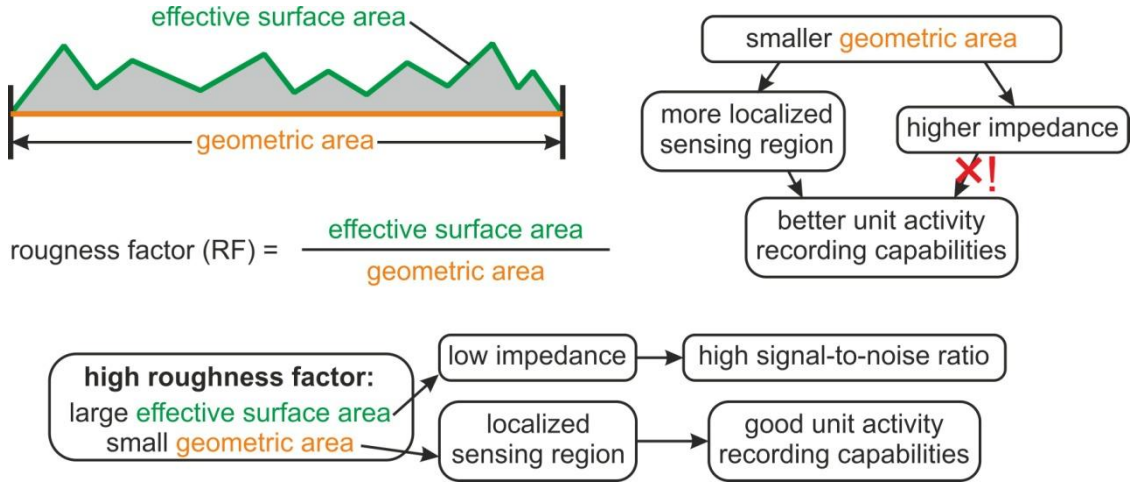

Fig.1.3. Illustration of the effective surface area and the geometric area of an extracellular neural electrode and the effect of these quantities on its performance

It is a quite common misunderstanding that high-impedance electrodes are more suitable for unit activity (spike) detection. This can in fact be true if we compare two microelectrodes of the same material. In this case, the higher impedance of the "better" electrode is a result of its smaller geometric area. In reality, this smaller geometric area causes both the better performance, due to a more localized sensor region, and the high impedance, due to the smaller area of the electrode surface. Therefore, its higher impedance is only an unfortunate consequence. This situation can falsely imply that good unit activity detection capability of an electrode is a result of its high impedance.

In summary, electrode impedances should be as low as possible, which can be obtained with high effective surface area. At the same time, the geometric area of an extracellular electrode is to be minimized in order to achieve high-quality unit activity recordings. This can be provided with the utilization of materials with large roughness

factor. Such solutions are presented in the last paragraph of section *1.3.4. Microelectrode arrays with special features.*

1.2.4. Biocompatibility

How does sensor-tissue interaction affect the quality of the measured signals? The question is still open, but it is obvious that it depends at least partially on the biocompatibility of the device. A slightly dated, but excellent review was published on this subject in the previous decade (Polikov et al., 2005).

The living neural tissue is a harsh, chemically active environment. It is important that the implanted probes make as little damage as possible and they remain stable at the same time. To meet these criteria, biocompatible materials are to be used for the construction of neural implants, which do not intoxicate living cells and can endure corrosive effects. Typical materials of microtechnology, such as Si, SiO_2, Si_3N_4 (Kotzar et al., 2002) and noble metals (Dymond et al., 1970) are non-toxic and inert. Yet even if the probes remain intact in the tissue, the functionality of their electrodes can be compromised by the foreign body response of the immune cells, which is triggered by the insults caused during the implantation and the intruding inorganic materials.

In the early period of the foreign body response the microglial cells, the resident macrophages of the nervous tissue, are activated. The ones located in the vicinity of the implant send projection towards it immediately after implantation (Kozai et al., 2012). In the following hours, through multiple steps, nearby microglial cells transform from their ramified (R) stage to a locomotory (L), amoeboid stage, in which they can move within the tissue rapidly (Stence et al., 2001). The activated microglia releases inflammatory factors and upregulates lytic enzymes as well (Polikov et al., 2005). Astrocytes, the other type of glial cells involved in the immune response are also activated and transform into reactive state, which is characterized by upregulation of GFAP, increased migration, proliferation, and enhanced matrix production (Landis, 1994). The increased glial cell activity changes into a sustained reactive response with time, during which a glial sheath is formed around the implant (Griffith and Humphrey, 2006; Szarowski et al., 2003; Turner et al., 1999; Ward et al., 2009).

The glial sheath has lower conductivity than the healthy tissue, which results in a signal-filtering effect. The question whether this phenomenon comprises unit activity (spike) detection, and if so, to what extent, is still open. Increase of electrode impedance during chronic use was reported (Lempka et al., 2009; Prasad and Sanchez, 2012), likely due to glial sheath formation. On the other hand, fortunately, numerous studies have been published of systems that are suitable for unit activity recordings for several months or years, e.g. utilizing a brush of 64 microwires in monkeys (Kruger et al., 2010) or a 10×10 silicon-based array in monkeys (Chestek et al., 2011) and humans (Simeral et al., 2011).

Nevertheless, the biocompatibility of extracellular electrode arrays is still a matter in focus, and several attempts have been made towards decreasing the deteriorative effect of the foreign body response. The effect of surface morphology on cell adhesion and patterning was characterized in vitro (Khan and Newaz, 2010), anti-inflammatory coatings such as hyaluronic acid, dextran, dexamethasone (Grand et al., 2010), interleukin receptor antagonists (IL1ra) (Taub et al., 2012) and bioactive coatings such as neural adhesion molecule L1 (Azemi et al., 2011) were tested in vivo. The concept of neurotrophic electrodes is based on the attraction of neuron processes into a glass cone with Matrigel and nerve growth factors. The cone is claimed to protect its inner electrodes from the insulating effects of the glial sheath (Guenther et al., 2009; Kennedy, 1989).

1.3. Microelectrode array types

1.3.1. Fine wires

Very common and trivial tools, employed for measuring extracellular potential changes are insulated, typically 20-50 μm fine wires. Such probes have been succesfully adapted for chronic use, giving insight into neural activity of freely moving, behaving animals since the late fifties (Strumwasser, 1958). The applied materials for such purposes can be teflon coated platinum-iridium (Chorover and Deluca, 1972; Palmer, 1978; Yamamoto, 1987), nichrome (Fontani, 1981) or polyimide insulated tungsten (Williams et al., 1999). A widely used method for improving SUA detection capabilities is bounding four wire electrodes together, forming a tetrode (Gray et al.,

1995). This technique allows one to monitor activities of tens of individual neurons simultaneously.

The yield of unit activities obtained with extracellular electrophysiology can be increased by orders of magnitude by employing not a single, but an array of electrodes. Furthermore, microelectrde arrays (MEAs) allow measurements of LFP with high spatial density, which makes CSD analysis a very powerful and robust method.

Arrays can be handcrafted with careful assembly of wire electrodes. With a construction of 3×11 tungsten wires, simultaneous recordings of 30-60 units can be achieved from guinea pig cortex (Williams et al., 1999). Four arrays of 12×12 individually drivable microelectrodes were used for interfacing with different cortical areas of macaque monkey, yielding recordings from a total of 800 individual cells (Hoffman and McNaughton, 2002).

1.3.2. Silicon-based devices

A huge progress was initiated in the fabrication of neural MEAs when the technological advancements of microelectronics industry were utilized. This process started in the late sixties (Wise et al., 1970). Since then these devices have been evolving along with microelectromechanical systems (MEMS) industry. The main advantages of utilizing MEMS technology over wire electrodes for the construction of neural MEAs are:

- The geometry of high density arrays can be custom-tailored to the structure of the brain region of interest, the shape and spatial arrangement of the sites can be formed with high precision and reproducibility.
- Integration of active electronic circuits is possible onto the same chip, which contains the electrodes.
- The possibility of batch fabrication provides high device yield.

Michigan arrays

The pioneering work of Wise, Angell and Starr (Wise and Angell, 1975; Wise et al., 1970) resulted in a brand of MEAs called Michigan arrays. These singe- or multi-

shank chips are fabricated out of single crystal silicon wafers and have a planar structure, as shown in Fig. 1.4. The microfabrication process flow involves boron diffusion, which creates etch-stop domains within the crystal, thus determining the three-dimensional shape of the probes, furthermore, the deposition and patterning of insulator thin-films and shaping a conductive (titanium/iridium) layer with lift-off technology.

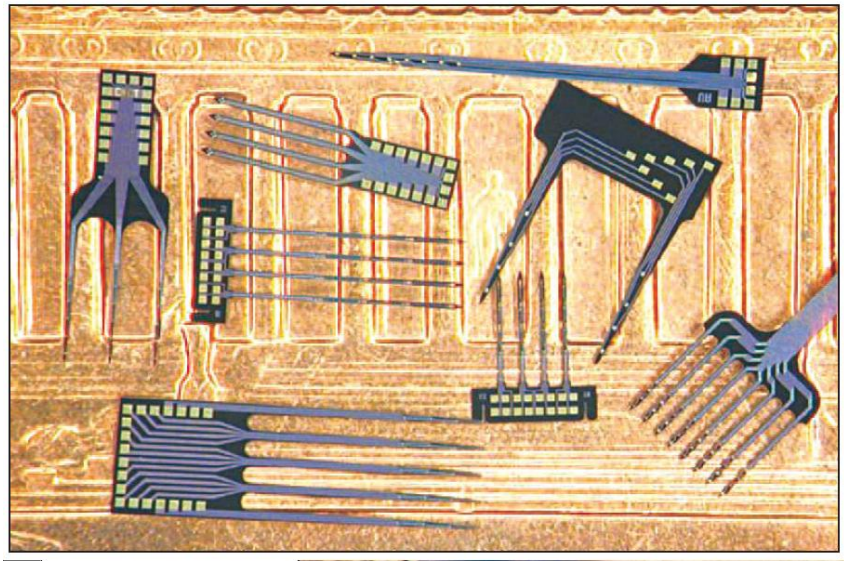

Fig. 1.4. Michigan microelectrode arrays (Wise, 2005)

These probes were commercialized by Neuronexus Technologies (Ann Arbor, MI, USA). The neuroscientific knowledge gained by the use of them is diverse. Csicsvari et al. tested three different Michigan MEA configurations on rat neocortex and hippocampus (Csicsvari et al., 2003). The first two contained 6 and 8 shanks, 96 and 64 electrodes, which covered two-dimensional areas of 1500×1500 μm^2 and 350×1400 μm^2, respectively. The third one was an 8-shank chip with 8 electrodes (octrodes) on the tip of each shank in zig-zag arrangement. The implants allowed the identification of the CA3 and CA1 pyramidal cell layers and dentate granule cell layers with CSD, the detection of 140-200 Hz ripple oscillations in the LFP. Spike sorting was performed on massively parallel unit recordings (typically 8-15 units per shank). Unit quality was similar to those obtained by tetrode wires, and even the speed of soma-dendritic backpropagation of action potentials could be measured. In vivo analysis of the rat hippocampus was carried on with other probes, e.g. 256-channel, multiplexed devices

(Berenyi et al., 2014). Michigan arrays were employed for the investigation of sleep spindles (Bartho et al., 2014). Four-shank probes equipped with octrodes were implanted into somatosensory thalamus of sleeping rats. Analyzing unit activities in that region, two types of spikes were distinguished: narrow spikes, corresponding to inhibitory reticular thalamic (nRT) neurons, and wide ones, corresponding to excitatory thalamocortical (TC) cells.

The Utah array

The Utah intracortical electrode array (UIEA), an also widely used silicon-based MEA, was developed at the University of Utah (Campbell et al., 1991; Jones et al., 1992). The device has a 4.2 mm × 4.2 mm square-shaped glass/silicon composite base, from which 10 × 10, approximately 1.5 mm long shafts protrude, formed by grinding and wet chemical etching of single-crystal silicon. During the original fabrication methodology, the shafts were coated with a metal, e.g. platinum, followed by polyimide. The latter was removed at the tip of the shafts, so they could function as electrodes. The manufacturing technology has been (and is being) modified and upgraded with slight alternations, such as replacing the polyimide insulation with parylene C (Hsu et al., 2009; Yoo et al., 2012), yet the main structure of the device has not changed considerably. In contrast to a typical Michigan array, the electrodes of the UIEA are arranged in a plane that is perpendicular to the direction of penetration (or slightly angled with varying shaft lengths, (Branner et al., 2001)).

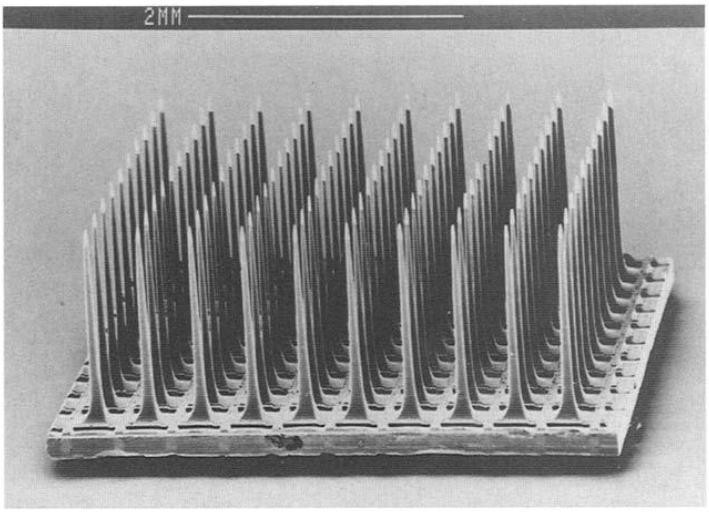

Fig. 1.5. A scanning electron microscopic image of the UIEA. Scale bar at top. (Nordhausen et al., 1996)

The device was brought to market by Blackrock Microsystems (Salt Lake City, UT, USA). It is most commonly utilized for neocortical recordings with high unit activity yield (Nordhausen et al., 1996; Reed et al., 2008). It was employed in numerous studies on laboratory animals, furthermore, it was approved for clinical trials in 2004 by the U.S. Food and Drug Administration (FDA). The majority of BMI systems which are based on extracellular recordings, utilize the UIEA.

Other silicon-based extracellular electrode arrays

Although the Michigan and the Utah MEAs are probably the two most well-known types of silicon-based extracellular neural probes, several other devices have been developed for similar purposes worldwide.

The European VSAMUEL and NeuroProbes projects, which were followed by the currently active NeuroSeeker project, facilitated the progress of silicon-based MEAs including the development of high density arrays and probes with special features. The members of the VSAMUEL consortium developed electrode arrays on planar, comb-like structures, which are similar to the Michigan probes (Hofmann et al., 2002; Norlin et al., 2002). The boron-diffusion controlled wet chemical etching, which determines the three-dimensional structure of the Michigan sensors, was substituted with deep reactive ion etching (DRIE) of silicon-on-insulator (SOI) substrates. In this case, a typically 1-2 μm thick buried oxide layer insulates the device layer (1-100 μm) from the several hundred μm thick bulk of the silicon substrate. The insulating oxide layer can function as an etch-stop for the DRIE, therefore this method allows precise control of device thickness. With the use of direct write laser lithography, different electrode arrangements could be realized by activating specific electrodes out of a standardized electrode array after the micromanufacturing processes were finished (Kindlundh et al., 2004).

The NeuroProbes consortium upgraded the technology comprising SOI substrates to a more cost-effective one, based on the DRIE of single crystal silicon (Neves and Ruther, 2007). A unique and innovative concept is the electronic depth control (EDC)

(Seidl et al., 2011; Torfs et al., 2011). The EDC probes contain very dense electrode arrays, e.g. on a four-shaft device 257 sites per each 8 mm long shaft. They are equipped with CMOS circuitry that includes preamplifiers and switch matrices, which makes the selection of active recording sites after the implantation possible. This allows neuroscientists to thoroughly analyze a large brain area with an electrode array of high spatial density or choose and observe a smaller area of interest without the necessity of relocating the probe. In vivo validation of such probes and the corresponding controlling systems was performed in the Institute of Cognitive Neuroscience and Psychology of the Research centre for Natural Sciences, Hungarian Academy of Sciences (RCNS-HAS), in rat cerebrum (Dombovari et al., 2013). Such devices are commercially available at ATLAS Neuroengineering (Leuven, Belgium).

Also beside the above mentioned European projects, the fabrication of silicon-based neural probes with DRIE is relatively common. This is possible with the utilization of SOI wafers (Cheung et al., 2000). An alternative to the expensive SOI substrates can be the use of thin (e.g. 25, 50 μm) single-crystal wafers, which can be attached to less fragile carrier substrates (e.g. 500 μm thick Si, Pyrex or quartz.) during the critical fabrication steps (Du et al., 2009b).

At the Department of Microtechnology of the Institute for Technical Physics and Materials Science (MFA), a single-shaft silicon probe was fabricated with the management of Dr. Anita Pongrácz, with a process flow employing special wet chemical etching techniques. Two anisotropic etching steps were utilized (Vázsonyi et al., 2003), with which 80 μm thick shafts were created and a third, isotropic one, which smoothened the edges of the shafts, thus made the implantation less invasive. Fig. 1.6. shows scanning electron microscopic (SEM) images of the unique, yacht bow-like sharp tip of the probe. A single column of square-shaped, 30 μm × 30 μm platinum electrodes were located on the probe. It was functionally tested by performing in vivo recordings in rat cortex and hippocampus (Grand et al., 2011).

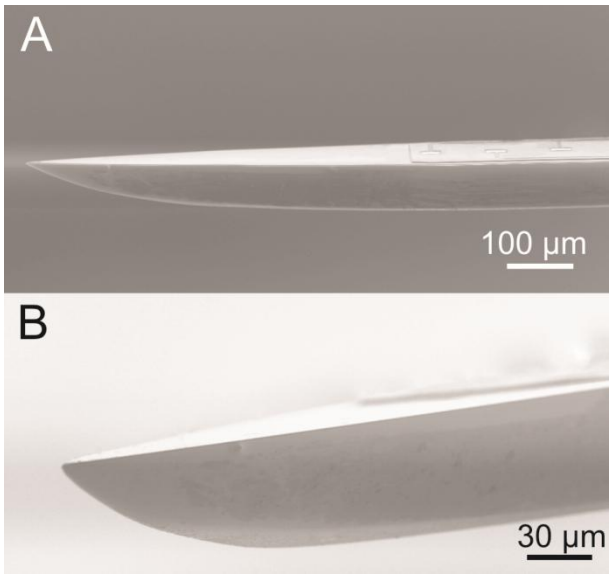

Fig. 1.6. The yacht bow-like sharp tip of the silicon probe fabricated with the utilization of special isotropic and anisotropic wet chemical etching techniques (Grand et al., 2011).

1.3.3. Polymer-based devices

As discussed in section *1.2.4. Biocompatibility*, extracellular probes made of inert and non-toxic materials also trigger the foreign body response of the immune system. The stiffness of silicon, in contrast to the flexibility of the neural tissue, is not advantageous in this aspect. Implants made of flexible materials provide smoother coupling with the soft tissue, they can follow small motions and pulsations of the brain, hence cause less disturbance in their environment (Hassler et al., 2011). Therefore mechanically flexible, polymer-based neural probes are subjects of active research. Several polymers, e.g. SU-8 photoresist (Nemani et al., 2013), Polyimide (PI) (Seymour et al., 2011) and Parylene C (Chang et al., 2007; von Metzen and Stieglitz, 2013) offer excellent biocompatibility. Acrylate and thiol-ene/acrylate shape memory polymers were characterized and fund to be suitable neural implant materials recently (Simon et al., 2013).

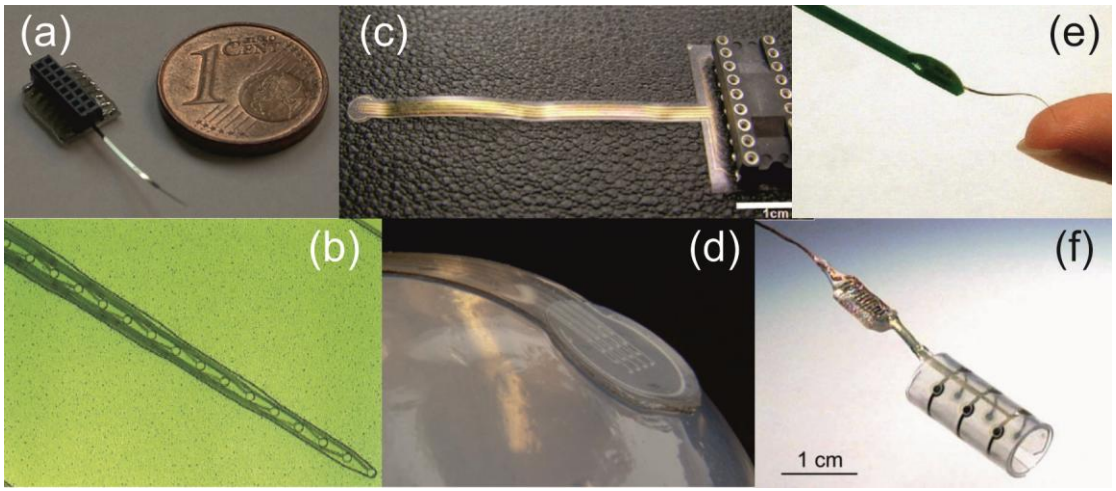

Fig. 1.7. Photographs of various polymer-based microfabricated electrode arrays. (a), (b) Implantable extracellular MEAs with polyimide-platinum-polyimide layer structure (Cheung et al., 2007). (c) (d) ECoG sensors made of parylene C, PDMS and gold. (Ochoa et al., 2013) (e) A polyimide-based probe with 16 electroplated gold electrodes (Chen et al., 2009). (f) Nerve cuff electrode, developed for interfacing with the peripheral nerves (Hassler et al., 2011).

Flexible probes were designed for implantation into peripheral nerves (Boretius et al., 2010; Stieglitz et al., 2002). Cerebral implants have been utilized for resistivity mapping (Béduer et al., 2014) or potential field recordings within the brain (Chen et al., 2009; Cheung, 2007; Kim et al., 2013; Mercanzini et al., 2008; Rousche et al., 2001). Several in vivo measurement situations do not require the implantation of a MEA into the neural tissue, rather contacting its outer surface with sensor or stimulator electrodes is sufficient. This can be achieved by employing microfabricated polymer sheets as well. Nerve cuff electrodes were developed for contacting peripheral nerves (Stieglitz et al., 2000) and various MEAs with larger size for ECoG in rats and higher mammals (Hollenberg et al., 2006; Myllymaa et al., 2009; Ochoa et al., 2013; Rubehn et al., 2009; Yeager et al., 2008).

In the clinics, retinal implants, which are polymer-based MEAs used as stimulators can be used for vision restoration for patients suffering from retinitis pigmentosa (Chader et al., 2009). Such systems have been commercialized by start-up

companies such as Second Sight Medical Products (Lausanne, Switzerland) and Retina Implant AG (Reutlingen, Germany).

1.3.4. Microelectrode arrays with special features

Three-dimensional arrays

It is a challenging idea to merge the two-dimensional shank arrangement of the Utah probe with the possibility of creating an array of electrodes on each shank, likewise to the Michigan and other planar-structured MEAs. Such a construction should result in a three-dimensional grid of electrodes. A solution was provided by assembling multiple comb-like Michigan arrays onto a common platform, parallel to each other. MEAs with various 3D array geometry, e.g. 8 × 16 shanks and 8 electrodes per shank were constructed this way (Bai et al., 2000). This concept was also realized by the NeuroProbes consortium, which resulted in a MEA with 4 × 4 shanks and 5 electrodes per shank, as shown in Fig. 1.8. (Neves and Ruther, 2007; Ruther et al., 2008).

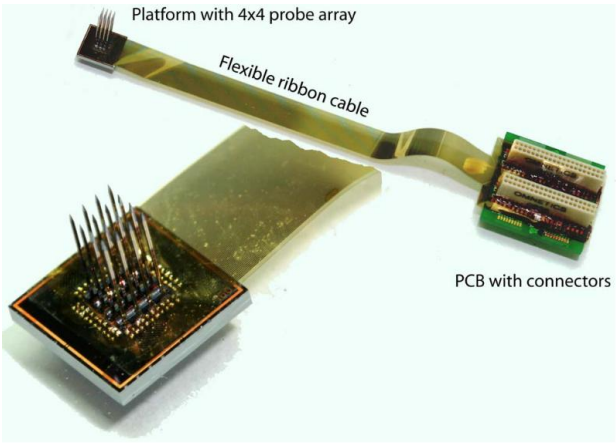

Fig. 1.8. A 4×4 array of 8-mm-long shanks, each of them containing five electrodes. The sensor is connected to the commercial connectors with a flexible ribbon cable. (Neves and Ruther, 2007)

Dual-side probes, 2 × 2 and 3 × 3 shank arrays were microfabricated at the California Institute of Technology (Du et al., 2009a; Du et al., 2009b). The dual-side 2 × 2 arrays were implanted into antennal lobes of locusts. A relatively dense array was formed: the midlines of the 50 μm thick shanks were 150 μm distant from each other to

the two corresponding directions. This construction yielded very rich recordings of spike waveforms in three geometric degrees of freedom. The results obtained by these recordings allowed the authors to gain insight into signal attenuation. For example, they claimed to observe the effect of extracellular current shielding at the substrate–fluid interface, and also approximated a characteristic decay length (33 ± 2 μm) for spikes, which is in consistence with former literature (Segev et al., 2004).

Microfluidic channels

Direct injection of solutions into the brain parenchyma is allowed by bulk flow of the cerebral interstitial fluid (Cserr and Ostrach, 1974). The method based on this phenomenon, i.e. convection-enhanced delivery (CED) makes possible the administration of substance molecules in a more controllable and effective manner than methods of diffusion-controlled release (Bobo et al., 1994; Morrison et al., 1994). Using CED, the blood-brain barrier (BBB) is circumvented, thus a wide spectrum of drugs can be applied, therefore this method has gained attention in the treatment of neurological disorders, such as epilepsy (Gasior et al., 2007), Parkinson's disease (Gill et al., 2003) and brain tumors (Lopez et al., 2006; Nakamura et al., 2011).

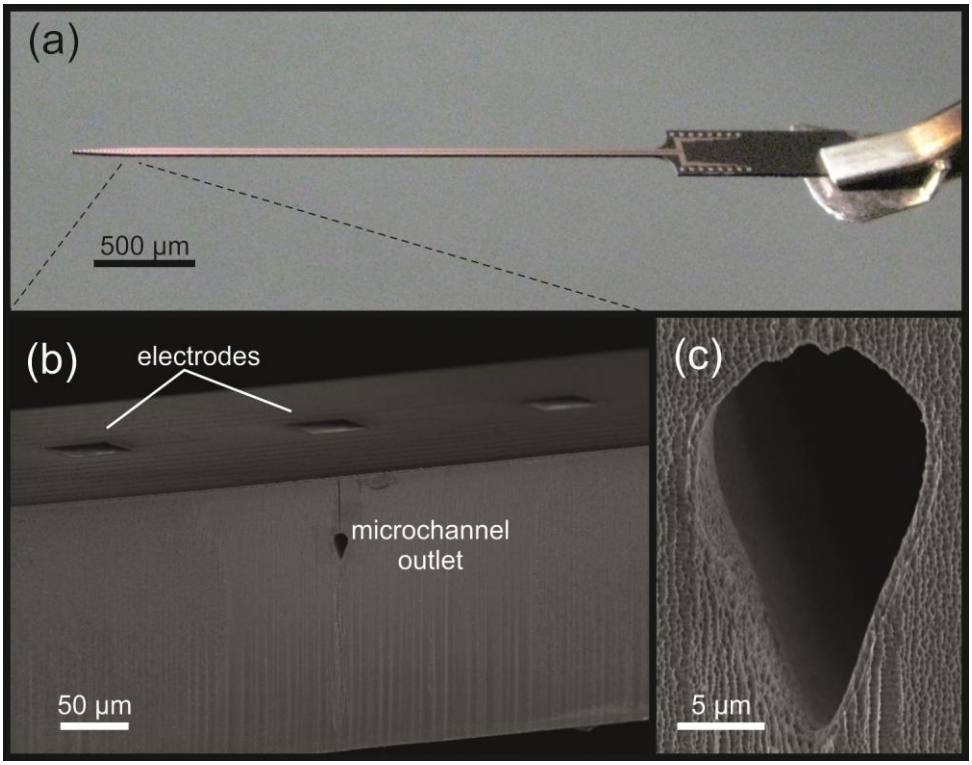

Fig. 1.9. (a) Photograph of a silicon-based neural probe for simultaneous in vivo electrophysiological recordings and drug delivery, microfabricated at the MFA. (b) Scanning electron microscopic image of the shaft section with electrodes on the front side and a microchannel outlet on the sidewall. (c) The profile of the microchannel.

The combination of CED with extracellular neural MEAs might open new possibilities in medical science, such as automated epileptic seizure detection and antiepileptic drug injection (Stein et al., 2000). MEMS technology makes possible the construction of neural implants with integrated fluidic ports and electrodes within the same probe shaft. A pioneering device of this sort was realized with anisotropic wet chemical etching of silicon (Chen et al., 1997) and was followed by several others (Liwei and Pisano, 1999; Papageorgiou et al., 2006; Retterer et al., 2004; Seidl et al., 2010). Fig. 1.9. shows images of a MEA with integrated microfluidic channels, developed at the Department of Microtechnology, MFA (Pongrácz et al., 2013).

Similarly to the silicon-based probes, the polymer-based devices can be equipped with channels, too (Metz et al., 2004).

Waveguides for optogenetics

Optogenetics is a technique based on the utilization of genetic modifications of cells in specific brain areas so that they express proteins that are light-sensitive. It allows neuroscientists to control neural activity with high spatial and temporal resolution. Genes encoding proteins such as channelrhodopsin, halorhodopsin and archaeorodopsin are available for such purposes (Boyden et al., 2005; Gradinaru et al., 2010; Han et al., 2011). To address the need of precise control of illumination with a microfabricated probe, the integration of waveguides onto silicon-based MEAs was solved recently (Wu et al., 2013). A polymer-based device was also constructed, combining electrode arrays with both drug and light delivery capabilities (Rubehn et al., 2011).

High surface area, low impedance microelectrodes

For the reasons presented in section *1.2.3. Roughness factor*, electrodes with large effective surface area, related to their geometric area are preferred. Several porous materials, with huge roughness factor have been developed for this purpose. Early methods for thus minimizing impedance values of neural electrodes were performed by electroplating platinum, e.g. in Kohlrausch's solution (3% $PtCl_2$ and 0.025% PbAc dissolved in 0.025N HCl) (Robinson, 1968). Recent studies involved diverse materials, such as carbon nanotubes (Baranauskas et al., 2011; Green et al., 2008b; Minnikanti et al., 2010) conducting polymers (Green et al., 2008a), polypyrrole/graphene oxide (Deng et al., 2011) and polypyrrole/carbon nanotube composites (Lu et al., 2010).

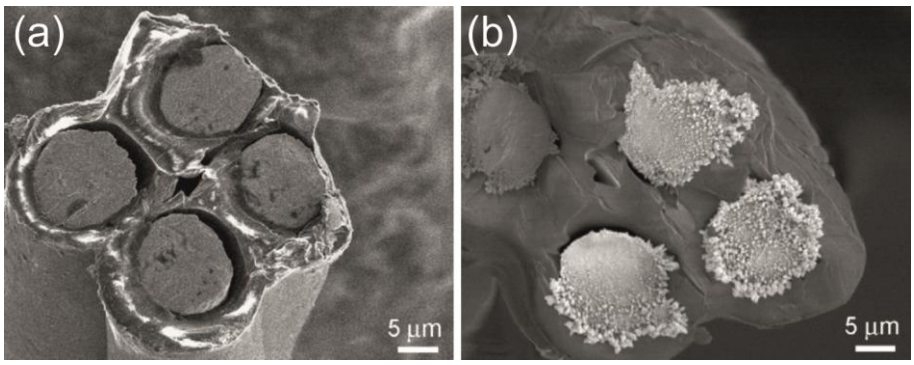

Fig. 1.10. (a) Fine wire tetrode. (b) A tetrode with low-impedance, electrochemically deposited gold electrodes (Ferguson et al., 2009).

Platinized platinum (Pt/Pt), due to its relatively simple deposition procedure and high roughness factor, would be an excellent candidate for large surface area coatings, but its mechanical stability is claimed to be poor (Desai et al., 2010; Heim et al., 2012b). Durability can be enhanced with the application of lead acetate (Robinson, 1968), the thus yielded deposit is usually referred to as Pt black. However, lead can be dissolved from the surface of the deposit, its application in implantable biosensors is hazardous (while electroplated Pt itself is non-toxic (Dymond et al., 1970)). Another approach to solve this problem is platinization with simultaneous ultrasonic agitation (sonicoplating) (Desai et al., 2010; Marrese, 1987). A review on various fabrication methods of porous platinum surfaces has been published (Kloke et al., 2011). These surfaces are applied in other microdevices besides neural electrodes, like pH (Noh et al., 2011) and glucose (Yuan et al., 2005) sensors.

In spite of the broad spectrum of the already published methods, impedance reduction of electrodes of neural MEAs is still an issue under active research.

2. SPECIFIC AIMS

2.1. In vivo recordings with silicon-based probes of extreme shaft length

Previous studies have confirmed that the shaft length of silicon-based probes, manufactured using standard MEMS technology can be increased from the common millimeter scale to a much greater one, up to several centimeters. However, in order to maintain mechanical robustness, it is beneficial if the cross-sectional dimensions of such extremely long probes are also increased (Fekete et al., 2013). We created probes with length of 1.5-7 cm and thickness and width of 200-400 μm, suitable for the penetration of the meninges (including the dura mater) and precise targeting. The scope of our experiments was to investigate the functionality of such devices during acute in vivo experiments, including their suitability for unit activity detection. The electrode arrays were tested within rat neocortex, hippocampus and thalamus.

2.2. Testing in vivo durability of platinized platinum electrodes

As described in section *1.3.4. Microelectrode arrays with special features*, low impedance electrodes can be created with high surface area deposits. A factor that has to be considered is whether these materials are durable enough to withstand direct interfacing with the neural tissue. As their manufacturing cost is still relatively high, electrode arrays are not disposable, they are usually used multiple times for acute in vivo measurements. According to the current catalog of Neuronexus Technologies Inc. (Ann Arbor, MI, USA), electrodes are reusable up to 15 times, if properly cleaned. The surface modification of electrode sites with coatings that repeatedly endure implantation and cleaning is not trivial.

In the chapters corresponding to this study, a Pt/Pt deposition procedure will be presented, created on a silicon-based extracellular MEA. The platinization method was developed with the variation of deposition parameters and applying ultrasonic treatment on the deposited layers afterwards. Parameters such as roughness factor, durability and controllability of the deposition were in our primary attention. The Pt/Pt deposits were tested with multiple acute in vivo experiments for durability and compatibility with acute stereotactic operation procedures.

2.3. Development and characterization of polymer-based microelectrode arrays with protruding sensor sites

As discussed in section *1.3.3. Polymer-based devices*, polymer-based MEAs are frequently used for ECoG. In this case, the electrodes are placed onto the surface of the brain tissue. Furthermore, they are also utilized as intracerebral implants, in which case they function as extracellular MEAs. We aimed to create and test a construction between these two variations: a row of electrodes with protruding sites, which can slightly penetrate into the tissue and record signals from below the surface of the brain.

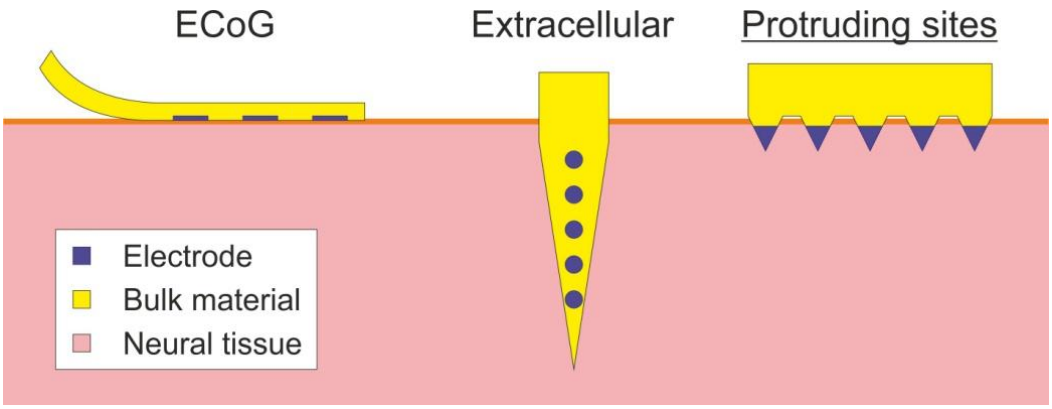

Fig. 2.1. Conceptual illustration of three different electrode array types. Our goal was to develop a novel polymer-based MEA, with protruding sensor sites and perform proof of concept characterization.

2.4. Development and characterization of a multimodal, polymer-based microelectrode system

We intended to create an all-flexible version of the “thumbtack” neural MEA, which had been successfully used for recording field potentials, multiple unit and SUA in behaving and anaesthetized humans (Ulbert et al., 2001). The preceding sensor contains a laminar array of polyimide isolated platinum–iridium electrodes on a single shaft with an outer diameter of 350 μm and length of 3 mm, which can be implanted into the cerebral cortex perpendicularly to the surface of the brain. The shaft perpendicularly protrudes out of the center of a silicone disk, which has a diameter of 8 mm. The disk facilitates the immobility of the shaft during recordings by plying to the brain surface. We aimed to modify this device by equipping the disk with an electrode array as well, thus making possible ECoG recordings in the vicinity of the implanted shaft. At the same time, we substituted the hand-made shaft with a polymer-based MEMS component in order to achieve a more precise and reproducible manner of fabrication and fine mechanical coupling between the probe and the tissue. The ECoG component was designed to be equipped with eight relatively large circular sites (d = 200 μm) for field potential recordings. The extracellular MEAs were designed to contain smaller electrodes (d = 30 μm), which might be suitable for the detection of action potentials of individual neurons within the tissue.

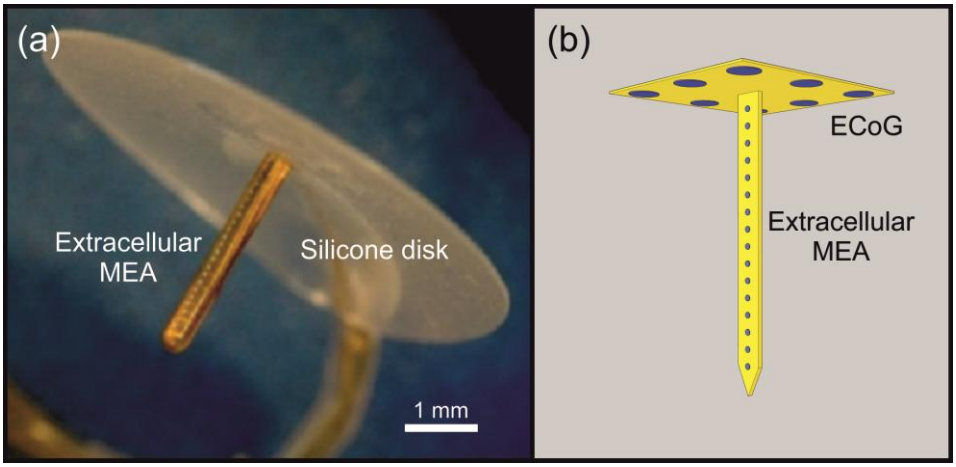

Fig. 2.2. (a) The thumbtack microelectrode array (www.plexon.com) (b) Conceptual illustration of the multimodal, polymer-based microelectrode system

3. METHODS

3.1. Methods related to in vivo recordings with silicon-based probes of extreme shaft length

3.1.1. Design and fabrication

Shaft thicknesses were defined by the substrate silicon wafers (200 μm and 380 μm), while their widths and lengths could be freely varied: 206 μm and 400 μm wide shafts with four different lengths (15 mm, 30 mm, 50 mm and 70 mm) were designed. These parameters have been thoroughly combined.

The electrodes (recording sites) on the probe tip were arranged as tetrodes (4 electrodes per probe in rhombus vertices) and linear arrays (12 or 16 sites in the midline of the front side of the shaft). Considering the latter, center-to-center distances of the 30 μm × 30 μm and 50 μm × 50 μm recording areas were 100 μm and 200 μm, respectively.

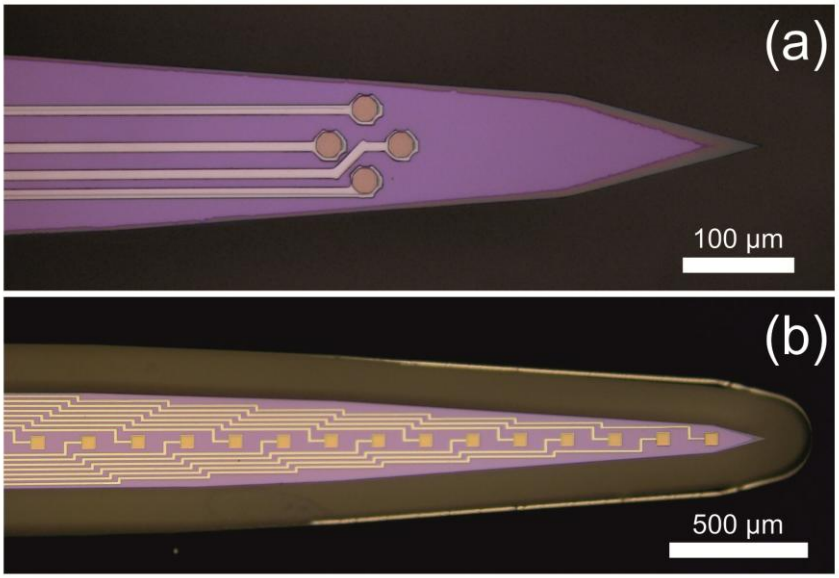

Fig. 3.1. (a) Tetrode and (b) linear electrode array configurations.

Tetrodes were optimized for measuring SUAs, therefore they were more compactly designed: the octagonal sites, 22 μm in diagonal, were located 46 μm distant from each other. Microscopic images, presenting different electrode arrangements are shown in Fig. 3.2.

The fabrication technology of the MEAs is based on a single-side, three mask bulk micromachining process sequence that proceeded in three phases. Schematic cross-sectional view of the probe during the fabrication process is shown in Fig. 3.2. 200 μm and 400 μm thick, double-side polished (100) oriented 4-inch silicon wafers were used for the probe fabrication. The initial phase consisted of thin-film depositions to form the bottom insulating layers, the electrodes and output leads (Fig. 3.2 (a)). In the second phase the upper passivation layers were deposited and the contact holes, bonding pads and contour of the probe body were formed by different etching steps (Fig. 3.2 (b)). In the last phase, DRIE was used to define the probe shafts and bases (Fig.3.2 (c)) followed by the removal of the different masking layers and packaging of the probe.

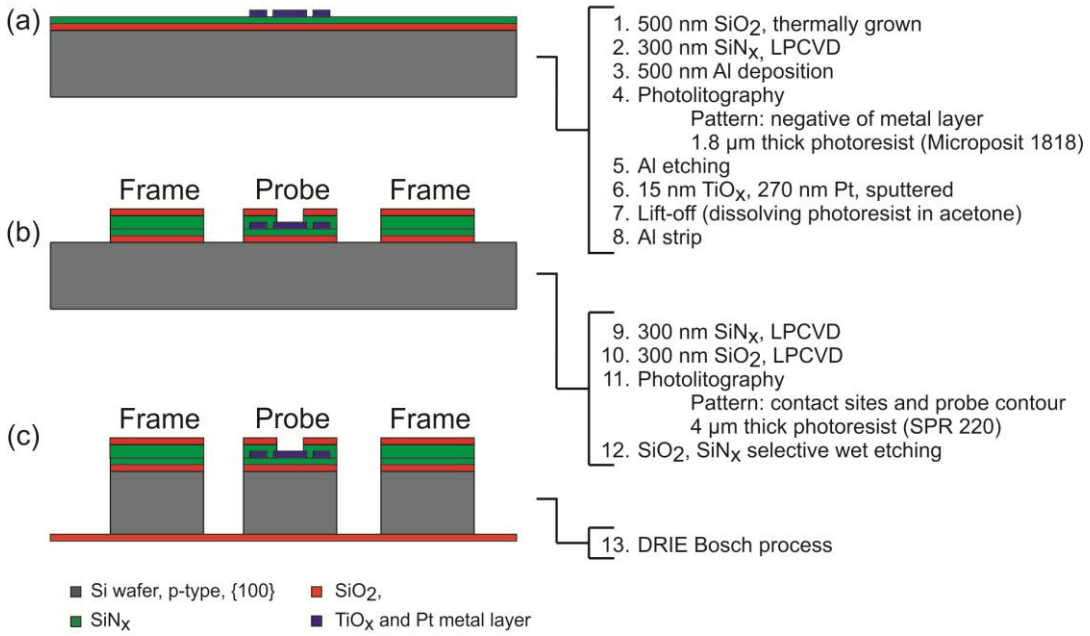

Fig. 3.2. Technological processes. (a) Forming lower insulator and patterned metal layers, (b) upper insulator layers, opened at the sites, (c) silicon dry etching with Bosch process.

Contact formation was carried out as follows. In the first step 500 nm thick SiO_2 layer was thermally grown on both sides of the wafer, followed by a deposition of 300 nm thick low-pressure chemical vacuum deposited (LPCVD) low stress silicon-nitride. The metal layer was then deposited and patterned by lift-off process. The lift-off structure composed of 1.8 μm thick photoresist (Microposit 1818) layer over patterned Al thin film of 500 nm. The metal layer consisted of a 15 nm thick adhesion layer of TiOx and Pt. TiO_x was formed by reactive sputtering of Ti in O_2 (Ar/O_2 ratio was 80:20) atmosphere. In the same vacuum cycle 270 nm thick Pt was sputtered on top of TiO_x. The lift-off was accomplished by dissolving the photoresist pattern in acetone, this process was optimized by using water-cooled substrate holder which diminished the resist distortion during TiO_x/Pt sputtering. Subsequently, the removal of Al patterns in four component etching solution and low pressure chemical vapor deposition of 300 + 300 nm thick SiN_x/SiO_2 insulating layer stack occurred. Contact holes through the insulating layers were created by selective wet etching processes. By these processing steps, Pt lines insulated by SiN_x/SiO_2 layers and formation of Pt contacts have been carried out.

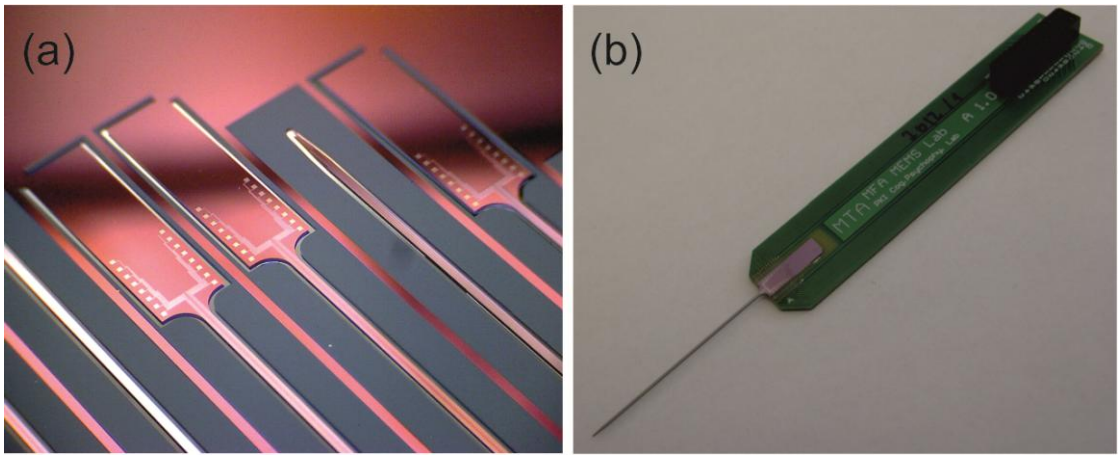

Fig. 3.3. (a) 16-channel multielectrodes on a micromachined silicon wafer. (b) A packaged silicon-based neural electrode on a PCB with shaft length of 3 cm

For probe shaping, a 500 nm thick Al layer was deposited on the front side and patterned by photolithography using 4 μm thick SPR220 photoresist. The body of the probe was defined by Al wet etching. SPR220 photoresist was spun also on the backside of the wafer used as a stopping layer during the subsequent DRIE of silicon. The 3D

micromachining process was performed in an Oxford Plasmalab System 100 chamber using Bosch process.

The probes were flipped out of the wafer and glued onto a printed circuit board (PCB) with a two-component epoxy resin (Araldit AY103/HY956). 50 μm thick Al wires have been employed to establish connection between the bonding pads and the PCB leads using a Kulicke-Soffa ultrasonic wire bonder. For the insulation and protection of the Al wires, the same resin has been used as for the gluing. Fig. 3.3. shows images of the MEAs during and after fabrication.

3.1.2. In vivo measurements

The MEAs were tested on Wistar rats (n=4) in the Institute of Cognitive Neuroscience and Psychology of the RCNS-HAS. Animal care and experiments were performed in compliance with Animal Care Regulations of the Institute of Cognitive Neuroscience and Psychology of the Hungarian Academy of Sciences and order 243/1988 of the Hungarian Government, which is an adaptation of directive 86/609/EGK of the European Committee Council. The animals were initially anesthetized via intraperitoneal injection of a mixture of 37.5 mg/ml ketamine and 5 mg/ml xylazine at 0.3 ml/100 g body weight injection volume. The sleeping state was maintained by intramuscular updates of the same solution (0.3 ml / hour). A drop of paraffin oil was applied in each eye in order to prevent them from drying. The body temperature was maintained at 37 °C with an electric heating pad. The animals were mounted in a stereotactic frame (David Kopf Instruments, Tujunga, CA, USA), restraining their heads. After shaving the scalp, it was incised in order to gain access to the skull. Soft tissues, including the periosteum covering the skull were removed with a scalpel. The bone was cleaned with 1% hyperol solution (Meditop Ltd., Pilisborosjenő, Hungary). The animal preparation procedures described hitherto were the same for other in vivo operations presented in this dissertation.

Crainotomy window was opened from -1 mm to -5 mm anteroposterior (AP), from 1 mm to 4 mm mediolateral (ML) in reference to the bregma. Each probe, attached to the micromanipulator arm of the stereotactic device was slowly inserted into the

cerebrum of an animal without removing or incising the dura mater. Stereotactic coordinates of the targets are presented in table 3.1.

Probe no.	Length [mm]	Width [μm]	Thickness [μm]	Electrode configuration	Implantation target, in reference to the bregma [mm]
1	3	400	380	Tetrode	AP: -3.0, ML: 3.2
2	3	400	200	Linear	AP: -3.0, ML: 3.2
3	3	400	200	Tetrode	AP: -3.0, ML: 3.0
4	5	206	380	Tetrode	AP: -3.0, ML: 3.0
5	7	400	200	Linear	AP: -2.0, ML: 3.5

Table 3.1. The main properties of the MEAs, functionally tested in vivo. Measurements performed with probe no. 3 are presented in details later. Probe no. 3 and 5 were implanted into the same animal, at different stereotactic coordinates.

3.1.3. Signal acquisition and data processing

Signals were recorded using a two-stage amplifier and a data acquisition system with a gain of 1000, 20 kHz sampling rate and 16 bit resolution (LabView, National Instruments Corp., Austin, TX, USA). Edit 4.5 software of Neuroscan (Charlotte, NC, USA) was used for off-line signal visualization, filtering and analysis. The Klusters free software was used for clustering unit activities (Hazan et al., 2006), which is currently (on October 15, 2014) available for free download from the website http://neurosuite.sourceforge.net/

3.2. Methods related to in vivo durability tests of platinized platinum electrodes

3.2.1. Silicon probes

The manufacturing technology and in vivo characterization of the probes employed for these experiments were described in detail by Grand et al. (Grand et al., 2011). In the midline of the single, 7 mm long, 280 µm wide, 80 µm thick probe shaft 24 sputter-deposited platinum electrodes had been manufactured with geometric areas of 30 µm × 30 µm. Fig. 3.4. shows microscopic images of such a device.

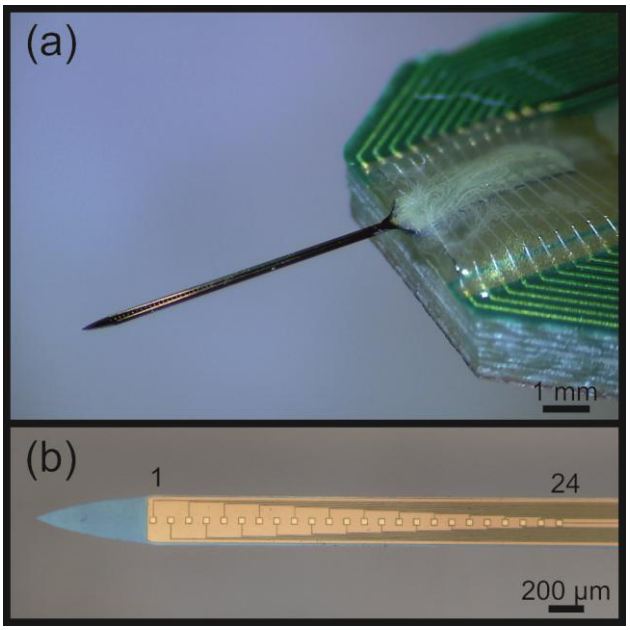

Fig. 3.4. (a) 7 mm long, 280 µm wide, 70 µm thick, 24-channel silicon-based neural probe with a pointed tip on a PCB. (b) The tip of the probe shaft.

3.2.2. Basic electrochemical measurements

Electrochemical impedance spectroscopy

Electrochemical impedance spectroscopy (EIS) measurements were performed in lactated Ringer's solution (Teva Pharmaceutical Industries Ltd., Israel), using an Ag/AgCl reference electrode (Radelkis Ltd., Hungary) and a counter electrode of platinum wire with relatively high surface area. The probe signal was sinusoidal, 25 mV RMS. A Reference 600 instrument (Gamry Instruments, PA, USA) was used as potentiostat and Gamry Framework 6.02 and Echem Analyst 6.02 software were used for experimental control, data collection and analysis. Experiments were performed in a Faraday cage.

Cyclic voltammetry

Cyclic voltammetry (CV) allowed sensitive measurements of the surface area of the electrodes. Curves were obtained with a PAR 283 potentiostat, in a three compartment electrochemical cell. 0.5 M H_2SO_4 solution has been deoxygenated with argon of 99.9995 purity and was used as electrolyte, isolated from air. A hydrogen electrode and a platinum sheet were used as reference and counter electrodes, respectively. The real surface areas of the recording sites were computed from the CV curves (Woods, 1976) and by dividing these data with their projected footprint area (geometric surface area), the roughness factor of the electrodes were determined.

3.2.3. Electrolytic deposition of platinum

In order to obtain electrodes with large effective surface area, Pt/Pt layers were electrochemically deposited using a PAR 283 potentiostat and a solution of 1 g $PtCl_4 \times 2HCl \times 6\ H_2O$ + 2 cm^3 conc. HCl + 200 cm^3 H_2O. Potentiostatic rather than galvanostatic deposition was chosen, since it yields a more controllable process and a more homogenous deposit. Parameters such as potential and time have been set to 100 mV (vs. reversible hydrogen electrode) and 10 minutes, respectively. During preliminary experiments, several other depositing parameters were also tested before

these were chosen. During these tests the roughness factor of the deposits as well as their durability against ultrasonic bath were kept in focus.

The 24-channel MEAs have been modified the following way. Platinum was electrochemically deposited onto every second (2^{nd}, 4^{th}, etc.) channel simultaneously using the above described plating method, while odd-numbered (1^{st}, 3^{rd}, etc.) channels were only immersed in the plating solution and no voltage was applied on them (these sites were used as controls in this study). Odd-numbered and even-numbered channels will be referred to as thin-film Pt and Pt/Pt electrodes, respectively.

The Pt/Pt structures were analyzed with optical microscopy and SEM. Focused ion beam (FIB) method with Ga ions accelerated to 30 keV was used to cut the Pt/Pt deposits in order to have cross-sectional view of them. SEM images of thin-film Pt and Pt/Pt electrodes are shown in Fig. 3.5. These images reveal that the electrochemically deposited Pt layer is thicker at the edges of the electrodes.

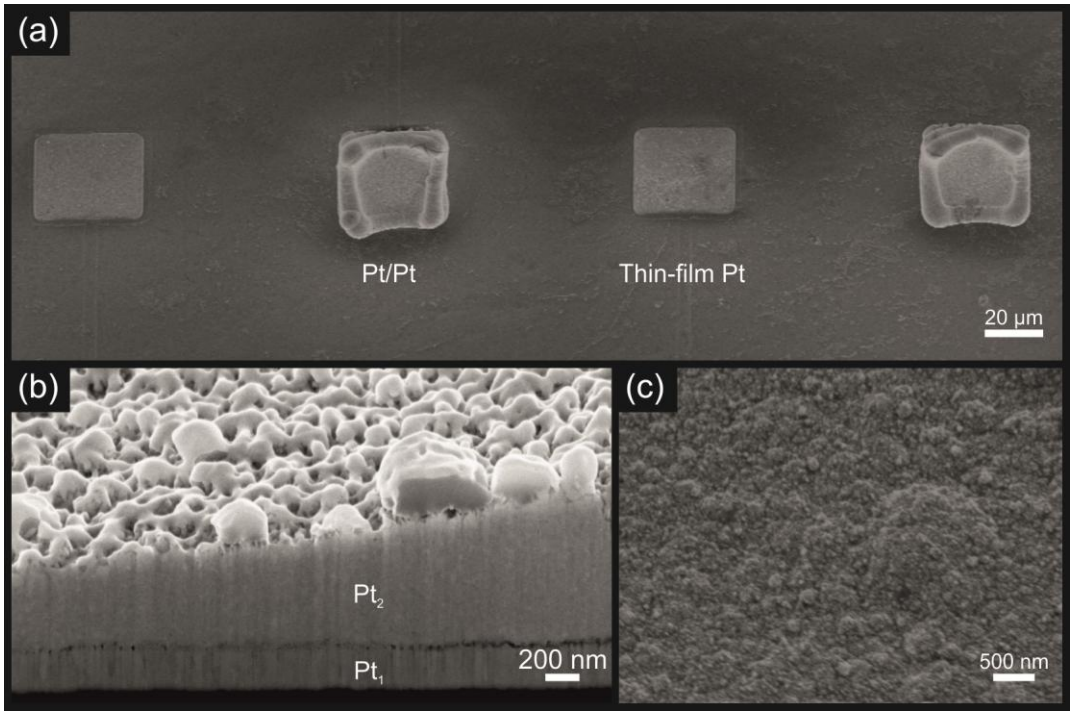

Fig. 3.5. (a) Scanning electron microscopic images of four neighboring electrode sites on the MEA, two of them coated with Pt/Pt. (b) A cross-sectional view of the Pt/Pt layer, sectioned with Focused Ion Beam (FIB). Pt_1 is the original thin-film layer, Pt_2 is electrochemically deposited. (c) The surface of a platinum deposit (Pt/Pt electrode).

3.2.4. In vivo measurements

The durability of the electrodes was tested via subjecting three of such prepared MEAs to in vivo measurement sessions, performed in rat cerebrum. Probes were implanted and used for extracellular recording twelve times. The course of in vivo experiments is summarized in Table 3.2. Before every third implantation, a cleaning process was performed in 0.5 M H_2SO_4, with the application of ±1.5 V DC voltage, for 3 seconds, 5 times, in reference to a Pt electrode with much larger surface area. The main purpose of this process was to detach the adsorbed particles from the surface of the electrodes.

Procedures performed on the probes	
Cleaning in H_2SO_4	
In vivo recordings: **#1,2,3**	In vivo recordings: #1,2,3
Storage in H_2O for days	Rinsing in H_2O
Cleaning in H_2SO_4	In vivo implantation #1
In vivo recordings: **#4,5,6**	In vivo recording #1
Storage in H_2O for days	Removal, rinsing, storage in H_2O for 30 minutes
Cleaning in H_2SO_4	In vivo implantation #2
In vivo recordings : **#7,8,9**	In vivo recording #2
Storage in H_2O for days	Removal, rinsing, storage in H_2O for 30 minutes
Cleaning in H_2SO_4	In vivo implantation #3
In vivo recordings : **#10,11,12**	In vivo recording #3
Storage in H_2O for days	Removal, rinsing in H_2O
Cleaning in H_2SO_4	

Table 3.2. Protocol of in vivo testing. Probes were subjected to 12 recording sessions. Cleaning procedures were performed before every third implantation.

Intracerebral measurements were performed as follows. 220-390 g Wistar rats (a total of 12) have been prepared for surgery as described previously, in the first paragraph of section *3.1.2. In vivo measurements.* Craniotomy was performed from -4.0 mm to -1.0 mm AP, from 1.0 mm to 4.0 mm ML in reference to the bregma. The dura mater was left intact. In order to reduce the number of animals used, a probe was implanted three times into a rat, at different locations. Implantations were targeted at AP/ML stereotactic locations of -3.6 mm/2 mm; -3.6 mm/3.6 mm; -3 mm/2.8 mm, which allowed us to reach the hippocampus and the thalamus with 4-5 mm deep implantations in reference to the surface of the brain for the recordings (Paxinos and Watson, 2009). In order to avoid large blood vessels, a maximal deviation of 0.15 mm from original target locations was in some cases necessary. Recordings were performed for about one hour, with the recording and signal processing system described previously in section *3.1.3. Signal acquisition and data processing*. After 12 implantations, thermal noise measurements were carried out, in vitro, in lactated Ringer's solution, with the same setup.

Electrode impedance values were measured before and after recordings at 1 kHz, using a BAK model (EASI-1, BAK Electronics, FL, USA), with sine wave current of less than 500 nA. The reference electrode for both in vivo recordings and impedance measurements was a pointed platinum wire located beneath the skin posterior to the scalp.

3.3. Methods related to the development and characterization of polymer-based microelectrode arrays with protruding sensor sites

3.3.1. Design and fabrication

The electrodes were arranged linearly in a single, 1.15 mm long row. Arrow-shaped recording sites were designed on the edges of microscopic spikes. The sites can be approximated with isosceles triangles with base lengths of 22 μm and heights of 20 μm. The geometric surface area of an electrode is approximately 220 μm^2. The

“spiky” geometry was chosen for the reason specified by our aims: to allow the electrodes to slightly penetrate into the cortex during in vivo experiments.

The microfabricated component of the device was manufactured on an oxidized Si substrate wafer. It consists of a bottom PI layer, a middle metal (TiO_x + Pt) layer and a top SU-8 layer. We have chosen this polymer composition in order to exploit the preferential features of the materials: PI sufficiently adheres to the substrate, yet it can be peeled off easily without the necessity of a sacrificial layer, while SU-8 can be conveniently patterned by photolithography, which makes it more suitable for forming the top layer. Two photolithographic masks with resolution of 1 μm defined the layout.

Fig. 3.6. shows a 3D schematic of the fabrication process. First, a 4-inch double-side polished, (100) oriented Si wafer was cleaned and a 1 μm thick thermal silicon-dioxide layer was grown on its sides. Then the wafer was spin-coated by a 7 μm thick P84 polyimide layer (step a). The conductive layer, which consists of 30 and 270 nm thick TiO_x and Pt layers, respectively, was deposited on the PI layer and patterned by lift-off technique. For this, a 500 nm thick sacrificial Al layer was deposited before the TiO_x/Pt layers by electron beam evaporation and patterned by lithography using a 1.8 μm-thick Microposit 1818 photoresist layer and wet chemical etching. The TiO_x was then deposited by reactive sputtering, the purpose of this thin layer was to provide sufficient adhesion. Following this, the Pt layer was sputtered onto the front side as well, and the sacrificial Al layer was etched away, yielding the patterned conductive layer (step b). Its different regions would be functioning as electrodes, bonding pads and wiring between them. The process flow was carried on by spin-coating a 20 μm thick SU-8 upper insulator layer onto the front side, which was patterned with photolithography (step c). Openings made on the SU-8 layer in this step defined the electrodes, bonding pads and the contour lines of the device. The contour line pattern was transferred onto the PI layer by reactive ion etching (RIE) (step d). In this step, the SU-8 was thinned on the top as well, while Pt functioned as a masking layer at the electrodes and bonding pads. Hence, the bottom PI layer was preserved below these structures, providing sufficient mechanical stability for them. Finally, the whole wafer was submerged into distilled water and the thus microfabricated device component could be peeled off from the oxidized Si substrate (step e).

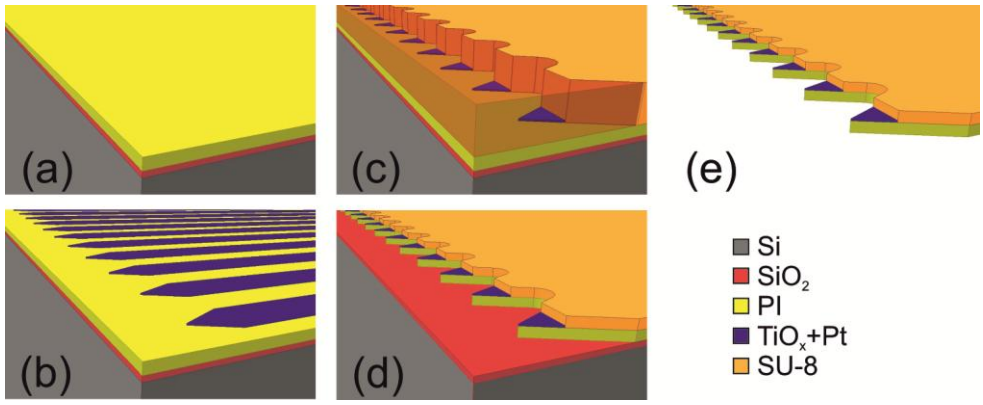

Fig. 3.6. Schematics of the fabrication process steps. Two photolithographic masks are utilized, the first in step (b) for pattering the metal layer and the second in step (c), for patterning the top SU-8 layer.

The electrode array was electrically and mechanically connected to a custom-made, 1 mm thick, 10 mm wide, 127 mm long printed circuit board (PCB), provided by Auter Ltd. (Budapest, Hungary). Metal pins were soldered to through-hole vias of the PCB and to the bonding pads at the base of the microfabricated component. The PCB was equipped with a Preci-Dip electrical connector for interfacing with the preamplifier.

3.3.2. In vitro and in vivo characterization

Characterization of the electrode impedances was performed in vitro, in physiological saline, by EIS with the apparatus which had been used for the characterization of high surface area deposits (see section *3.2.2. Basic electrochemical measurements*).

For in vivo testing, rats were anesthetized and prepared for stereotactic operation as described previously, in the first paragraph of section *3.1.2. In vivo measurements.* Craniotomy was performed from -1.0 mm to -4.0 mm AP, from 1.0 mm to 5.0 mm ML in reference to the bregma. The MEAs were mounted on a micromanipulator. The microdevice was adjusted into a transverse plane, its longitudinal axis was perpendicular to the surface of the neocortex. The dura mater was removed at the target location. The spiky tips, containing the electrodes were submerged into the tissue and brain signals were recorded with the system described previously in section *3.1.3.*

Signal acquisition and data processing. This procedure was performed at several locations in the craniotomy window. Fig. 3.7. demonstrates the placement of the MEA during a recording.

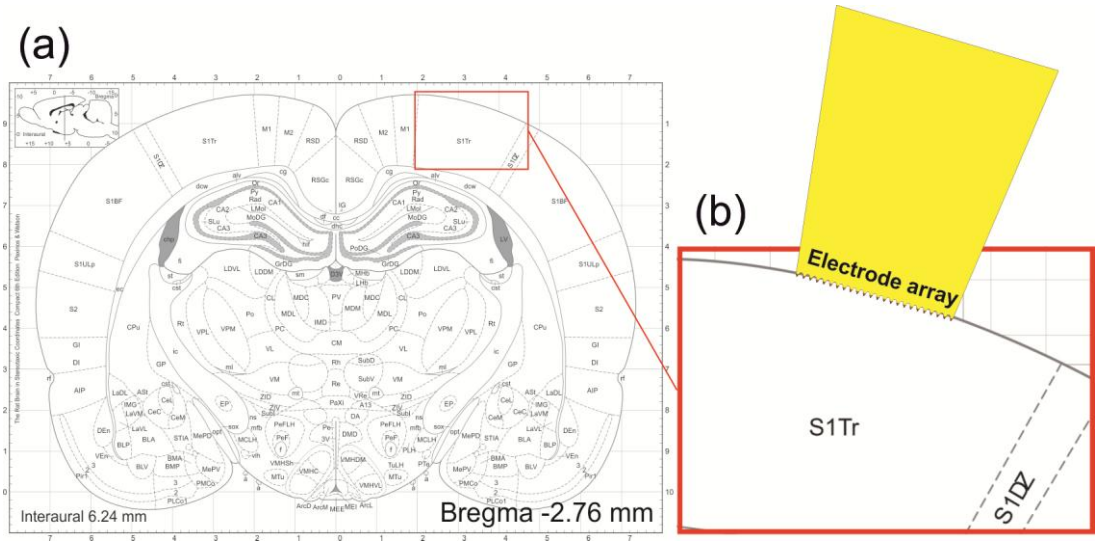

Fig. 3.7. (a) Coronal section of the rat brain -2.76 mm posterior to the bregma. Illustration is based on Figure 56 of (Paxinos and Watson, 2009). (b) Zoomed view of a somatosensory area and a proportional representation of the MEA on the cortex.

3.4. Methods related to the development and characterization of a multimodal, polymer-based microelectrode system

3.4.1. Fabrication

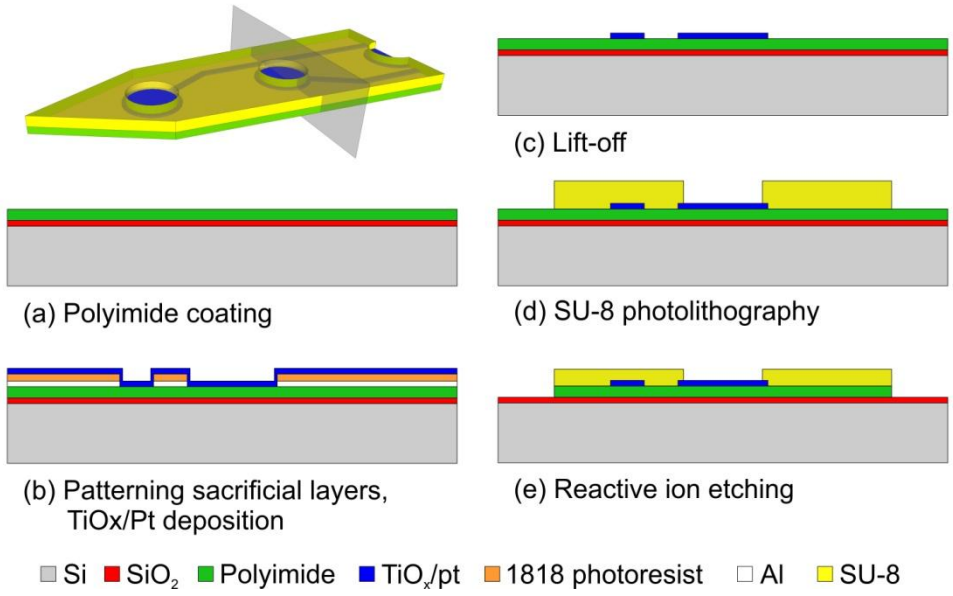

Fig. 3.8. Steps of microfabrication. The processes yield a PI (bottom insulator) – TiO_x/Pt (conductive) – SU-8 (top insulator) layer structure.

In order to realize the device concept presented in section *2.4. Development and characterization of a multimodal, polymer-based microelectrode system*, the same rapid and cost-effective process flow was utilized, which had been successfully employed previously for the construction of the electrode array with protruding sites. The processes resulted in a PI (bottom insulator) – TiO_x/Pt (conductive) – SU-8 (top insulator) layer structure. Photographs of the two microfabricated components of the device are shown in Fig. 3.9.

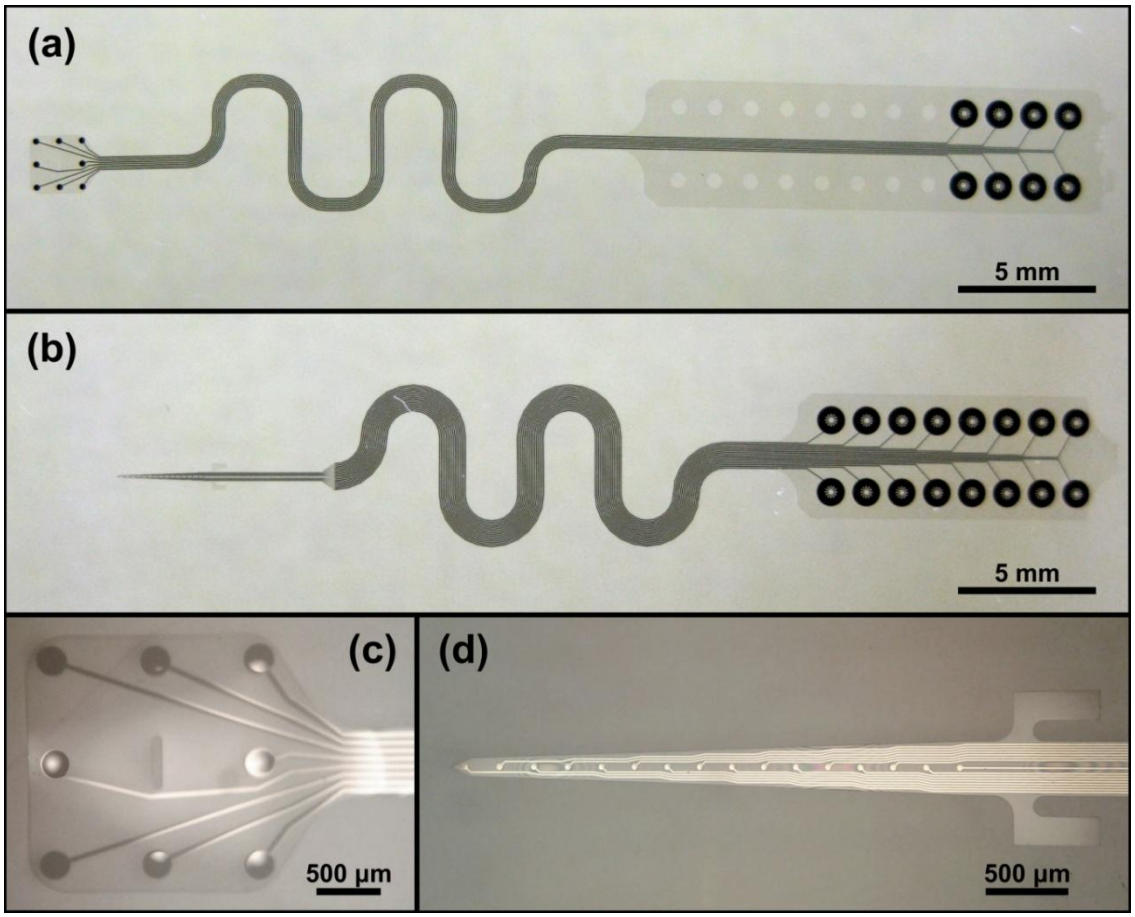

Fig. 3.9. The microfabricated components. The ECoG part, shown in (a) and (c) is provided with a hole in the middle of the array, into which the extracellular MEA (shown in (b) and (d)) can be inserted. Above the extracellular electrodes, two handles protrude from the sides of the shank.

3.4.2. Assembly and packaging

In order to assemble the device, we clamped the ECoG component between four pieces of 1 mm thick glass slides. Two slides held in place the bonding pads, the leads and a segment of the sensor region, containing three ECoG electrodes, located closest to the connector. The other two slides clamped the segment of the sensor region containing three electrodes farthest from the connector. The part of the sensor region containing the two middle ECoG sites and the hole was not covered by any of the glass slides. The shank of the extracellular electrodes was inserted into the hole with a pair of tweezers. The shank was equipped with two handles, located on the sides of the shank, 300 µm

above the electrode array. The insertion was complete when these handles mechanically contacted the ECoG component. Following this, the two components were fixed together with a drop of epoxy resin, at their backsides, avoiding the electrodes. In the final step, the devices were equipped with connectors (Preci-Dip, Delémont, Switzerland). Their pins were stitched through holes at the bonding pads of the microfabricated components and bonded onto exposed platinum sites, which had been formed in the vicinity of the holes with the same methodology as the electrodes.

3.4.3. Electrode impedance measurement and reduction methods

Characterization of electrode impedances was performed by electrochemical impedance spectroscopy (EIS) in physiological saline. Impedance reduction was only performed on the sites of the implantable (extracellular) electrode array. The electrolytic deposition procedure was identical to the one utilized for the Pt/Pt durability study, detailed in section *3.2.3. Electrolytic deposition of platinum.*

3.4.4. In vivo characterization

We performed electrophysiological recordings in the cerebrum of rats in order to test the functionality of the MEAs. A total of 5 Wistar rats, weighing 270-400 g have been anesthetized and prepared for stereotactic operation as described previously, in the first paragraph of section *3.1.2. In vivo measurements.* Craniotomy was performed from -1.0 mm to -6.0 mm AP, from 2.0 mm to 7.0 mm ML in reference to the bregma. The implantation of the extracellular MEAs were targeted at the stereotactic location of -3.36 mm AP, 5.5 mm ML, perpendicularly to the brain surface, which allowed us to perform laminar measurements in the barrel cortex and reach into the hippocampus (Paxinos and Watson, 2009), as shown in Fig. 3.10. The dura mater was incised above the target location in order to achieve a smooth implantation. The probes were handled and implanted with a forceps, attached to a moving arm of the stereotactic apparatus. The signal recordings were carried out using a 32-channel Intan RDH-2000 amplifier system (Intan Technologies LLC., Los Angeles, CA, USA) connected to a computer via USB 2.0, sampling with a frequency of 20 kHz.

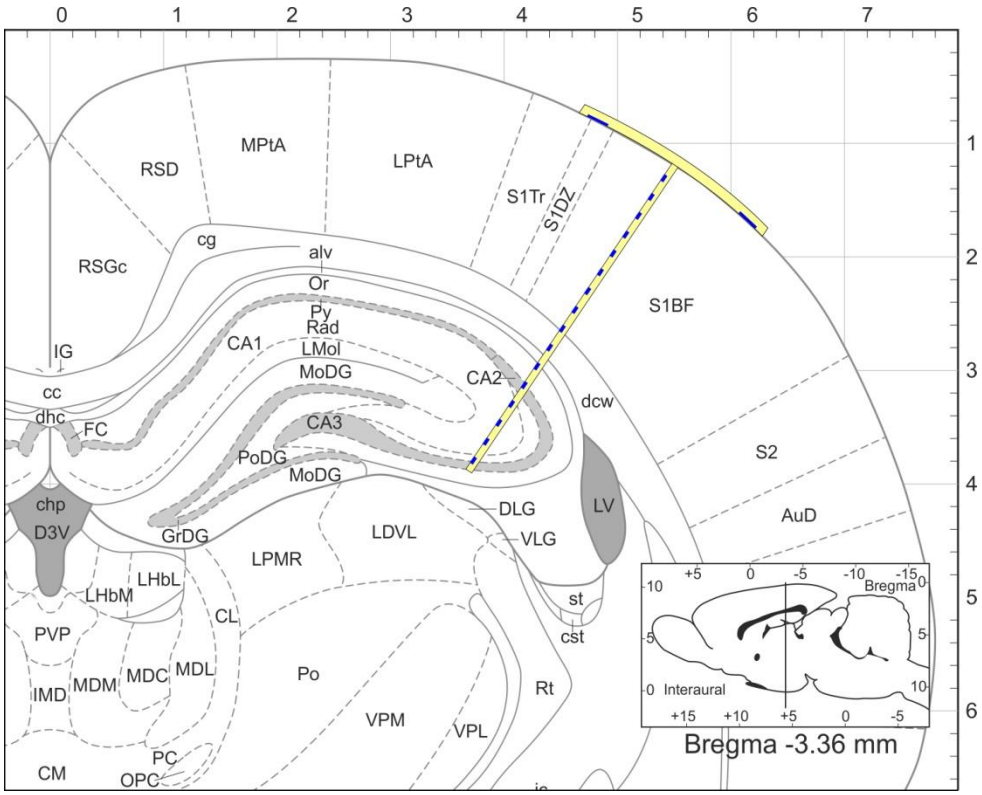

Fig. 3.10. Implantation plan for in vivo functional characterization of the MEA. Principal somatosensory areas of the rat neocortex and the hippocampus underneath them were targeted. Illustration based on Figure 61. of (Paxinos and Watson, 2009).

After the recording sessions, the probes were removed from the brain and cleaned. We soaked them in an aqueous solution of 10 mg/ml Terg-A-Zyme (by Alconox Inc., White Plains, NY, USA) for 10-15 minutes. 3-4 times during this period and after it we removed the probes from the solution to rinse with distilled water.

Signals obtained by the laminar (extracellular) MEA were subjected to CSD analysis. CSD was calculated with the MATLAB 2014b software (MathWorks Inc., Natick, MA, USA), with the utilization of the CSDplotter toolbox. For a clearer visualization, the CSD of 10 periods were averaged and plotted. The periods were aligned to each other based on the start of the upstates, i.e. the initiation of multiunit activity.

4. RESULTS AND DISCUSSION

4.1. Results and discussion concerning in vivo recordings with silicon-based probes of extreme shaft length

The probes tolerated the implantation through the intact dura mater without bending or breaking. Good quality single and multiple unit activities were recorded from the cortex and thalamus. Fig. 4.1. shows representative unit activity signals (recorded with probe no. 3.) A total of 35 cells were recorded from the cortical and thalamic areas (cortex, n = 13; thalamus, n = 22) and two or three clusters could be separated in general from the recorded unit activity at one recording position. The mean peak-to-peak amplitude of the averaged action potentials of the cells was 128.9 ± 54.3 μV (range: 43.6 – 244.5 μV) and the number of spikes in a sorted unit cluster was 1452 ± 1829 on average (range: 47-9433). Clusters clearly separated on one plane of the feature space (first three principal components) were selected as putative neurons. Clear refractory periods (1-2 ms) visible on the autocorrelograms of the separated clusters were signs of appropriate spike sorting. In most cases the action potential waveforms of the same unit could be detected on several of the four channels simultaneously (Fig. 4.1. (c)). The distribution of the channels were calculated where the largest negative peak of the spikes of the recorded neurons was detected, but no significant differences between the channels were found (Channel 1: 8 units, 22.9 %; Channel 2: 12 units, 34.3 %, Channel 3: 5 units, 14.3 %; Channel 4: 10 units, 28.5 %). These results indicate that the spatial position of the tetrode contacts had no effect on the action potential recording capabilities of the probe.

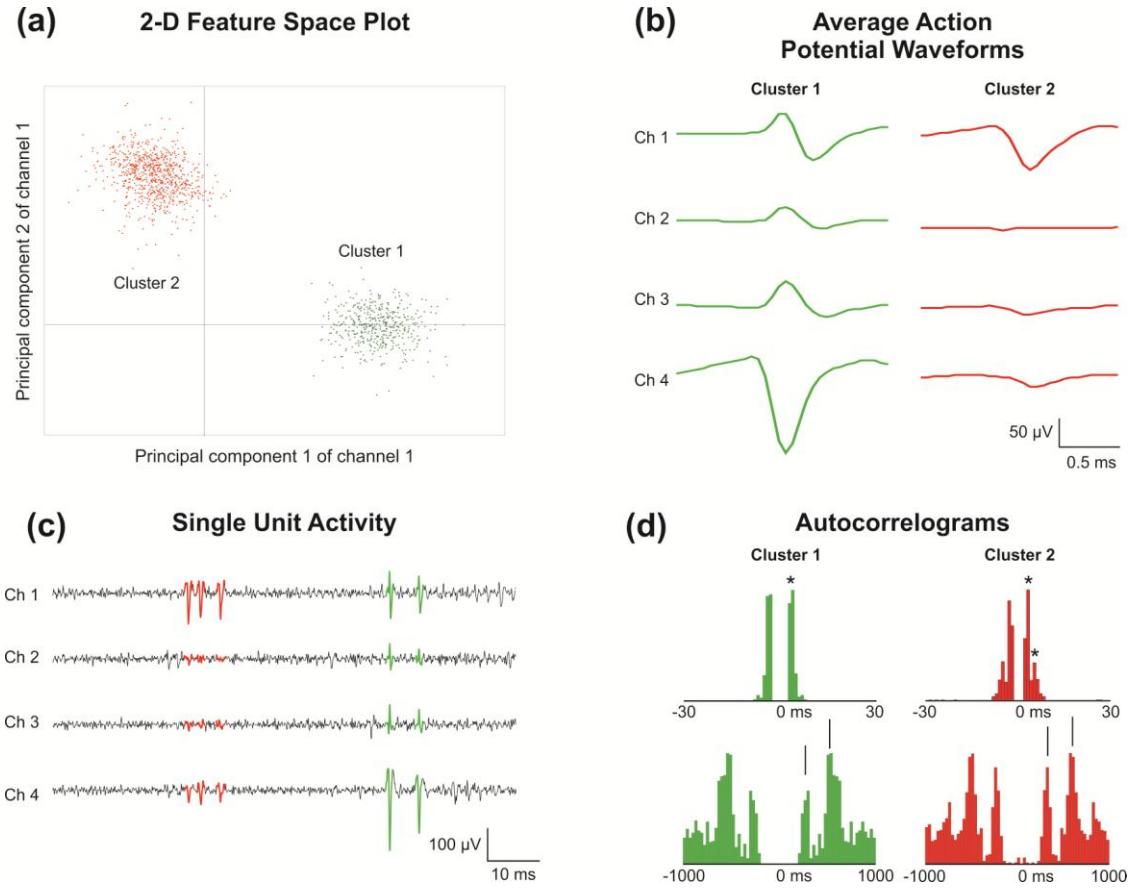

Fig. 4.1. The result of spike sorting performed on a tetrode recording from the thalamus (a) The 2-D feature space plot with two well separable single unit clusters (red and green cloud of dots). (b) Average action potential waveforms of the two separated unit clusters on different recording channels. Cluster 1 (green unit) has clearly visible action potentials on all four channels with different peak amplitudes. (c) A 100 ms segment of a bandpass filtered (500-5000 Hz) unit activity recording with sample spikes of the two isolated clusters. The green unit was a bursting TC neuron with two action potentials per burst on average, whereas the other thalamic cell (red unit) fired mostly three spikes during one burst. (d) Autocorrelograms of the red and green clusters on two different timescales. The upper pictures show clear refractory periods (no spiking between 0-1 ms) in case of both of the clusters and several peaks (asterisks) between 2 and 5 ms that refer to the bursting nature of the TC neurons during anesthesia. The peaks (arrows) on the bottom autocorrelograms around 250 and 500 ms implies a strong correlation between the unit activity and the ongoing delta (2-4 Hz) and slow (0.5-2 Hz) oscillations which are the major brain rhythms in the thalamus during sleep and anesthesia.

The majority of the neurons were excitatory pyramidal cells (n = 13) and TC cells (n = 21) with wide spikes (half-amplitude duration: 319 ± 69.4 μs, range: 208.5 - 452 μs), except for one neuron with narrow action potentials (164.5 μs) probably recorded from the nucleus reticularis thalami (nRt). The nRt consists of GABAergic inhibitory cells that send their axon collaterals to several „first order" and „higher order" thalamic nuclei. Representative spike waveforms of neurons recorded from different thalamic nuclei and cortical layers are shown in Fig. 4.2. Bursting neurons with 2-6 spikes in one burst event are typical to the somatosensory nuclei (e.g. ventral posterolateral nucleus – (VPL), ventral posteromedial nucleus (VPM), Fig 4.2. (a)-(b)) of the thalamus during anesthesia. The nRt neuron fired bursts containing 6-10 action potentials (Fig 4.2. (c)), while the recorded cortical cells discharged mostly single spikes, spike doublets or triplets (Fig. 4.2. (d)-(f)). During deep sleep and anesthesia brain rhythms with lower frequencies (slow oscillation, 0.5-2 Hz; delta, 2-4 Hz can be recorded from the thalamus and cortex and the neuron discharges are time locked to the active phases of these oscillations (Fig. 4.2. (d)) (Steriade, 2003).

In spite of the extreme length of the devices, the relatively thick shanks made the implantation through the intact dura mater without noticeable bending possible. The effect of probe thickness is not understood on the performance of acutely, let alone chronically implanted probes. Presumably, the thinner the probe is, the less disturbance it should cause e.g. in blood vessels (Kozai et al., 2010), and therefore more capable it should be of unit activity recordings. Recently, measurements performed by Scott et. al. gave a surprising result, showing that there was no difference between spike recording performance of probes with different width (40 μm vs. 85 μm) (Scott et al., 2012).

Our experiments yielded qualitative information about the spike detection capabilities of arrays with extreme shaft dimensions in rat cortex, hippocampus and thalamus. Although the access of these anatomical structures would not necessitate such long (15 - 70 mm) probe shafts, these regions are suitable targets in order to validate the probes, thus bringing the possibilities lying in the utilization of silicon-based MEAs one step further. The results underscore that Si-based MEMS technology allows rapid and precise manufacturing of MEAs, which might prove to be applicable for a very wide range of neurophysiological measurements, including deep-brain extracellular recordings in higher mammals.

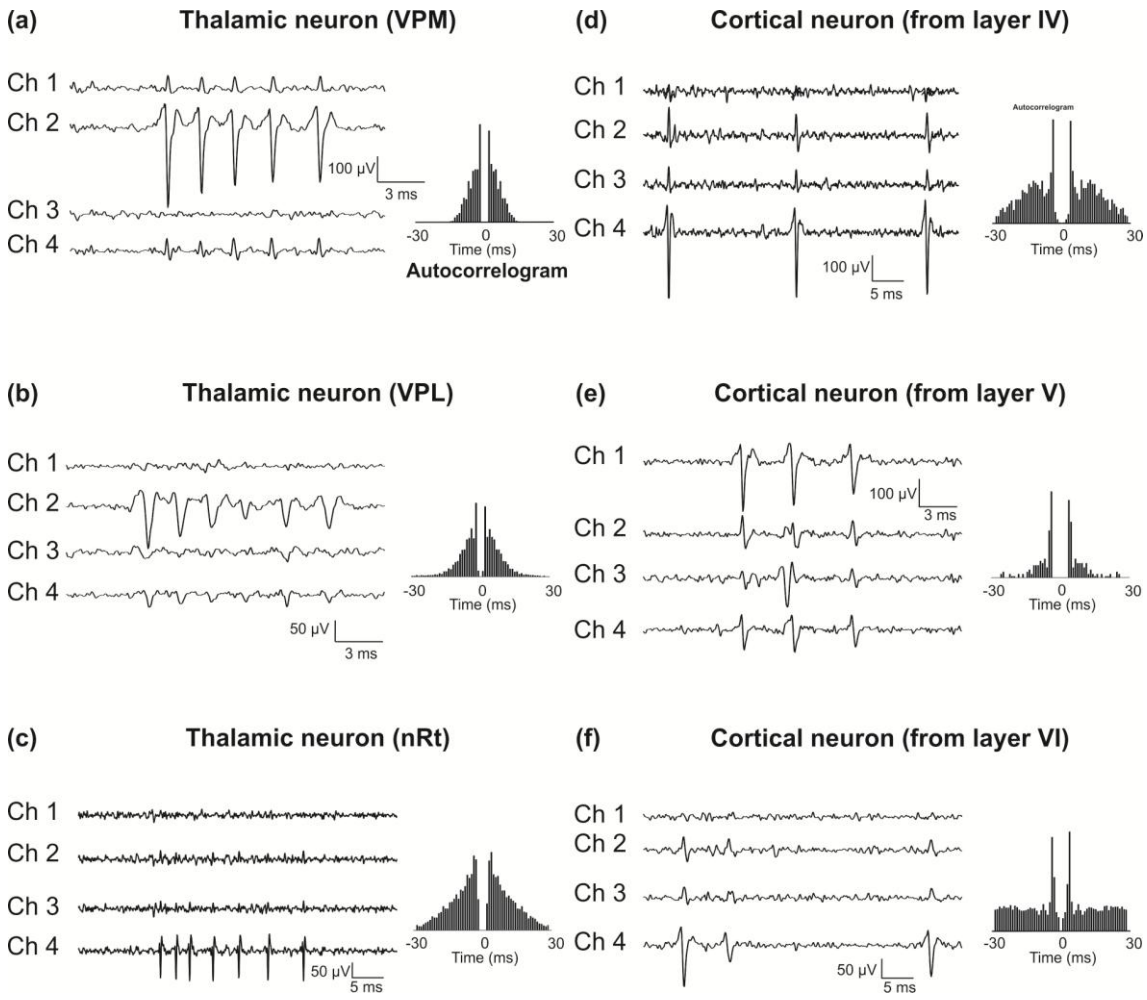

Fig. 4.2. Representative samples of the spike waveforms (left) and corresponding autocorrelograms (right) recorded with the silicon tetrode from the thalamus and cortex during anesthesia. Peak-to-peak action potential amplitudes ranged from a few dozen microvolts up to 400 microvolts and the spikes of the same unit were in most cases clearly visible on more than one channel. Most of the sorted neurons were bursting cells with 2-6 spikes per burst.

4.2. Results and discussion concerning in vivo durability tests of platinized platinum electrodes

4.2.1. Results of in vitro measurements

CV curves of an original, thin-film Pt site and a platinized Pt site are presented in Fig. 4.3. Data obtained from CV indicate that the electrochemical cell configuration and plating parameters allowed formation of platinum deposits with average roughness factor of 950. The electrolytic Pt deposition reduced the impedance of the electrodes (in physiological saline) with several orders of magnitude in the frequency range of 0.1 Hz - 1 kHz, as shown in Fig. 4.4.

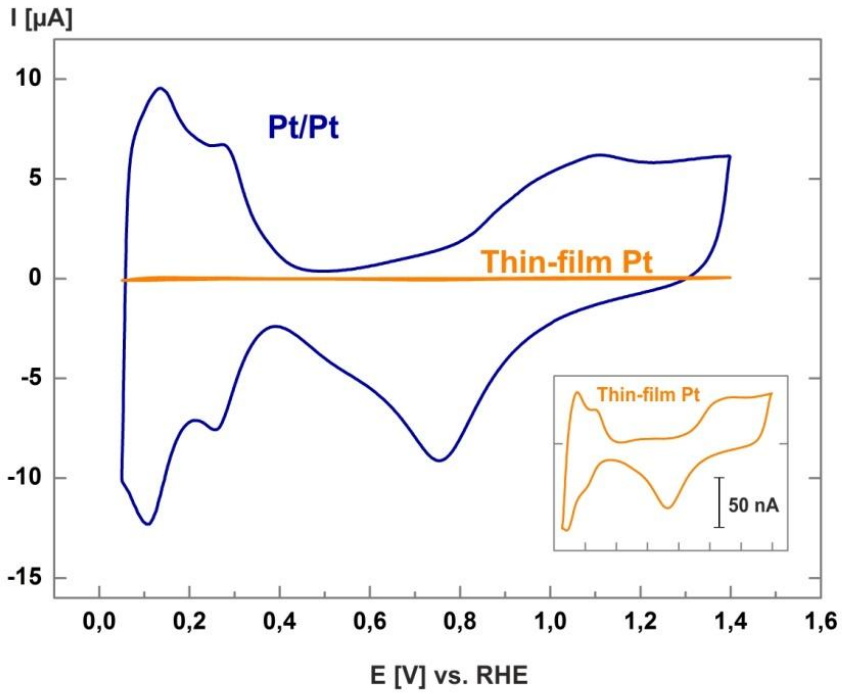

Fig. 4.3. Cyclic voltammetric curves of thin-film Pt and a Pt/Pt electrodes of a probe. Potentials are given on the reversible hydrogen electrode (RHE) scale.

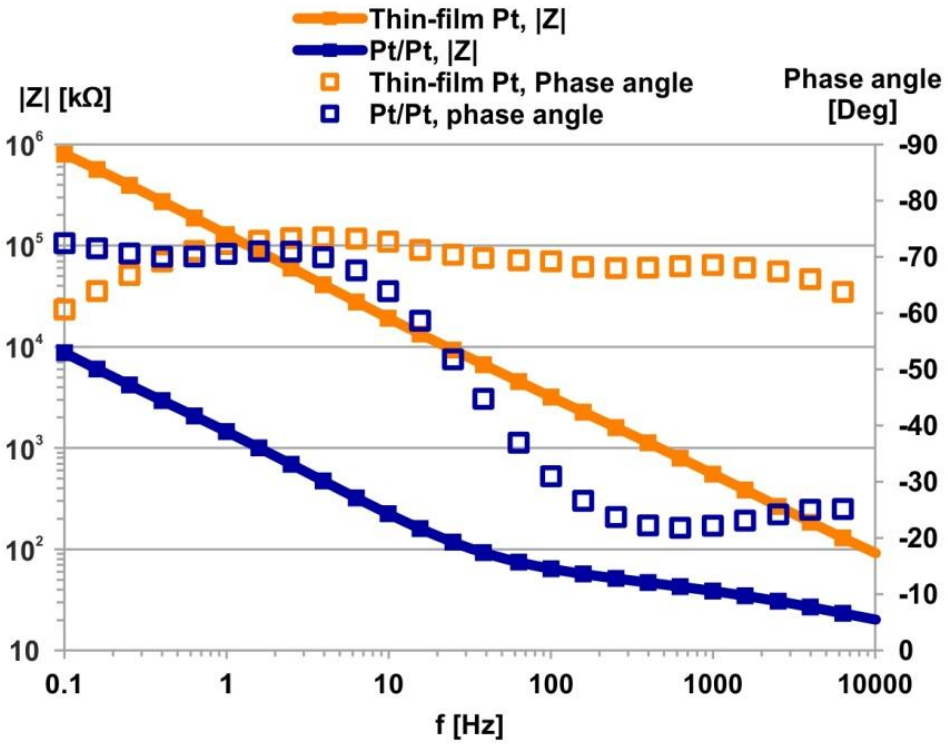

Fig. 4.4. Average EIS spectra of original thin-film Pt and Pt/Pt electrodes on a probe.

4.2.2. Variation of impedance magnitudes in vivo

Fig. 4.5. shows impedance values at 1 kHz, obtained after in vivo recordings, merged from measurements with 69 electrodes of 3 probes (three electrodes were excluded, which had extremely large impedance values, probably due to wiring failure). Averaging all of the presented values, 616 ± 129 kΩ for thin-film Pt and 112 ± 36 kΩ for Pt/Pt electrodes are yielded. These are different from those values, which could be extracted from the EIS measurements in lactated Ringer's solution (at 1 kHz, EIS yielded 552 ± 151 kΩ and 38.7 ± 2.25 kΩ on the average for thin-film Pt and Pt/Pt electrode impedances, respectively). The difference between in vitro and in vivo impedance is not surprising, since impedance depends not only on electrode, but on solution properties as well (Abidian and Martin, 2008; Franks et al., 2005; Wise et al., 1970).

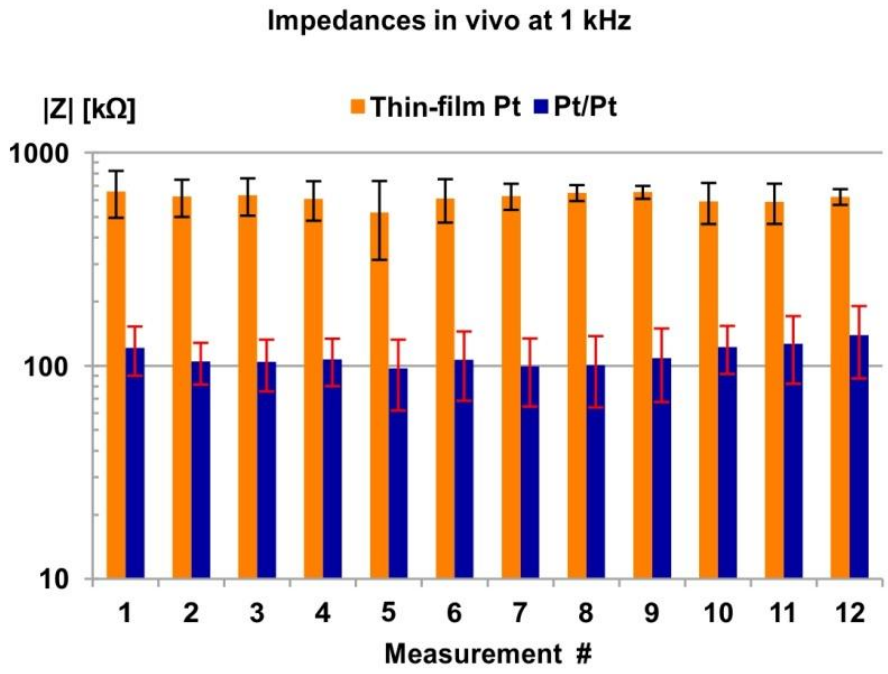

Fig. 4.5. Variation of average impedance values at 1 kHz during 12 in vivo recording sessions of the electrodes. The data are presented as mean ± standard error.

4.2.3. Effects of 12 acute implantations on the electrodes

After the in vivo measurements the probes were subjected to CV in order to quantify how in vivo use modified the effective surface area of the electrodes. These measurements revealed that as a result of the 12 implants, the effective surface / geometric area ratio dropped from 950 to 330 in case of Pt/Pt electrodes, and from 1.0 to 0.85 in case of thin-film Pt electrodes, as shown in Fig. 4.6. We assume that either the roughness factor of the Pt/Pt structure decreased, or organic residuals passivated a part of the surface of the electrodes. Although it is a considerable decrease, the effective surface of Pt/Pt electrodes, on the average, was still more than two orders of magnitude higher to what original thin-film Pt electrodes provided.

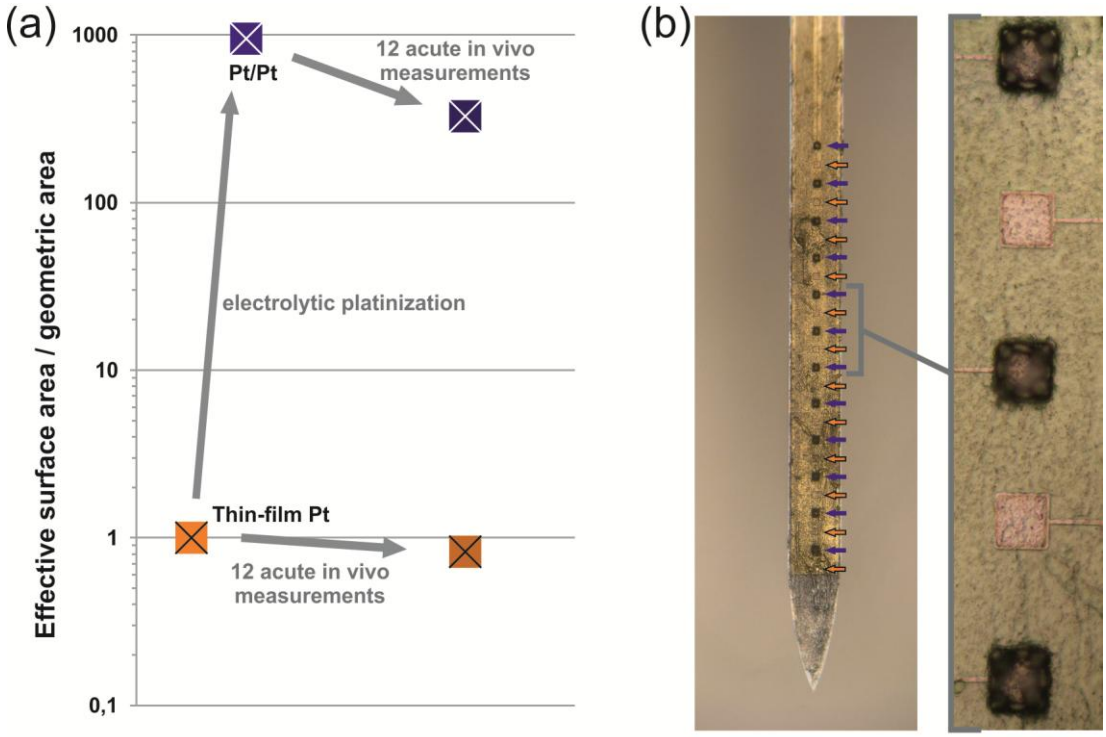

Fig. 4.6. (a) The variation of average effective surface area with electrolytic platinum deposition and multiple acute use of the MEAs. (b) Optical microscopic images of a probe after 12 acute implantations. Pt/Pt and thin-film Pt electrodes are marked with blue and orange arrows, respectively.

It is worthwhile to discuss why a decrease in effective surface area did not cause large increase in electrode impedances at 1 kHz, in vivo (presented in Fig. 4.5.). As previously described (in section *1.2.2. Impedance),* and illustrated in Fig. 1.2, the electrode impedance can be modeled with an equivalent circuit containing a spreading resistance (R_S), a charge transfer resistance (R_{CT}) and a constant phase element (CPE). The latter two are characteristic of the electrode surface and can be unified to a single impedance (Z_{SUR}).

These equivalent circuit parameter values for Pt/Pt electrodes in vivo can be roughly estimated as follows. Lactated Ringer's solution provide surface conditions for electrodes similar to in vivo, therefore in order to calculate impedance corresponding to electrode surface (Z_{SUR}), in vitro EIS curves of the Pt/Pt electrodes can be fitted onto the equivalent circuit model. Thus computing the impedance corresponding to the electrode surface yields $Z_{SUR,Pt/Pt} = 0.609 \pm 0.132$ kΩ. In order to estimate the spreading resistance (R_S), we cannot adapt in vitro EIS data, since this parameter should describe the unique

resistance of the brain tissue, where ion flow is limited by the low volume fraction and tortuosity of the extracellular space (Nicholson and Phillips, 1981). Analytically, in case of square sites, R_S can be calculated as

$$R_S = \qquad (4.1)$$

where ρ is the solution resistivity and l is the length of the electrode side. Thus R_S depends on the geometric area, while it is independent of the effective surface area of the electrodes (Franks et al., 2005). A review study evaluated average electrical conductivity of 4.11 ± 2.37 Ωm in gray matter (Latikka et al., 2001). Substituting this value and the 30 μm length of electrode sides into (4.1), R_S of 60.4 ± 34.8 kΩ is yielded in vivo.

According to these estimations for Pt/Pt electrodes in vivo, the spreading resistance (R_S) is about two orders of magnitude higher than the impedance corresponding to electrode surfaces. Therefore R_S can clearly suppress a small variation in the impedances of the electrode surfaces. For these reasons, the results of in vivo impedance testing (shown in Fig. 4.5.) need to be considered with limitations: they show that the impedance of Pt/Pt electrode-electrolyte interface remains so low that the spreading resistance remains the dominant factor of the total impedance even after multiple acute use of the probes, but they give no quantitative information about the effective surface area of the Pt/Pt deposits.

4.2.4. Noise of different electrodes after 12 implantations

One of the main purposes of electrolytic Pt deposition on neural electrodes is noise reduction. In order to learn whether Pt/Pt electrodes are superior to thin-film Pt sites in this aspect, even after multiple acute use of them, the data presented here are only obtained from measurements performed during or after the last (12^{th}) measurements. Representative graphs of PSDs of signals measured in vivo and in vitro with thin-film Pt and Pt/Pt electrodes are shown in Fig. 4.7.

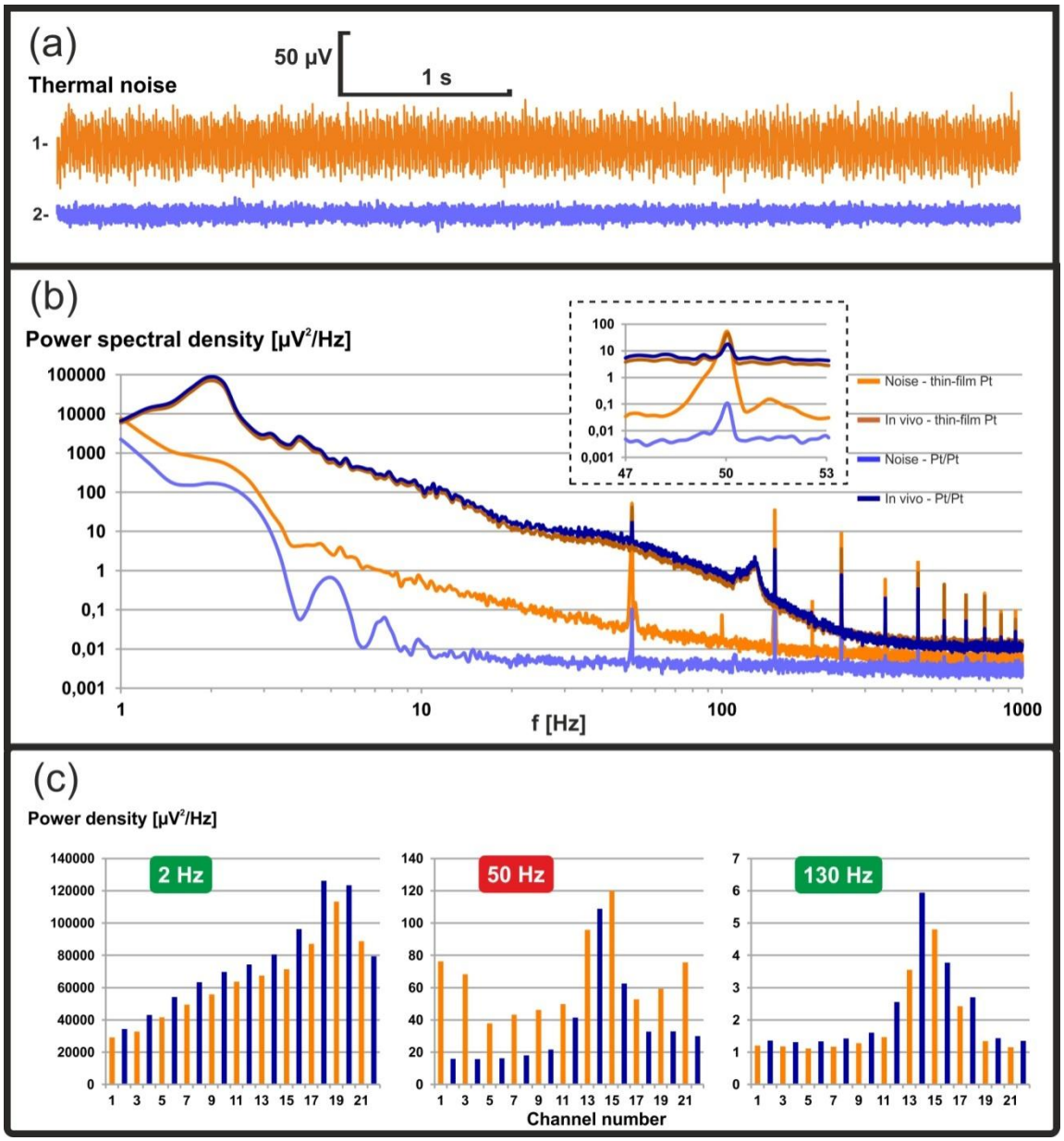

Fig. 4.7. (a) Thermal noise of thin-film Pt (1) and Pt/Pt (2) electrodes above 500 Hz, measured in lactated Ringer's solution. Pt/Pt sites provide less noise. (b) Power spectral density of neural signals and noise, recorded after the 12th implantation. (c) Power densities of in vivo recorded signals at biologically relevant frequencies (2Hz, 130 Hz) and at line frequency (50 Hz) of original thin-film Pt and Pt/Pt electrodes (orange and blue columns, respectively). Platinized sites provided signals with slightly more power at biologically relevant frequencies and less noise.

On the power spectra of in vivo signals, increased amplitude at the 1.5-2.5 Hz bandwidth can be observed. This slow oscillation is the result of ketamine-xylazine anesthesia (Fontanini et al., 2003). Another hump is visible between 110 and 135 Hz, which we assume to be related to the fast gamma (epsilon) oscillation and sharp waves (Buzsáki and Silva, 2012; Sullivan et al., 2011) of the hippocampus. The sharp peaks of the graphs, e.g. at 50 Hz, correspond to noise. Integrating the power spectrum of in vitro measured noise in the 1 Hz - 1 kHz region, we have found that the power on Pt/Pt sites is on the average 17.5% of the noise on original sites in this bandwidth.

It has been suggested by E. W. Keefer et al. that a further advantage of impedance reduction is increased signal power (Keefer et al., 2008). However, other researchers observed no such effect (Scott et al., 2012). Our measurements only indicated a slight increase, while the power of in vivo recorded signals greatly depended on electrode location, as shown in Fig. 4.7. (c). Calculations based on recordings in the lower regions (e.g. channel 1-10 in Fig. 4.7. (c)) revealed that platinization resulted in averagely 27% and 18% more power at 2 Hz and 130 Hz, respectively.

4.3. Results and discussion concerning the development and characterization of a novel polymer-based microelectrode arrays with protruding sensor sites

Images of the MEA, prior to bonding to the PCB are shown in Fig. 4.8. (a) and (b). The microfabrication process flow was carried out with high yield. Failures, such as imperfections in the pattern of the conductive layer, or tearing the foils while peeling them off of the substrate occurred with a prevalence of less than 10%. The complete device had a width of 10 mm and a length of 134 mm.

To my knowledge, this device was the first microfabricated neural electrode array with layer composition of PI - Pt - SU-8 (bottom insulator – conductor – top insulator). It is rather common that the top insulator layer is PI as well (A. Fomani and Mansour, 2011; Stieglitz et al., 1997). The advantage of the novel composition is that during the contour etching step it does not require an additional masking layer (e.g. aluminium) to be formed onto the top of the MEMS component, since the top SU-8 layer (which can

be directly patterned with photolithography) and the platinum layer have both proven to be suitable for masking the dry etching process, thus defining the contour.

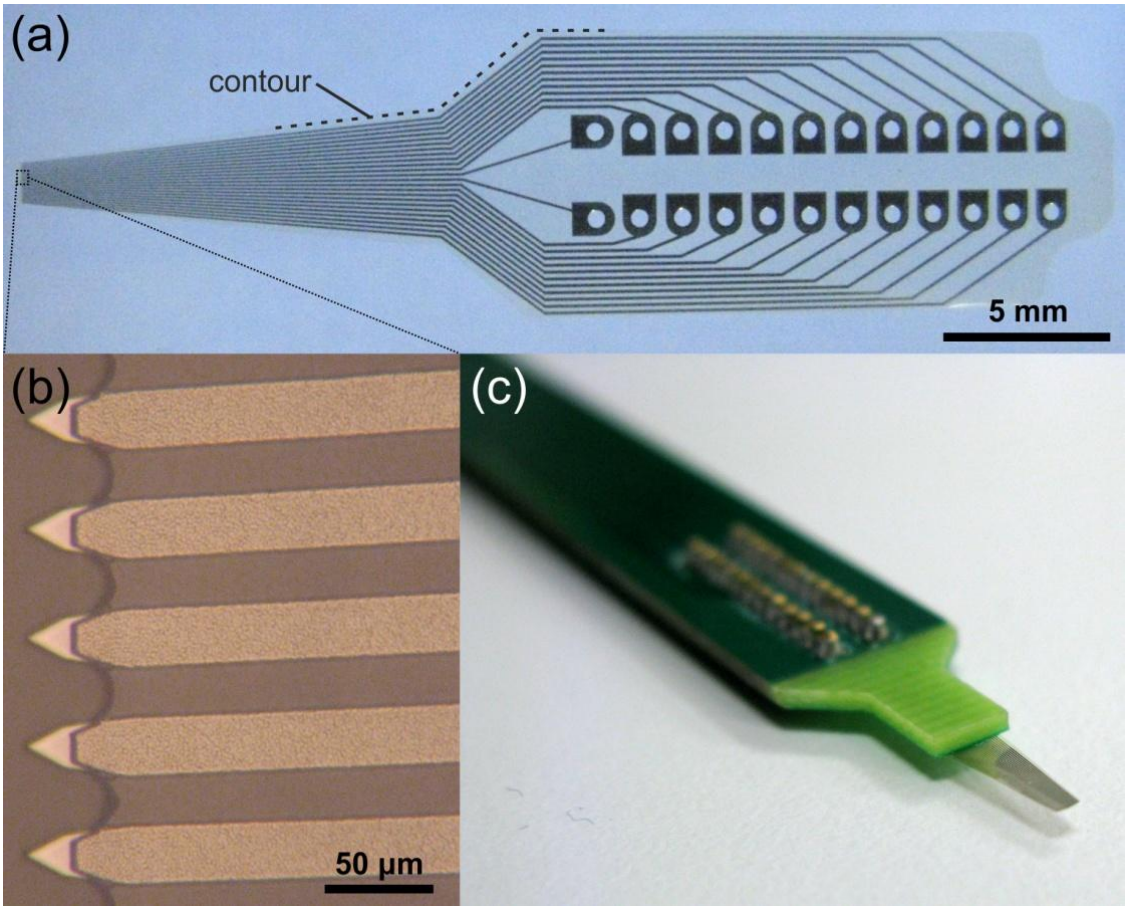

Fig. 4.8. (a) The microfabricated component with electrodes, corresponding bonding pads and lead wires. The bottom PI and top SU-8 isolating polymer layers are almost totally transparent. (b) Image of the spiky electrode array at the tip. The center-to center distance of the sensors is 50 µm. (c) The microfabricated component mounted on a PCB. The MEMS component is turned over, so the electrode surfaces are facing downwards.

Fig. 4.9. shows the average curve of the EIS measurements of an electrode array. The obtained values are in agreement with the literature of thin-film platinum electrodes (Franks et al., 2005; Kisban et al., 2007; Schuettler, 2007). The data suggests that SU-8 and PI layers insulate the metal wires properly, otherwise abnormally low impedances should have been measured. Also, there was no observable sign of insulation failure after seven days of soaking.

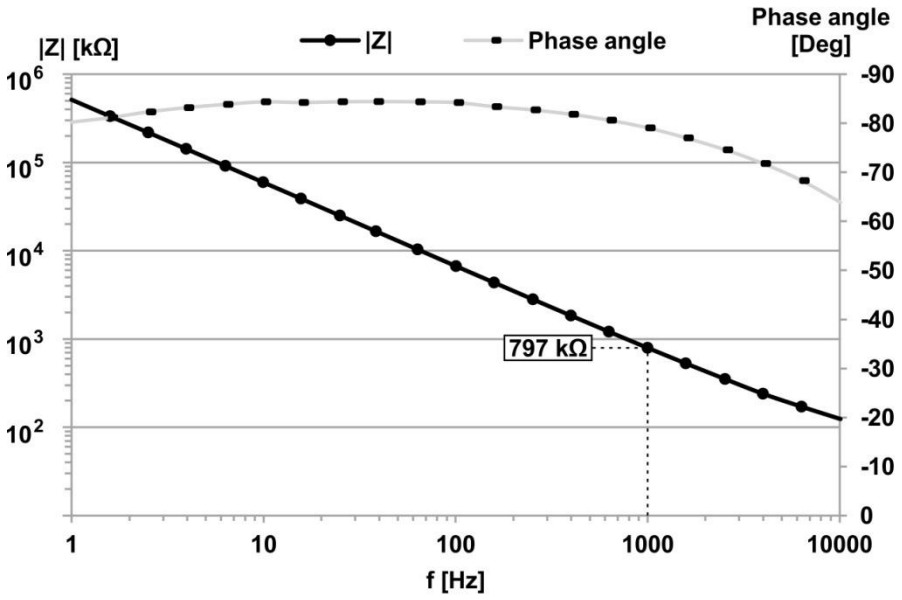

Fig. 4.9. Bode plot of average electrochemical impedance spectrum of the microelectrodes on a microelectrode array.

Fig. 4.10. shows waveforms of a representative in vivo recording above the somatosensory cortex and a microscopic image of the probe during measurement. The microdevice came into contact with the brain surface without causing visible bleeding in all cases, the arrow-shaped sites could visibly penetrate into the neural tissue. An oscillation of approximately 1.6 Hz is visible on all of the sensor channels due to the anesthesia (Fontanini et al., 2003; Steriade et al., 1993). Comparing them to each other, a divergence is observable in the waveforms, showing the spatial variation of the LFP in the cortex along the 1.15 mm length of the array.

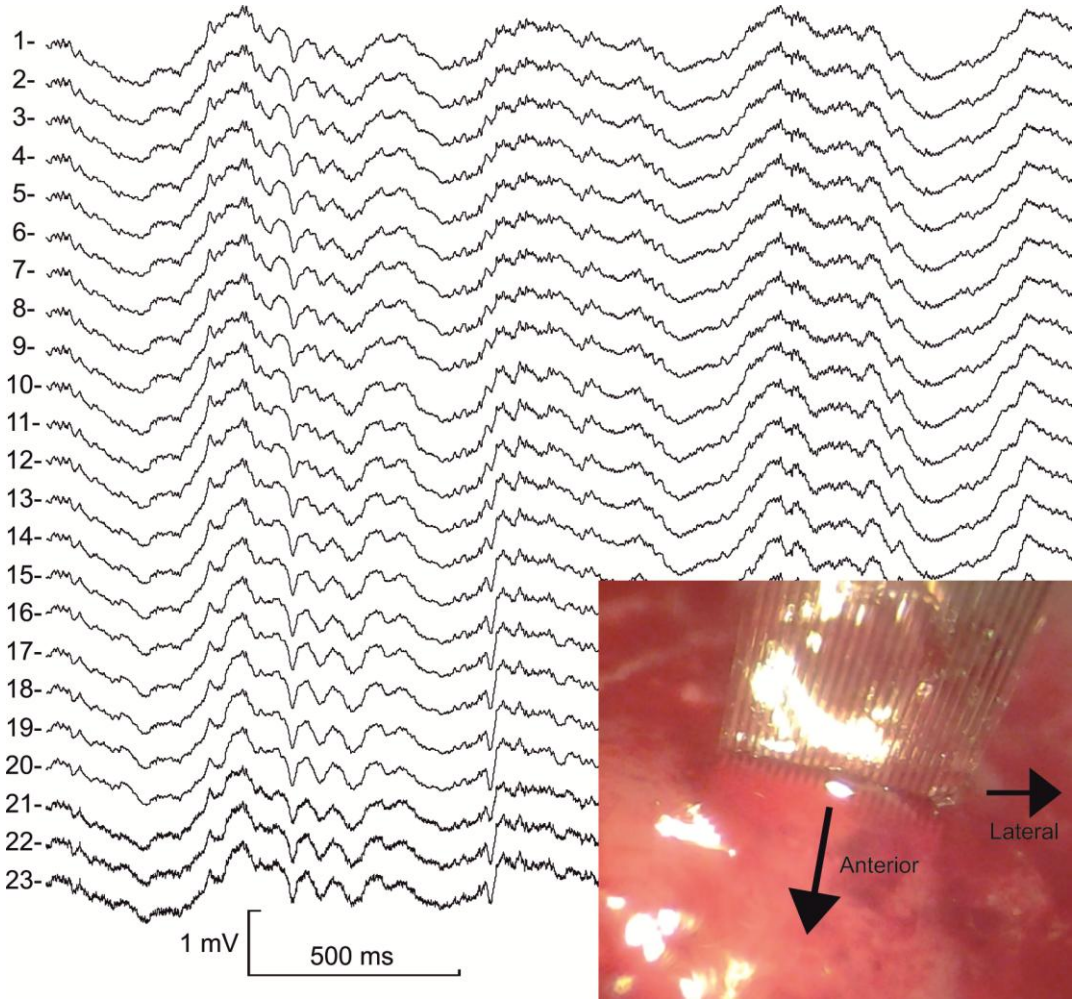

Fig. 4.10. Representative electrophysiological signals and a microscopic image obtained from the in vivo experiments on rat neocortex. The frequency of the slow oscillation is approximately 1.6 Hz, indicating a state of slow-wave sleep, caused by ketamine - xylazine anesthesia.

The microdevice has some limitations and disadvantages. One of these is the necessity of the removal of the dura mater. Otherwise, the soft and flexible sites were not able to enter into the tissue medium. This is not a serious issue during acute recordings, but if such a device was intended to be used chronically, it would be a severe disadvantage due to the risk of drying and infections (Jackson and Muthuswamy, 2008). A further limitation derives from the one-dimensional geometry of the electrode array. In order to upgrade the concept to create a two-dimensional MEA with protruding sensor sites, multiple one-dimensional arrays are to be integrated together or a more subtle microfabrication technology is to be developed.

4.4. Results and discussion concerning the development and characterization of a polymer-based multimodal microelectrode system

4.4.1. Microfabricated and assembled devices

An image of a device and a magnified view of its sensor region, containing the electrodes are presented in Fig. 4.11. The microtechnological and assembly processes resulted in the unique, three-dimensional probe geometry consistent with our design. The attachment of the shank (containing the extracellular electrodes) to the ECoG component was sufficient, the connection remained intact in all cases during the in vitro and in vivo tests. The similarly flexible meander wiring leads provided mechanical decoupling between the sensor region and the connector. The mechanical robustness of the lead was adequate, failures only occurred as a result of extreme pulling forces. Our overall experience was that these flexible tools do not require so much care during handling compared to the more brittle silicon-based extracellular MEAs.

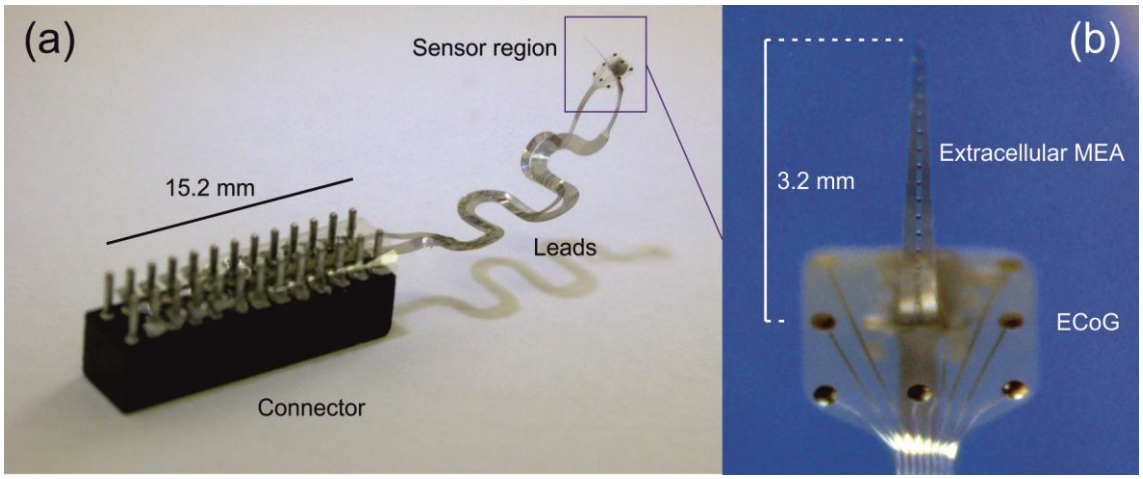

Fig. 4.11. (a) Macroscopic view of the assembled device. (b) A microscopic image of the multimodal sensor region with its unique three-dimensional formation, containing the two types of microelectrodes.

4.4.2. Original and reduced electrode impedances in saline

Results of average values yielded by in vitro impedance measurements on a probe are shown in Fig. 4.12. The original, sputtered thin-film Pt extracellular electrodes (with geometric area of 707 μm^2) had an average impedance magnitude of 559.5±148.4 kΩ at 1 kHz. We decided to reduce this value in order to obtain a better SNR during measurements. The electrolytic deposition of platinum yielded a Pt/Pt layer of high roughness factor, hence the average impedance magnitude at 1 kHz reduced to 27.6±8 kΩ. As expected, the ECoG sites of larger (31400 μm^2) geometric area had much lower original impedances: 18.6±0.5 kΩ on the average. ECoG electrodes are only expected to record LFP without unit activities and we found this value to be sufficient for this purpose and did not apply electrolytic deposition on these sites.

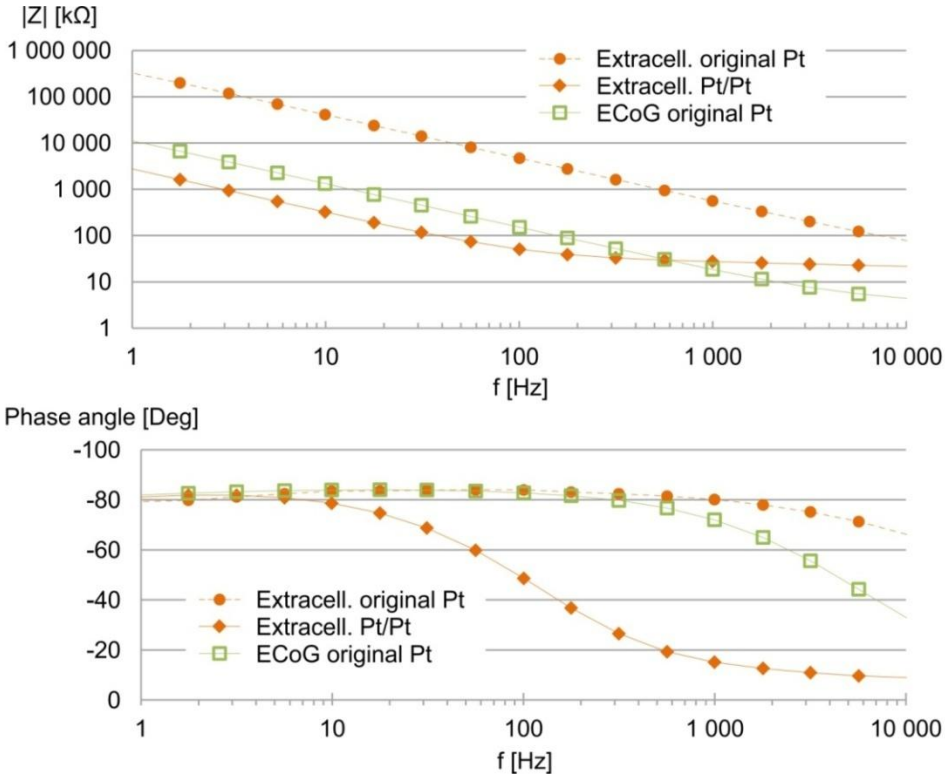

Fig. 4.12. The average magnitude and phase values of electrode impedances at different frequencies, measured in physiological saline. The extracellular electrodes were subjected to electrochemical deposition of Pt, which reduced the impedance magnitudes from 559.5±148.4 kΩ to 27.6±8 kΩ at 1 kHz. The impedance of the ECoG sites were 18.6±0.5 kΩ on the average at 1 kHz, no modification was performed on them.

4.4.3. In vivo experimental results and discussion

The extracellular component of the device was suitable for implantation after the incision of the dura mater, and signals could be recorded with the ECoG and the extracellular component, simultaneously. The recordings were followed by the above described cleaning process, after which no sign of organic residues was found on the probes.

A sample of the recorded waveforms is presented in Fig. 4.13. Channels no. 1-8 represent LFP changes detected by ECoG electrodes. Channels no. 9-24 correspond to the extracellular sites. Similarly to the in vivo signals obtained with electrode array with protruding sensor sites, a synchronous slow wave oscillation with up- and downstates can be seen on all channels, indicating slow-wave sleep (SWS).

LFP has a positive peak during upstates on the brain surface and in the outer cortical layers, while in the deeper layers the LFP polarity of the waves is reversed. This phenomenon can be observed regarding the ECoG channels and channels 9-18 of the implanted component. Elevated activity in higher frequency domains of the LFP signals on channels 19-24 indicate that the tip of the implanted shank reaches down into the hippocampus, as expected.

Unit activities of the neighboring cells were revealed by filtering the frequencies below 500 Hz out of the signals. In the cortex, high intensity of multiunit activity can be observed within the upstate periods. In the hippocampus, unit activities do not follow the oscillation closely, which meets our expectations, since slow waves are supposedly generated by neocortical and thalamic oscillators (Crunelli and Hughes, 2010).

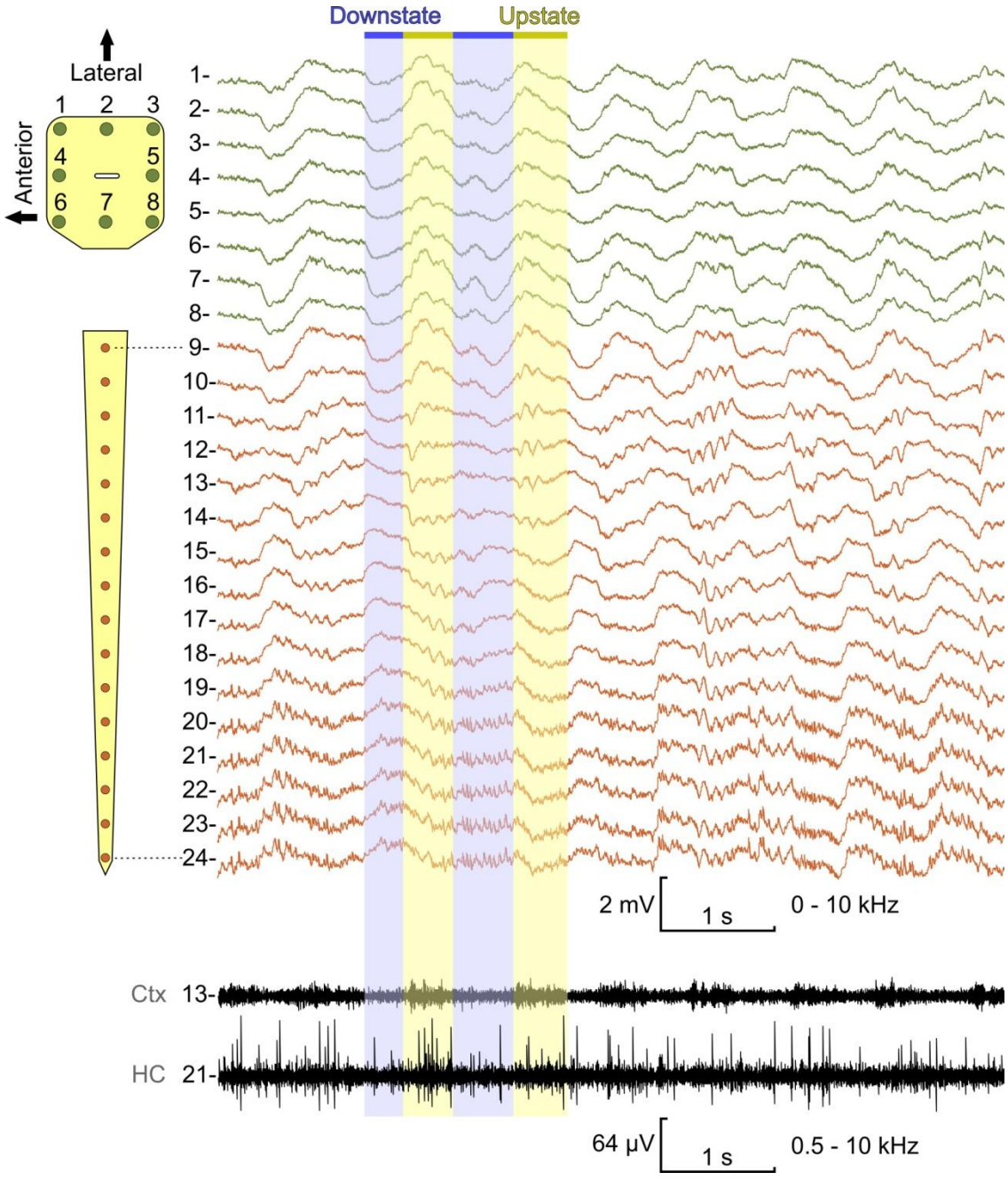

Fig. 4.13. Simultaneously recorded waveforms from the ECoG (channels no. 1-8, green curves) and the implanted component (channels no. 9-24, red curves). The 1-1.5 Hz oscillation is the result of ketamine-xylazine anesthesia. During its upstates, positive LFP can be detected on the brain surface and the outer cortical layers and negative LFP in deeper cortical layers. The intensity of unit activity (black curves) closely correlates with the upstate periods in the cortex, but not in the hippocampus.

Fig. 4.14. shows the results of CSD analysis. The upstate phase of the oscillation begins with the formation of a current source in the outer and inner layers of the cortex and a massive sink in the middle layers. Entering the downstate phase, the CSD is transformed into a sink-source-sink pattern in the cortex. This trend was also observed in humans during slow-wave sleep, although with different pattern (Cash et al., 2009; Csercsa et al., 2010). The CSD variation presented in Fig. 4.14. is consistent with the results of recent, not yet published experiments on the somatosensory cortex of anesthetized rats, obtained with silicon-based laminar MEAs, performed by Richárd Fiáth. He provides a thorough discussion on the subject, including comparison with the data yielded by human patients.

The experiment suggests that in case the investigated neural tissue has a laminar structure, the probe makes possible the determination of current sinks and sources as well.

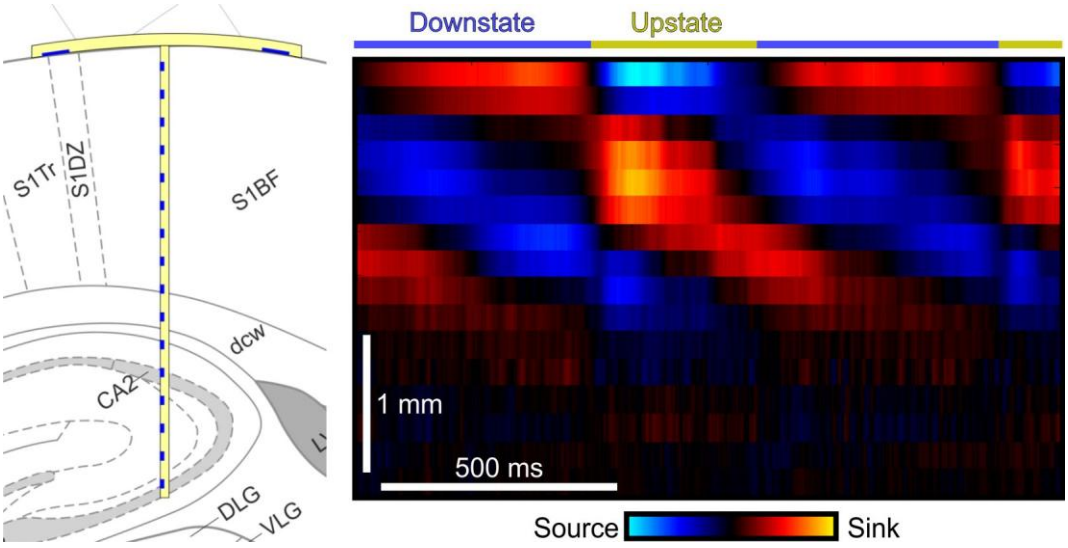

Fig. 4.14. Changes of current sources and sinks in time, yielded from the signals recorded by the laminar electrode array. Illustration of the implantation (left) is based on Figure 61. of (Paxinos and Watson, 2009).

There are examples in the literature for the realization of ECoG measurements and simultaneous extracellular recordings underneath the ECoG-covered region with separate devices. MEMS MEAs with Parylene C – gold – Parylene C layer structure were used on rat brain surface, along with tungsten fine wire microelectrodes, which

could be inserted into the brain through holes on the surface arrays (Toda et al., 2011). The configuration allowed LFP recordings with both the MEA and the fine wires, and the detection of unit activities with the latter. Flexible ECoG arrays along with 32-channel silicon MEAs and 16-channel platinum probes were used in rat (Watanabe et al., 2014) and monkey (Watanabe et al., 2012) brains, respectively. Surface grids were synchronously used with the "thumbtack" laminar array and similar depth electrodes in humans with epilepsy (Matsuo et al., 2013; Ulbert et al., 2004). The main concept of applying a surface MEA and an implantable component, integrated orthogonally to the surface array was patented in the United States (Anderson et al., 2012). However, to my best knowledge, the inventors did not fabricate and utilize such a device for neurophysiology.

The novelty of the herein demonstrated device (apart from the special, reliable and rapid technological process flow) is its multimodality, which is provided by its unique three-dimensional structure, assembled from two two-dimensional components, showing that these functions can be integrated into a single, all-flexible probe. The necessity of the incision of the dura mater is a disadvantage of the presented system, similarly to the polymer-based electrode arrays with protruding sites. An advantage is its high customizability, allowed by the applied MEMS technology. The number of electrodes on the ECoG and implantable component, as well as their size and distance from each other can be adjusted in a wide range and realized with high precision. Neither the microfabrication technology, nor the assembly processes exclude the possibility of extending the implanted component to a multishank MEA.

5. CONCLUSIONS

- Not only local field potential changes, but activities of single cells can be detected acutely in the extracellular space of the central nervous system of a rat using silicon-based microelectrode arrays fabricated with MEMS technology, with shaft length ranging from 15-70 mm, thickness and width ranging from 200 to 400 μm. Such probes are suitable for implantation through the intact dura mater.

- Low impedance extracellular neural microelectrodes can be realized with electrochemical deposition of high surface area platinum, furthermore, the deposition parameters can be chosen so that the electrodes with lowered impedances will be able to withstand 12 acute implantation-recording sessions.

- Following the removal of the dura mater of rats, a microelectrode array with a row of protruding sensor sites can be inserted underneath the cortical surface, allowing recordings of local field potential changes. The array can be constructed with an SU-8 – TiO_x/Pt – polyimide layer structure, which can be realized with the utilization of MEMS technology.

- Simultaneous electrocorticographic and laminar extracellular recordings can be obtained acutely in the central nervous system of rats with a multimodal, flexible, polymer-based microelectrode array constructed with an SU-8 – TiO_x/Pt – polyimide layer structure.

6. SUMMARY

In the recent years the number of neuroscientific experiments utilizing MEAs created with MEMS technology continued to increase. The dominance of silicon-based devices lessened and polymer-based electrode arrays are getting more and more into focus, due to their flexibility. Special elements have also been developed, such as microfluidic channels for drug delivery, high surface area deposits for increased SNR, etc. This work comprises four different novelties related to neural MEAs. It includes various technological developments and their functional characterization with acute in vivo measurements in rat cerebrum.

Probes with extreme shaft length (15-70 mm) were fabricated from single-crystal Si wafers utilizing SiO_2 and SiN_x thin-film deposition, TiO_x/Pt lift-off and DRIE (Bosch process). The corresponding in vivo recordings yielded qualitative data, confirming that the probes are suitable for unit activity detection.

An electrolytic platinization method was developed for creating high surface area Pt/Pt deposits in order to realize low impedance electrodes. 10-minute potentiostatic deposition at 100 mV vs. reversible hydrogen electrode from 1 g $PtCl_4 \times 2HCl \times 6\ H_2O$ + 2 cm^3 conc. HCl + 200 cm^3 H_2O solution was used. The impedance at 1 kHz reduced from 552 kΩ to 38.7 kΩ in vitro and from 616 kΩ to 112 kΩ in vivo. The compatibility of the porous deposits with acute extracellular recordings was tested with 12 measurement sessions for each probe, which the Pt/Pt structures could withstand.

We realized a polymer-based electrode array with protruding sensor sites that can slightly pierce into the brain tissue, with a novel MEMS process flow, comprising polyimide spin-coating onto Si wafers, TiO_x/Pt lift-off, SU-8 photolithography and RIE. The same microfabrication methodology was utilized for creating the components of a flexible multimodal sensor system, which includes brain surface electrodes and an implantable probe shank for laminar recordings. In vitro characterization of these devices in physiological saline, impedance reduction with the previously described

method and in vivo functional tests on somatosensory cortices of anesthetized rats yielded the expected impedance values and signal quality.

7. ÖSSZEFOGLALÓ

Az utóbbi években a mikroeletromechanikai rendszerek (MEMS) technológiájával létrehozott multielektródokat alkalmazó idegtudományos kísérletek száma tovább gyarapodott. A szilícium alapú eszközök dominanciája némileg csökkent a polimer alapú elektródok előtérbe kerülésével, ami utóbbi eszközök flexibilitásának köszönhető. A MEMS technológiai háttere speciális elemeket integráltan tartalmazó szenzorok kialakítását is lehetővé teszi. Például mikrofluidikai csatornákat hozhatunk létre gyógyszeradagolás céljából, nagy fajlagos felületű bevonatokat választhatunk le a jel-zaj viszony növeléséhez, stb. Munkánk során négy, neurális mikroelektródokkal kapcsolatos újdonságot hoztunk létre, beleértve azok technológiai fejlesztését és funkcionális tesztelését patkányagyban.

Különösen hosszú (15-70 mm) szárú multielektródokat alakítottunk ki egykristály szilícium szeletekből SiO_2, SiNx vékonyréteg-leválasztással, TiO_x/Pt lift-off eljárással történő ábrakialakítással, valamint mély reaktív ionmarással. Az eszközökkel kivitelezett in vivo mérések adatainak kvalitatív értékelése megmutatta, hogy azok alkalmasak egysejt aktivitások érzékelésére.

Elektrolitikus leválasztással nagy fajlagos felületű platinázott platinaréteget alakítottunk ki elektródimpedancia-csökkentés céljából. A 10 perces, 1 g $PtCl_4 \times 2HCl \times 6\ H_2O$ + 2 cm^3 konc. HCl + 200 cm^3 H_2O oldatból 100 mV-on (reverzibilis hidrogénelektródhoz képest) történő, poteciosztatikus leválasztás eredményeképp az 1 kHz-en mért átlagos impedancia 552 kΩ-ról 38.7 kΩ-ra redukálódott in vitro, 616 kΩ-ról 112 kΩ-ra in vivo. Az akut implantálásra szánt porózus szenzorfelületek felhasználhatóságát a 12-12 elektrofiziológiai méréssel validáltuk, melyeknek sikeresen ellenálltak.

Polimer alapú multielektródot alakítottunk ki az eszköz törzséből kinyúló szenzorfelületekkel, melyek képesek enyhén az agyfelszín alá hatolni. Az egyedi MEMS technológiai sor poliimid Si szeletekre történő felpörgetést, TiO_x/Pt ábrakialakítást, SU-8 fotolitográfiát és reaktív ionmarást tartalmazott. Ezt a

mikromegmunkálási eljárást felhasználtuk egy multimodális szenzorrendszer elemeinek a kialakítására is, mely agyfelszíni elektródokat és egy implantálható, lamináris multielektródot tartalmazott. A szenzorok in vitro karakterizációja, impedanciacsökkentése a korábban említett módszerrel, valamint a patkányok szomatoszenzoros agykérgén végzett in vivo funkcionális tesztek az elvárt impedanciaértékeket és jelminőséget szolgáltatták.

8. REFERENCES

A. Fomani A, Mansour RR. (2011) Fabrication and characterization of the flexible neural microprobes with improved structural design. Sensor Actuat A-Phys, 168: 233-241.

Abidian MR, Martin DC. (2008) Experimental and theoretical characterization of implantable neural microelectrodes modified with conducting polymer nanotubes. Biomaterials, 29: 1273-1283.

Anderson D, Kipke DR, Hetke JF, Vetter RJ, Kong K, Seymour J. Hybrid clustered interface neural system. Patent no. US2012/0323288A1, United States, 2012. Asano E, Juhasz C, Shah A, Muzik O, Chugani DC, Shah J, Sood S, Chugani HT. (2005) Origin and propagation of epileptic spasms delineated on electrocorticography. Epilepsia, 46: 1086-1097.

Azemi E, Lagenaur CF, Cui XT. (2011) The surface immobilization of the neural adhesion molecule L1 on neural probes and its effect on neuronal density and gliosis at the probe/tissue interface. Biomaterials, 32: 681-692.

Bai Q, Wise KD, Anderson DJ. (2000) A high-yield microassembly structure for three-dimensional microelectrode arrays. IEEE Trans Biomed Eng, 47: 281-289.

Baranauskas G, Maggiolini E, Castagnola E, Ansaldo A, Mazzoni A, Angotzi GN, Vato A, Ricci D, Panzeri S, Fadiga L. (2011) Carbon nanotube composite coating of neural microelectrodes preferentially improves the multiunit signal-to-noise ratio. J Neural Eng, 8: 1741-2560.

Bartels J, Andreasen D, Ehirim P, Mao H, Seibert S, Wright EJ, Kennedy P. (2008) Neurotrophic electrode: method of assembly and implantation into human motor speech cortex. J Neurosci Methods, 174: 168-176.

Bartho P, Slezia A, Matyas F, Faradzs-Zade L, Ulbert I, Harris KD, Acsady L. (2014) Ongoing network state controls the length of sleep spindles via inhibitory activity. Neuron, 82: 1367-1379.

Béduer A, Joris P, Mosser S, Delattre V, Fraering PC, Renaud P. (2014) Accurate resistivity mouse brain mapping using microelectrode arrays. Biosens Bioelectron, 60: 143-153.

Berenyi A, Somogyvari Z, Nagy AJ, Roux L, Long JD, Fujisawa S, Stark E, Leonardo A, Harris TD, Buzsaki G. (2014) Large-scale, high-density (up to 512 channels) recording of local circuits in behaving animals. J Neurophysiol, 111: 1132-1149.

Bliss TV, Collingridge GL. (1993) A synaptic model of memory: long-term potentiation in the hippocampus. Nature, 361: 31-39.

Bliss TV, Lomo T. (1973) Long-lasting potentiation of synaptic transmission in the dentate area of the anaesthetized rabbit following stimulation of the perforant path. J Physiol, 232: 331-356.

Bobo RH, Laske DW, Akbasak A, Morrison PF, Dedrick RL, Oldfield EH. (1994) Convection-enhanced delivery of macromolecules in the brain. Proc of the Nat Academy of Sci, 91: 2076-2080.

Boretius T, Badia J, Pascual-Font A, Schuettler M, Navarro X, Yoshida K, Stieglitz T. (2010) A transverse intrafascicular multichannel electrode (TIME) to interface with the peripheral nerve. Biosens Bioelectron, 26: 62-69.

Boyden ES, Zhang F, Bamberg E, Nagel G, Deisseroth K. (2005) Millisecond-timescale, genetically targeted optical control of neural activity. Nat Neurosci, 8: 1263-1268.

Branner A, Stein RB, Normann RA. (2001) Selective Stimulation of Cat Sciatic Nerve Using an Array of Varying-Length Microelectrodes, 85: 1585-1594.

Brumberg JS, Nieto-Castanon A, Kennedy PR, Guenther FH. (2010) Brain-Computer Interfaces for Speech Communication. Speech Commun, 52: 367-379.

Buzsáki G, Anastassiou CA, Koch C. (2012) The origin of extracellular fields and currents — EEG, ECoG, LFP and spikes. Nat Rev Neurosci, 13: 407-420.

Buzsáki G, Silva FLd. (2012) High frequency oscillations in the intact brain. Prog Neurobiol, 98: 241-249.

Campbell PK, Jones KE, Huber RJ, Horch KW, Normann RA. (1991) A silicon-based, three-dimensional neural interface: manufacturing processes for an intracortical electrode array. IEEE Trans Biomed Eng, 38: 758-768.

Cash SS, Halgren E, Dehghani N, Rossetti AO, Thesen T, Wang C, Devinsky O, Kuzniecky R, Doyle W, Madsen JR, Bromfield E, Eross L, Halasz P, Karmos G, Csercsa R, Wittner L, Ulbert I. (2009) The human K-complex represents an isolated cortical down-state. Science, 324: 1084-1087.

Chader GJ, Weiland J, Humayun MS. (2009) Artificial vision: needs, functioning, and testing of a retinal electronic prosthesis. Prog Brain Res, 175: 317-332.

Chang TY, Yadav VG, De Leo S, Mohedas A, Rajalingam B, Chen CL, Selvarasah S, Dokmeci MR, Khademhosseini A. (2007) Cell and protein compatibility of parylene-C surfaces. Langmuir, 23: 11718-11725.

Chauvette S, Crochet S, Volgushev M, Timofeev I. (2011) Properties of slow oscillation during slow-wave sleep and anesthesia in cats. J Neurosci, 31: 14998-15008.

Chauvette S, Volgushev M, Timofeev I. (2010) Origin of Active States in Local Neocortical Networks during Slow Sleep Oscillation. Cerebral Cortex, 20: 2660-2674.

Chen J, Wise KD, Hetke JF, Bledsoe SC, Jr. (1997) A multichannel neural probe for selective chemical delivery at the cellular level. IEEE Trans Biomed Eng, 44: 760-769.

Chen YY, Lai HY, Lin SH, Cho CW, Chao WH, Liao CH, Tsang S, Chen YF, Lin SY. (2009) Design and fabrication of a polyimide-based microelectrode array: application in neural recording and repeatable electrolytic lesion in rat brain. J Neurosci Methods, 182: 6-16.

Chestek CA, Gilja V, Nuyujukian P, Foster JD, Fan JM, Kaufman MT, Churchland MM, Rivera-Alvidrez Z, Cunningham JP, Ryu SI, Shenoy KV. (2011) Long-term stability of neural prosthetic control signals from silicon cortical arrays in rhesus macaque motor cortex. J Neural Eng, 8: 1741-2560.

Cheung K, Gun L, Djupsund K, Yang D, Lee LP (Year) A new neural probe using SOI wafers with topological interlocking mechanisms. Microtechnologies in Medicine and Biology, 1st Annual International, Conference On. 2000. City. p. 507-511.

Cheung KC. (2007) Implantable microscale neural interfaces. Biomed Microdevices, 9: 923-938.

Cheung KC, Renaud P, Tanila H, Djupsund K. (2007) Flexible polyimide microelectrode array for in vivo recordings and current source density analysis. Biosens Bioelectron, 22: 1783-1790.

Chorover SL, Deluca A-M. (1972) A sweet new multiple electrode for chronic single unit recording in moving animals. Physiol Behav, 9: 671-674.

Cooke SF, Bliss TV. (2006) Plasticity in the human central nervous system. Brain, 129: 1659-1673.

Crunelli V, Hughes SW. (2010) The slow (<1 Hz) rhythm of non-REM sleep: a dialogue between three cardinal oscillators. Nat Neurosci, 13: 9-17.

Csercsa R, Dombovari B, Fabo D, Wittner L, Eross L, Entz L, Solyom A, Rasonyi G, Szucs A, Kelemen A, Jakus R, Juhos V, Grand L, Magony A, Halasz P, Freund TF, Magloczky Z, Cash SS, Papp L, Karmos G, Halgren E, Ulbert I. (2010) Laminar analysis of slow wave activity in humans. Brain, 133: 2814-2829.

Cserr HF, Ostrach LH. (1974) Bulk flow of interstitial fluid after intracranial injection of Blue Dextran 2000. Exp Neur, 45: 50-60.

Csicsvari J, Henze DA, Jamieson B, Harris KD, Sirota A, Bartho P, Wise KD, Buzsaki G. (2003) Massively parallel recording of unit and local field potentials with silicon-based electrodes. J Neurophysiol, 90: 1314-1323.

Deng M, Yang X, Silke M, Qiu W, Xu M, Borghs G, Chen H. (2011) Electrochemical deposition of polypyrrole/graphene oxide composite on microelectrodes towards tuning the electrochemical properties of neural probes. Sensor Actuat B-Chem, 158: 176-184.

Desai SA, Rolston JD, Guo L, Potter SM. (2010) Improving impedance of implantable microwire multi-electrode arrays by ultrasonic electroplating of durable platinum black. Front Neuroeng, 3: 00005.

Dombovari B, Fiath R, Kerekes BP, Toth E, Wittner L, Horvath D, Seidl K, Herwik S, Torfs T, Paul O, Ruther P, Neves H, Ulbert I. (2013) In vivo validation of the electronic depth control probes. Biomed Tech, 11: 1-7.

Du J, Blanche TJ, Harrison RR, Lester HA, Masmanidis SC. (2011) Multiplexed, high density electrophysiology with nanofabricated neural probes. PLoS One, 6: 12.

Du J, Riedel-Kruse IH, Nawroth JC, Roukes ML, Laurent G, Masmanidis SC. (2009a) High-Resolution Three-Dimensional Extracellular Recording of Neuronal Activity With Microfabricated Electrode Arrays. J Neurophys, 101: 1671-1678.

Du J, Roukes ML, Masmanidis SC. (2009b) Dual-side and three-dimensional microelectrode arrays fabricated from ultra-thin silicon substrates. Journal of Micromechanics and Microengineering, 19: 075008.

Dymond AM, Kaechele LE, Jurist JM, Crandall PH. (1970) Brain tissue reaction to some chronically implanted metals. J Neurosurg, 33: 574-580.

Eccles JC. (1951) Interpretation of action potentials evoked in the cerebral cortex. Electroen Clin Neuro, 3: 449-464.

Fekete Z, Hajnal Z, Márton G, Fürjes P, Pongrácz A. (2013) Fracture analysis of silicon microprobes designed for deep-brain stimulation. Microel Eng, 103: 160-166.

Ferguson JE, Boldt C, Redish AD. (2009) Creating low-impedance tetrodes by electroplating with additives. Sensor Actuat A-Phys, 156: 388-393.

Fontani G. (1981) A technique for long term recording from single neurons in unrestrained behaving animals. Physiol Behav, 26: 331-333.

Fontanini A, Spano P, Bower JM. (2003) Ketamine-xylazine-induced slow (< 1.5 Hz) oscillations in the rat piriform (olfactory) cortex are functionally correlated with respiration. J Neurosci, 23: 7993-8001.

Franks W, Schenker I, Schmutz P, Hierlemann A. (2005) Impedance characterization and modeling of electrodes for biomedical applications. IEEE Trans Biomed Eng, 52: 1295-1302.

Freeman JA, Nicholson C. (1975) Experimental optimization of current source-density technique for anuran cerebellum. J Neurophysiol, 38: 369-382.

Gasior M, White NA, Rogawski MA. (2007) Prolonged attenuation of amygdala-kindled seizure measures in rats by convection-enhanced delivery of the N-type calcium channel antagonists omega-conotoxin GVIA and omega-conotoxin MVIIA. J Pharmacol Exp Ther, 323: 458-468.

Gelbard-Sagiv H, Mukamel R, Harel M, Malach R, Fried I. (2008) Internally generated reactivation of single neurons in human hippocampus during free recall. Science, 322: 96-101.

Gill SS, Patel NK, Hotton GR, O'Sullivan K, McCarter R, Bunnage M, Brooks DJ, Svendsen CN, Heywood P. (2003) Direct brain infusion of glial cell line-derived neurotrophic factor in Parkinson disease. Nat Med, 9: 589-595.

Goto T, Hatanaka R, Ogawa T, Sumiyoshi A, Riera J, Kawashima R. (2010) An evaluation of the conductivity profile in the somatosensory barrel cortex of Wistar rats. J Neurophysiol, 104: 3388-3412.

Gradinaru V, Zhang F, Ramakrishnan C, Mattis J, Prakash R, Diester I, Goshen I, Thompson KR, Deisseroth K. (2010) Molecular and cellular approaches for diversifying and extending optogenetics. Cell, 141: 154-165.

Graimann B, Huggins JE, Levine SP, Pfurtscheller G. (2004) Toward a direct brain interface based on human subdural recordings and wavelet-packet analysis. IEEE Trans Biomed Eng, 51: 954-962.

Grand L, Pongrácz A, Vázsonyi É, Márton G, Gubán D, Fiáth R, Kerekes BP, Karmos G, Ulbert I, Battistig G. (2011) A novel multisite silicon probe for high quality laminar neural recordings. Sensor Actuat A-Phys, 166: 14-21.

Grand L, Wittner L, Herwik S, Gothelid E, Ruther P, Oscarsson S, Neves H, Dombovari B, Csercsa R, Karmos G, Ulbert I. (2010) Short and long term biocompatibility of NeuroProbes silicon probes. J Neurosci Meth, 189: 216-229.

Gray CM, Maldonado PE, Wilson M, McNaughton B. (1995) Tetrodes markedly improve the reliability and yield of multiple single-unit isolation from multi-unit recordings in cat striate cortex. J Neurosci Meth, 63: 43-54.

Green RA, Lovell NH, Wallace GG, Poole-Warren LA. (2008a) Conducting polymers for neural interfaces: Challenges in developing an effective long-term implant. Biomaterials, 29: 3393-3399.

Green RA, Williams CM, Lovell NH, Poole-Warren LA. (2008b) Novel neural interface for implant electrodes: improving electroactivity of polypyrrole through MWNT incorporation. J Mater Sci Mater Med, 19: 1625-1629.

Griffith RW, Humphrey DR. (2006) Long-term gliosis around chronically implanted platinum electrodes in the Rhesus macaque motor cortex. Neurosci Lett, 406: 81-86.

Guenther FH, Brumberg JS, Wright EJ, Nieto-Castanon A, Tourville JA, Panko M, Law R, Siebert SA, Bartels JL, Andreasen DS, Ehirim P, Mao H, Kennedy PR. (2009) A Wireless Brain-Machine Interface for Real-Time Speech Synthesis. PLoS ONE, 4: e8218.

Hackett TA, Barkat TR, O'Brien BM, Hensch TK, Polley DB. (2011) Linking topography to tonotopy in the mouse auditory thalamocortical circuit. J Neurosci, 31: 2983-2995.

Hafting T, Fyhn M, Molden S, Moser MB, Moser EI. (2005) Microstructure of a spatial map in the entorhinal cortex. Nature, 436: 801-806.

Han X, Chow BY, Zhou H, Klapoetke NC, Chuong A, Rajimehr R, Yang A, Baratta MV, Winkle J, Desimone R, Boyden ES. (2011) A high-light sensitivity optical neural silencer: development and application to optogenetic control of non-human primate cortex. Front Syst Neurosci, 5: 18.

Hashiguchi K, Morioka T, Yoshida F, Miyagi Y, Nagata S, Sakata A, Sasaki T. (2007) Correlation between scalp-recorded electroencephalographic and electrocorticographic activities during ictal period. Seizure, 16: 238-247.

Hassler C, Boretius T, Stieglitz T. (2011) Polymers for neural implants. Journal of Polymer Science Part B: Polymer Physics, 49: 18-33.

Hazan L, Zugaro M, Buzsaki G. (2006) Klusters, NeuroScope, NDManager: a free software suite for neurophysiological data processing and visualization. J Neurosci Meth, 155: 207-216.

Heim M, Rousseau L, Reculusa S, Urbanova V, Mazzocco C, Joucla S, Bouffier L, Vytras K, Bartlett P, Kuhn A, Yvert B. Combined macro-/mesoporous microelectrode arrays for low-noise extracellular recording of neural networks, 2012a.

Heim M, Yvert B, Kuhn A. (2012b) Nanostructuration strategies to enhance microelectrode array (MEA) performance for neuronal recording and stimulation. J Physiol Paris, 106: 137-145.

Hochberg LR, Serruya MD, Friehs GM, Mukand JA, Saleh M, Caplan AH, Branner A, Chen D, Penn RD, Donoghue JP. (2006) Neuronal ensemble control of prosthetic devices by a human with tetraplegia. Nature, 442: 164-171.

Hoeltzell PB, Dykes RW. (1979) Conductivity in the somatosensory cortex of the cat -- evidence for cortical anisotropy. Brain Res, 177: 61-82.

Hoffman KL, McNaughton BL. (2002) Coordinated reactivation of distributed memory traces in primate neocortex. Science, 297: 2070-2073.

Hofmann UG, Folkers A, Mosch F, Hohl D, Kindlundh M, Norlin P. (2002) A 64(128)-channel multisite neuronal recording system. Biomed Tech, 1: 194-197.

Hollenberg BA, Richards CD, Richards R, Bahr DF, Rector DM. (2006) A MEMS fabricated flexible electrode array for recording surface field potentials. J Neurosci Meth, 153: 147-153.

Homer ML, Nurmikko AV, Donoghue JP, Hochberg LR. (2013) Sensors and decoding for intracortical brain computer interfaces. Annu Rev Biomed Eng, 15: 383-405.

Hsu JM, Rieth L, Normann RA, Tathireddy P, Solzbacher F. (2009) Encapsulation of an integrated neural interface device with Parylene C. IEEE Trans Biomed Eng, 56: 23-29.

Jackson N, Muthuswamy J. (2008) Artificial dural sealant that allows multiple penetrations of implantable brain probes. J Neurosci Meth, 171: 147-152.

Jenison RL, Rangel A, Oya H, Kawasaki H, Howard MA. (2011) Value encoding in single neurons in the human amygdala during decision making. J Neurosci, 31: 331-338.

Jones KE, Campbell PK, Normann RA. (1992) A glass/silicon composite intracortical electrode array. Ann Biomed Eng, 20: 423-437.

Jones MS, Barth DS. (1999) Spatiotemporal organization of fast (>200 Hz) electrical oscillations in rat Vibrissa/Barrel cortex. J Neurophysiol, 82: 1599-1609.

Kanas VG, Mporas I, Benz HL, Sgarbas KN, Bezerianos A, Crone NE. (2014) Joint spatial-spectral feature space clustering for speech activity detection from ECoG signals. IEEE Trans Biomed Eng, 61: 1241-1250.

Keefer EW, Botterman BR, Romero MI, Rossi AF, Gross GW. (2008) Carbon nanotube coating improves neuronal recordings. Nat Nanotechnol, 3: 434-439.

Kennedy PR. (1989) The cone electrode: a long-term electrode that records from neurites grown onto its recording surface. J Neurosci Meth, 29: 181-193.

Khan S, Newaz G. (2010) A comprehensive review of surface modification for neural cell adhesion and patterning. J Biomed Mater Res A, 93: 1209-1224.

Kim BJ, Kuo JT, Hara SA, Lee CD, Yu L, Gutierrez CA, Hoang TQ, Pikov V, Meng E. (2013) 3D Parylene sheath neural probe for chronic recordings. J Neural Eng, 10: 1741-2560.

Kindlundh M, Norlin P, Hofmann UG. (2004) A neural probe process enabling variable electrode configurations. Sensor Actuat B-Chem, 102: 51-58.

Kisban S, Herwik S, Seidl K, Rubehn B, Jezzini A, Umilta MA, Fogassi L, Stieglitz T, Paul O, Ruther P. (2007) Microprobe array with low impedance electrodes and highly flexible polyimide cables for acute neural recording. Conf Proc IEEE Eng Med Biol Soc: 175-178.

Kloke A, von Stetten F, Zengerle R, Kerzenmacher S. (2011) Strategies for the fabrication of porous platinum electrodes. Adv Mater, 23: 4976-5008.

Komura Y, Tamura R, Uwano T, Nishijo H, Ono T. (2005) Auditory thalamus integrates visual inputs into behavioral gains. Nat Neurosci, 8: 1203-1209.

Kotzar G, Freas M, Abel P, Fleischman A, Roy S, Zorman C, Moran JM, Melzak J. (2002) Evaluation of MEMS materials of construction for implantable medical devices. Biomaterials, 23: 2737-2750.

Kozai TD, Marzullo TC, Hooi F, Langhals NB, Majewska AK, Brown EB, Kipke DR. (2010) Reduction of neurovascular damage resulting from microelectrode insertion into the cerebral cortex using in vivo two-photon mapping. J Neural Eng, 7: 1741-2560.

Kozai TDY, Vazquez AL, Weaver CL, Kim S-G, Cui XT. (2012) In vivo two-photon microscopy reveals immediate microglial reaction to implantation of microelectrode through extension of processes. J Neural Eng, 9: 066001.

Kruger J, Caruana F, Volta RD, Rizzolatti G. (2010) Seven years of recording from monkey cortex with a chronically implanted multiple microelectrode. Front Neuroeng, 3.

Kuruvilla A, Flink R. (2003) Intraoperative electrocorticography in epilepsy surgery: useful or not? Seizure, 12: 577-584.

Landis DM. (1994) The early reactions of non-neuronal cells to brain injury. Annu Rev Neurosci, 17: 133-151.

Latikka JA, Hyttinen JA, Kuurne TA, Eskola HJ, Malmivuo JA (Year) The conductivity of brain tissues: comparison of results in vivo and in vitro measurements. Vol. 1, Engineering in Medicine and Biology Society, 2001. Proceedings of the 23rd Annual International Conference of the IEEE. City. p. 910-912 vol.911.

Lempka SF, Johnson MD, Moffitt MA, Otto KJ, Kipke DR, McIntyre CC. (2011) Theoretical analysis of intracortical microelectrode recordings. J Neural Eng, 8: 1741-2560.

Lempka SF, Miocinovic S, Johnson MD, Vitek JL, McIntyre CC. (2009) In vivo impedance spectroscopy of deep brain stimulation electrodes. J Neural Eng, 6: 1741-2560.

Lewicki MS. (1998) A review of methods for spike sorting: the detection and classification of neural action potentials. Network: Computation in Neural Systems, 9: 53-78.

Liu X, Demosthenous A, Donaldson N. (2008) Platinum electrode noise in the ENG spectrum. Med Biol Eng Comput, 46: 997-1003.

Liwei L, Pisano AP. (1999) Silicon-processed microneedles. J Microelectromech Syst, 8: 78-84.

Lopez KA, Waziri AE, Canoll PD, Bruce JN. (2006) Convection-enhanced delivery in the treatment of malignant glioma. Neurol Res, 28: 542-548.

Lu Y, Li T, Zhao X, Li M, Cao Y, Yang H, Duan YY. (2010) Electrodeposited polypyrrole/carbon nanotubes composite films electrodes for neural interfaces. Biomaterials, 31: 5169-5181.

Mailley S, Hyland M, Mailley P, McLaughlin JA, McAdams ET. (2004) Thin film platinum cuff electrodes for neurostimulation: in vitro approach of safe neurostimulation parameters. Bioelectrochemistry, 63: 359-364.

Marrese CA. (1987) Preparation of strongly adherent platinum black coatings. Anal Chem, 59: 217-218.

Matsuo T, Kawai K, Uno T, Kunii N, Miyakawa N, Usami K, Kawasaki K, Hasegawa I, Saito N. (2013) Simultaneous recording of single-neuron activities and broad-area intracranial electroencephalography: electrode design and implantation procedure. Neurosurgery, 73: 146-154.

Mercanzini A, Cheung K, Buhl DL, Boers M, Maillard A, Colin P, Bensadoun JC, Bertsch A, Renaud P. (2008) Demonstration of cortical recording using novel flexible polymer neural probes. Sens Actuat A-Phys, 143: 90-96.

Merrill DR, Bikson M, Jefferys JG. (2005) Electrical stimulation of excitable tissue: design of efficacious and safe protocols. J Neurosci Meth, 141: 171-198.

Metherate R, Ashe JH. (1993) Ionic flux contributions to neocortical slow waves and nucleus basalis-mediated activation: whole-cell recordings in vivo. J Neurosci, 13: 5312-5323.

Metin C, Frost DO. (1989) Visual responses of neurons in somatosensory cortex of hamsters with experimentally induced retinal projections to somatosensory thalamus. Proc Natl Acad Sci U S A, 86: 357-361.

Metz S, Bertsch A, Bertrand D, Renaud P. (2004) Flexible polyimide probes with microelectrodes and embedded microfluidic channels for simultaneous drug delivery and multi-channel monitoring of bioelectric activity. Biosens Bioelectron, 19: 1309-1318.

Minnikanti S, Pereira MG, Jaraiedi S, Jackson K, Costa-Neto CM, Li Q, Peixoto N. (2010) In vivo electrochemical characterization and inflammatory response of multiwalled carbon nanotube-based electrodes in rat hippocampus. J Neural Eng, 7: 1741-2560.

Moffitt MA, McIntyre CC. (2005) Model-based analysis of cortical recording with silicon microelectrodes. Clin Neurophysiol, 116: 2240-2250.

Morrison PF, Laske DW, Bobo H, Oldfield EH, Dedrick RL. (1994) High-flow microinfusion: tissue penetration and pharmacodynamics. Am J Physiol, 266: R292-305.

Moser EI, Kropff E, Moser MB. (2008) Place cells, grid cells, and the brain's spatial representation system. Annu Rev Neurosci, 31: 69-89.

Myllymaa S, Myllymaa K, Korhonen H, Töyräs J, Jääskeläinen JE, Djupsund K, Tanila H, Lappalainen R. (2009) Fabrication and testing of polyimide-based microelectrode arrays for cortical mapping of evoked potentials. Biosens Bioelectron, 24: 3067-3072.

Nakamura T, Saito R, Sugiyama S-i, Sonoda Y, Kumabe T, Tominaga T. (2011) Local convection-enhanced delivery of chemotherapeutic agent transiently opens blood–brain barrier and improves efficacy of systemic chemotherapy in intracranial xenograft tumor model. Cancer Lett, 310: 77-83.

Nemani KV, Moodie KL, Brennick JB, Su A, Gimi B. (2013) In vitro and in vivo evaluation of SU-8 biocompatibility. Mat Sci Eng: C, 33: 4453–4459

Neves HP, Ruther P. (2007) The NeuroProbes Project. Conf Proc IEEE Eng Med Biol Soc, 5: 6443-6445.

Nicholson C, Freeman JA. (1975) Theory of current source-density analysis and determination of conductivity tensor for anuran cerebellum. J Neurophysiol, 38: 356-368.

Nicholson C, Phillips JM. (1981) Ion diffusion modified by tortuosity and volume fraction in the extracellular microenvironment of the rat cerebellum. J Physiol, 321: 225-257.

Noh J, Park S, Boo H, Kim HC, Chung TD. (2011) Nanoporous platinum solid-state reference electrode with layer-by-layer polyelectrolyte junction for pH sensing chip. Lab Chip, 11: 664-671.

Nordhausen CT, Maynard EM, Normann RA. (1996) Single unit recording capabilities of a 100 microelectrode array. Brain Res, 726: 129-140.

Norlin P, Kindlundh M, Mouroux A, Yoshida K, Hofmann UG. (2002) A 32-site neural recording probe fabricated by DRIE of SOI substrates. J Micromech Microeng, 12: 414.

O'Keefe J, Conway DH. (1978) Hippocampal place units in the freely moving rat: why they fire where they fire. Experimental brain research. Experimentelle Hirnforschung. Exp Cerebr, 31: 573-590.

O'Keefe J, Dostrovsky J. (1971) The hippocampus as a spatial map. Preliminary evidence from unit activity in the freely-moving rat. Brain Res, 34: 171-175.

Ochoa M, Wei P, Wolley AJ, Otto KJ, Ziaie B. (2013) A hybrid PDMS-Parylene subdural multi-electrode array. Biomed Microdevices, 15: 437-443.

Ojemann GA. (1997) Treatment of temporal lobe epilepsy. Annu Rev Med, 48: 317-328.

Pajkossy T, Wandlowski T, Kolb DM. (1996) Impedance aspects of anion adsorption on gold single crystal electrodes. J Electroanal Chem, 414: 209-220.

Palmer C. (1978) A microwire technique for recording single neurons in unrestrained animals. Brain Res Bull, 3: 285-289.

Papageorgiou DP, Shore SE, Bledsoe SC, Wise KD. (2006) A shuttered neural probe with on-chip flowmeters for chronic in vivo drug delivery. J Microelectromech Syst, 15: 1025-1033.

Paxinos G, Watson C. The rat brain in stereotaxic coordinates: compact sixth edition. Academic Press, New York, 2009.

Pedreira C, Martinez J, Ison MJ, Quian Quiroga R. (2012) How many neurons can we see with current spike sorting algorithms? J Neurosci Meth, 211: 58-65.

Polikov VS, Tresco PA, Reichert WM. (2005) Response of brain tissue to chronically implanted neural electrodes. J Neurosci Meth, 148: 1-18.

Pongrácz A, Fekete Z, Márton G, Bérces Z, Ulbert I, Fürjes P. (2013) Deep-brain silicon multielectrodes for simultaneous in vivo neural recording and drug delivery. Sensor Actuat B-Chem, 189: 97-105.

Prasad A, Sanchez JC. (2012) Quantifying long-term microelectrode array functionality using chronic in vivo impedance testing. J Neural Eng, 9: 026028.

Quiroga RQ, Nadasdy Z, Ben-Shaul Y. (2004) Unsupervised spike detection and sorting with wavelets and superparamagnetic clustering. Neural Comput, 16: 1661-1687.

Reed JL, Pouget P, Qi HX, Zhou Z, Bernard MR, Burish MJ, Haitas J, Bonds AB, Kaas JH. (2008) Widespread spatial integration in primary somatosensory cortex. Proc Natl Acad Sci U S A, 105: 10233-10237.

Retterer ST, Smith KL, Bjornsson CS, Neeves KB, Spence AJ, Turner JN, Shain W, Isaacson MS. (2004) Model neural prostheses with integrated microfluidics: a potential intervention strategy for controlling reactive cell and tissue responses. IEEE Trans Biomed Eng, 51: 2063-2073.

Robinson DA. (1968) The electrical properties of metal microelectrodes. Proceedings of the IEEE, 56: 1065-1071.

Rousche PJ, Pellinen DS, Pivin DP, Jr., Williams JC, Vetter RJ, Kipke DR. (2001) Flexible polyimide-based intracortical electrode arrays with bioactive capability. IEEE Trans Biomed Eng, 48: 361-371.

Rubehn B, Bosman C, Oostenveld R, Fries P, Stieglitz T. (2009) A MEMS-based flexible multichannel ECoG-electrode array. J Neural Eng, 6: 1741-2560.

Rubehn B, Wolff SB, Tovote P, Schuettler M, Luthi A, Stieglitz T. (2011) Polymer-based shaft microelectrodes with optical and fluidic capabilities as a tool for optogenetics. Conf Proc IEEE Eng Med Biol Soc, 72: 6090815.

Ruther P, Aarts A, Frey O, Henrik S, Kisban S, Seidl K, Spieth S, Scumacher A, Koudelka-Hep M, Paul O, Stieglitz T, Zengerle R, Neves H (Year) The NeuroProbes project – multifunctional probe arrays for neural recording and stimulation. 13th Annual Conference of the IFESS. City.

Rutishauser U, Schuman EM, Mamelak AN. (2006) Online detection and sorting of extracellularly recorded action potentials in human medial temporal lobe recordings, in vivo. J Neurosci Meth, 154: 204-224.

Sachdev RN, Ebner FF, Wilson CJ. (2004) Effect of subthreshold up and down states on the whisker-evoked response in somatosensory cortex. J Neurophysiol, 92: 3511-3521.

Scherer R, Zanos SP, Miller KJ, Rao RP, Ojemann JG. (2009) Classification of contralateral and ipsilateral finger movements for electrocorticographic brain-computer interfaces. Neurosurg Focus, 27.

Schuettler M (Year) Electrochemical Properties of Platinum Electrodes in Vitro: Comparison of Six Different Surface Qualities. Engineering in Medicine and Biology Society, 2007. EMBS 2007. 29th Annual International Conference of the IEEE. City. p. 186-189.

Scott KM, Du J, Lester HA, Masmanidis SC. (2012) Variability of acute extracellular action potential measurements with multisite silicon probes. J Neurosci Meth, 211: 22-30.

Segev R, Goodhouse J, Puchalla J, Berry MJ, 2nd. (2004) Recording spikes from a large fraction of the ganglion cells in a retinal patch. Nat Neurosci, 7: 1154-1161.

Seidl K, Herwik S, Torfs T, Neves HP, Paul O, Ruther P. (2011) CMOS-Based High-Density Silicon Microprobe Arrays for Electronic Depth Control in Intracortical Neural Recording. J Microelectromech Syst, 20: 1439-1448.

Seidl K, Spieth S, Herwik S, Steigert J, Zengerle R, Paul O, Ruther P. (2010) In-plane silicon probes for simultaneous neural recording and drug delivery. J Micromech and Microeng, 20: 105006.

Seymour JP, Langhals NB, Anderson DJ, Kipke DR. (2011) Novel multi-sided, microelectrode arrays for implantable neural applications. Biomed Microdev, 13: 441-451.

Simeral JD, Kim SP, Black MJ, Donoghue JP, Hochberg LR. (2011) Neural control of cursor trajectory and click by a human with tetraplegia 1000 days after implant of an intracortical microelectrode array. J Neural Eng, 8: 1741-2560.

Simon D, Ware T, Marcotte R, Lund B, Smith D, Jr., Di Prima M, Rennaker R, Voit W. (2013) A comparison of polymer substrates for photolithographic processing of flexible bioelectronics. Biomed Microdev, 15: 925-939.

Somogyvari Z, Cserpan D, Ulbert I, Erdi P. (2012) Localization of single-cell current sources based on extracellular potential patterns: the spike CSD method. Eur J Neurosci, 36: 3299-3313.

Spencer K, Kai M, Kyle T, Richard B, Paul H, Bradley G. (2010) Decoding spoken words using local field potentials recorded from the cortical surface. J Neur Eng, 7: 056007.

Stein AG, Eder HG, Blum DE, Drachev A, Fisher RS. (2000) An automated drug delivery system for focal epilepsy. Epilepsy Res, 39: 103-114.

Stence N, Waite M, Dailey ME. (2001) Dynamics of microglial activation: a confocal time-lapse analysis in hippocampal slices. Glia, 33: 256-266.

Steriade M. (2003) The corticothalamic system in sleep. Front Biosci, 1: d878-899.

Steriade M, Nunez A, Amzica F. (1993) A novel slow (< 1 Hz) oscillation of neocortical neurons in vivo: depolarizing and hyperpolarizing components. J Neurosci, 13: 3252-3265.

Stieglitz T, Beutel H, Meyer JU. (1997) A flexible, light-weight multichannel sieve electrode with integrated cables for interfacing regenerating peripheral nerves. Sensor Actuat A-Phys, 60: 240-243.

Stieglitz T, Beutel Hr, Schuettler M, Meyer JU. (2000) Micromachined, Polyimide-Based Devices for Flexible Neural Interfaces. Biomed Microdev, 2: 283-294.

Stieglitz T, Ruf HH, Gross M, Schuettler M, Meyer JU. (2002) A biohybrid system to interface peripheral nerves after traumatic lesions: design of a high channel sieve electrode. Biosens Bioelectron, 17: 685-696.

Strumwasser F. (1958) Long-term recording' from single neurons in brain of unrestrained mammals. Science, 127: 469-470.

Sugano H, Shimizu H, Sunaga S. (2007) Efficacy of intraoperative electrocorticography for assessing seizure outcomes in intractable epilepsy patients with temporal-lobe-mass lesions. Seizure, 16: 120-127.

Sullivan D, Csicsvari J, Mizuseki K, Montgomery S, Diba K, Buzsaki G. (2011) Relationships between hippocampal sharp waves, ripples, and fast gamma oscillation: influence of dentate and entorhinal cortical activity. J Neurosci, 31: 8605-8616.

Szarowski DH, Andersen MD, Retterer S, Spence AJ, Isaacson M, Craighead HG, Turner JN, Shain W. (2003) Brain responses to micro-machined silicon devices. Brain Res, 983: 23-35.

Takekawa T, Isomura Y, Fukai T. (2010) Accurate spike sorting for multi-unit recordings. Eur J Neurosci, 31: 263-272.

Taub AH, Hogri R, Magal A, Mintz M, Shacham-Diamand Y. (2012) Bioactive anti-inflammatory coating for chronic neural electrodes. J Biomed Mater Res A, 100: 1854-1858.

Toda H, Suzuki T, Sawahata H, Majima K, Kamitani Y, Hasegawa I. (2011) Simultaneous recording of ECoG and intracortical neuronal activity using a flexible multichannel electrode-mesh in visual cortex. NeuroImage, 54: 203-212.

Torfs T, Aarts AA, Erismis MA, Aslam J, Yazicioglu RF, Seidl K, Herwik S, Ulbert I, Dombovari B, Fiath R, Kerekes BP, Puers R, Paul O, Ruther P, Van Hoof C, Neves HP. (2011) Two-dimensional multi-channel neural probes with electronic depth control. IEEE Trans Biomed Circuits Syst, 5: 403-412.

Toth A, Gyengesi E, Zaborszky L, Detari L. (2008) Interaction of slow cortical rhythm with somatosensory information processing in urethane-anesthetized rats. Brain Res, 21: 99-110.

Truccolo W, Friehs GM, Donoghue JP, Hochberg LR. (2008) Primary motor cortex tuning to intended movement kinematics in humans with tetraplegia. J Neurosci, 28: 1163-1178.

Turner JN, Shain W, Szarowski DH, Andersen M, Martins S, Isaacson M, Craighead H. (1999) Cerebral astrocyte response to micromachined silicon implants. Exp Neurol, 156: 33-49.

Ulbert I, Halgren E, Heit G, Karmos G. (2001) Multiple microelectrode-recording system for human intracortical applications. J Neurosci Methods, 106: 69-79.

Ulbert I, Heit G, Madsen J, Karmos G, Halgren E. (2004) Laminar analysis of human neocortical interictal spike generation and propagation: current source density and multiunit analysis in vivo. Epilepsia, 4: 48-56.

Vargas-Irwin C, Donoghue JP. (2007) Automated spike sorting using density grid contour clustering and subtractive waveform decomposition. J Neurosci Meth, 164: 1-18.

Vázsonyi É, Vértesy Z, Tóth A, Szlufcik J. (2003) Anisotropic etching of silicon in a two-component alkaline solution. J Micromech Microeng, 13: 165.

Velliste M, Perel S, Spalding MC, Whitford AS, Schwartz AB. (2008) Cortical control of a prosthetic arm for self-feeding. Nature, 453: 1098-1101.

von Metzen R, Stieglitz T. (2013) The effects of annealing on mechanical, chemical, and physical properties and structural stability of Parylene C. Biomed Microdev, 15: 727-735.

Ward MP, Rajdev P, Ellison C, Irazoqui PP. (2009) Toward a comparison of microelectrodes for acute and chronic recordings. Brain Res, 28: 183-200.

Watanabe H, Sakatani T, Suzuki T, Sato MA, Nishimura Y, Nambu A, Kawato M, Isa T. (2014) Reconstruction of intracortical whisker-evoked local field potential from electrocorticogram using a model trained for spontaneous activity in the rat barrel cortex. Neurosci Res, 87: 40-48.

Watanabe H, Sato MA, Suzuki T, Nambu A, Nishimura Y, Kawato M, Isa T. (2012) Reconstruction of movement-related intracortical activity from micro-electrocorticogram array signals in monkey primary motor cortex. J Neural Eng, 9: 1741-2560.

Williams JC, Rennaker RL, Kipke DR. (1999) Long-term neural recording characteristics of wire microelectrode arrays implanted in cerebral cortex. Brain Research Protocols, 4: 303-313.

Wise KD. (2005) Silicon microsystems for neuroscience and neural prostheses. IEEE Eng Med Biol Mag, 24: 22-29.

Wise KD, Angell JB. (1975) A Low-Capacitance Multielectrode Probe for Use in Extracellular Neurophysiology. Biomedical Engineering, IEEE Transactions on, BME-22: 212-219.

Wise KD, Angell JB, Starr A. (1970) An Integrated-Circuit Approach to Extracellular Microelectrodes. Biomedical Engineering, IEEE Transactions on, BME-17: 238-247.

Woldring S, Dirken MN. (1950) Spontaneous unit-activity in the superficial cortical layers. Acta Physiol Pharmacol Neerl, 1: 369-379.

Woods R. Chemisorption at electrodes: hydrogen and oxygen on noble metals and their alloys. In: Bard AJ (szerk.) Electroanalytical Chemistry: A Series of Advances. Dekker, New York, 1976.

Wu F, Stark E, Im M, Cho I-J, Yoon E-S, Buzsáki G, Wise KD, Yoon E. (2013) An implantable neural probe with monolithically integrated dielectric waveguide and recording electrodes for optogenetics applications. J Neur Eng, 10: 056012.

Yamamoto T. (1987) Easy construction of an improved fine wire electrode for chronic single neuron recording in freely moving animals. Phys Behav, 39: 649-652.

Yang K-L, Yiacoumi S, Tsouris C. (2004) Electrical double-layer formation. Dekker Enc Nanosci Nanotech: 1001.

Yeager JD, Phillips DJ, Rector DM, Bahr DF. (2008) Characterization of flexible ECoG electrode arrays for chronic recording in awake rats. J Neurosci Meth, 173: 279-285.

Yoo J-M, Sharma A, Tathireddy P, Rieth LW, Solzbacher F, Song J-I. (2012) Excimer-laser deinsulation of Parylene-C coated Utah electrode array tips. Sensor Actuat B-Chem, 166–167: 777-786.

Yuan JH, Wang K, Xia XH. (2005) Highly Ordered Platinum-Nanotubule Arrays for Amperometric Glucose Sensing. Advanced Functional Materials, 15: 803-809.

Zoltowski P. (1998) On the electrical capacitance of interfaces exhibiting constant phase element behaviour. J Electroanal Chem, 443: 149-154.

9. AUTHOR'S PUBLICATION LIST

9.1. Papers closely related to the PhD dissertation

Márton G, Kiss M, Orbán G, Pongrácz A, Ulbert I. (2014) A polymer-based spiky microelectrode array for electrocorticography. Microsyst Technol, In press.

Márton G, Bakos I, Fekete Z, Ulbert I, Pongrácz A. (2014) Durability of high surface area platinum deposits on microelectrode arrays for acute neural recordings. J Mat Sci: Mat Med, 25: 931-940.

Fekete Z, Hajnal Z, Márton G, Fürjes P, Pongrácz A. (2013) Fracture analysis of silicon microprobes designed for deep-brain stimulation. Microelectron Eng, 103: 160-166.

Márton G, Fekete Z, Fiáth R, Baracskay P, Ulbert I, Juhász G, Battistig G, Pongrácz A. (2013) In vivo measurements with robust silicon-based multielectrode arrays with extreme shaft lengths. IEEE Sens J, 13: 3263-3269.

Márton G, Fekete Z, Bakos I, Battistig G, Pongrácz A, Baracskay P, Juhász G, Bársony I. (2012) Deep-brain silicon multielectrodes with surface-modified Pt recording sites. Proceedings of IEEE Sensors 2012 conference, Taipei City, Taiwan. Paper 6411325

9.2. Papers not closely related to the PhD dissertation

Fekete Z, Pongrácz A, Márton G, Fürjes P. (2013) On the fabrication parameters of buried microchannels integrated in in-plane silicon microprobes. Mat Sci Foum 729: pp. 210-215.

Pongrácz A, Fekete Z, Márton G, Bérces Z, Ulbert I, Fürjes P. (2013) Deep-brain silicon multielectrodes for simultaneous in vivo neural recording and drug delivery. Sensor Actuat B-Chem, 189: 97-105.

Pongrácz A, Fekete Z, Márton G, Fiáth R, Fürjes P, Ulbert I, Battistig G. (2013) Deep-brain silicon multielectrodes for simultaneous neural recording and drug delivery. Pro Eng 47: 281-284.

Fiáth R, Grand L, Kerekes BP, Pongrácz A, Vázsonyi É, Márton G, Battistig G, Ulbert I. (2011) A novel multisite silicon probe for laminar neural recordings. Pro Comp Sci 7: 310-311.

Grand L, Pongrácz A, Vázsonyi É, Márton G, Gubán D, Fiáth R, Kerekes BP, Karoms G, Ulbert I, Battistig G. (2011) A novel multisite silicon probe for high quality laminar neural recordings. Sensor Actuat A-Phys, 166: 14-21.

10. ACKNOWLEDGEMENTS

I am glad to acknowledge the enormous support I received from Dr. Anita Pongrácz, who managed my work regarding microfabrication technology in the early years of my Ph.D. studies, and of course the support of my tutor, Dr. István Ulbert.

Several people contributed to this work, including Károlyné Payer, Magdolna Erős, Róbert Hodován, András Lőrincz, András Strasszner, Tibor Csarnai, János Ferencz, Dr. Zoltán Fekete, Dr. István Bakos, Dr. Tamás Pajkossy, Dr. Péter Fürjes, Attila Nagy, István Réti, Éva Vázsonyi, Richárd Fiáth, Péter Kottra, Dr. László Grand, Dr. Péter Baracskay, Dr. Gábor Juhász and other scientists and laboratory personnel.

I would like to express gratitude to Dr. Gábor Battistig and Dr. István Bársony for providing a vivid and encouraging working environment at the Microtechnology Department of the Institute for Technical Physics and Materials Science.

I am thankful for the support I received from students, Gábor Orbán, Zsófia Sztyéhlikné Bérces, and others. I owe special thanks to Marcell Kiss for challenging me with a deadline for the preparation of a first draft.

I consider myself very lucky that many of my colleagues I can also call friends.

I am also very grateful to my family. Without them I never could have created this work.